THESIS

USE OF INNOVATIVE TECHNIQUES TO OPTIMIZE THE RESIDENCE TIME

DISTRIBUTION OF DRINKING WATER CONTACT TANKS

Submitted by

Justin J. Kattnig

Department of Civil and Environmental Engineering

In partial fulfillment of the requirements

For the Degree of Master of Science

Colorado State University

Fort Collins, Colorado

Summer 2014

Master's Committee:

    Advisor: S. Karan Venayagamoorthy

    Timothy K. Gates
    Hiroshi Sakurai

ABSTRACT

USE OF INNOVATIVE TECHNIQUES TO OPTIMIZE THE RESIDENCE TIME

DISTRIBUTION OF DRINKING WATER CONTACT TANKS

The focus of this study is to understand the complex nature of flow dynamics within water disinfection contact tanks and to use this understanding in the development of beneficial tank modifications. In particular this study focuses on systems classified as small by the United States Environmental Protection Agency (USEPA). Methods involved in this process included the use of computational fluid dynamics (CFD), physical tracer studies, and acoustic doppler velocimetry (ADV). Attempted tank alterations included the installation of baffles, inlet modification, and the use of industrial packing material. Tested modifications aimed at altering existing velocity fields in order to increase the hydraulic disinfection efficiency of a given system. Hydraulic disinfection efficiency was measured through the use of residence time distribution (RTD) curves and the well-known baffling factor (BF) (as defined by the USEPA).

The principal system that was investigated was a 1500 gallon rectangular concrete tank with a sharp circular inlet. A physical prototype of this system currently resides at Colorado State University's (CSU) Engineering Research Center (ERC) and was used for all physical testing. CFD models were used to compute the average velocity fields within the tank and to produce modeled RTD curves. This was done for the empty tank and for 37 different baffled configurations. Baffles were placed parallel to the longest axis of the tank and varied in number and length. Optimal configurations yielded baffling factors between 0.70 and 0.8, which is more than thirteen times as efficient as the original system. Several configurations were selected and

physically constructed in the existing tank in order to validate the applied numerical methodology.

After CFD models were experimentally validated, random packing material was placed within the tank at areas of high velocity and flow separation (at the inlet and at baffle turns). An extensive parametric study was conducted in order to determine the effects of using packing material as an inlet modifier within the open tank. Packing material was placed in box-like structures and fastened over the inlet. Dimensions of these packing boxes were systematically varied and tested at different flow rates. Observed baffling factors were as high as 0.36, which represents an improvement over the basic system by a factor of six.

Resulting findings from the inlet modification study were then used to design and test internal modifications for a baffled system. In addition to material being placed over the inlet, structures were placed over channel openings at baffle turns. Configurations were tested at a number of flow rates in order to determine relative effects on gains in efficiency. The most effective system obtained a baffling factor of 0.72, representing an increase from the base system by a factor of 13. ADV measurements were conducted within the baffled system in order to assess changes in the velocity field and explain observed increases in baffling factor. Packing material was not modeled due to complexity and high computational cost.

Results from this study show that the innovative use of industrial packing material and other modifications can significantly increase the hydraulic disinfection efficiency of simple systems. It also shows that the use of CFD is an invaluable guide in this endeavor. The work summarized in this thesis aids in an ongoing effort to understand the hydraulic characteristics of small scale drinking water systems. The findings summarized here will help to shape the designs of the future.

ACKNOWLEDGEMENTS

TABLE OF CONTENTS

CHAPTER 1: INTRODUCTION

1.1 Background

Over 71% of the earth's surface is covered with water, which is one of the most precious and essential ingredients for the sustainment of life. The majority of earth's water is saline and exists in oceans, seas, and bays, accounting for over 96% of the world's total water supply. The remaining 4% of terrestrial water is fresh and helps support the life of billions of land-dwelling organisms. 68% of earth's freshwater is trapped in ice caps, glaciers, and permanent snow pack, and what remains is divided between surface and ground water features. These features have supported civilizations across the globe for centuries (USGS, 2014).

In addition to supporting human life, freshwater provides an ample breeding ground for the growth of microscopic organisms and allows for the transport of chemical contaminants. The presence of these constituents diminishes water quality, which provides significant challenges in terms of human health. More than 3.4 million people die each year from water related illnesses (water.org, 2014). The majority of these deaths occur outside of the United States, but even the most advanced nation in the world suffers from water borne outbreaks.

In the period between 1971 and 2002, 689 outbreaks of waterborne disease were reported in the U.S that involved public water systems. The worst of these outbreaks occurred in April 1993, where Cryptosporidium affected over 400,000 people in Milwaukee (Lansey & Boulos, 2005). Outbreaks such as this are what originally spurred the development of the Safe Drinking Water Act (SDWA), which was passed in 1974. Forming a cooperative between local, state, and federal agencies, the SDWA allowed the USEPA to research, establish, and enforce national drinking water standards (USEPA, 2012; USEPA, 2004). Under the SWDA the first set of National Interim Primary Drinking Water Regulations (NIODWRs) was proposed in 1975 and

passed in 1977 (Wilson, 2011). Since that time a number of rules and amendments have been

added to the SWDA. A number of these include the Surface Water Treatment Rule (SWTR), the

Ground Water Rule, and the Disinfectants/Disinfection By-Products Rule (D/DBPR) (Lansey &

Boulos, 2005; Wilson, 2011). Both the SWTR and the Ground Water Rule use log inactivation of

viruses as a measure of disinfection (USEPA, 1991). Surface and ground water treatment plants

are regulated under the SDWA by whichever agency acquires primacy (USEPA, 2012).

The state of Colorado has primacy for drinking water regulation. Under Colorado's

primacy the Water Quality Division of the Colorado Department for Public Health and

Environment (CDPHE) is directly responsible for the regulation of Colorado's drinking water

systems. CDPHE determines disinfection (log inactivation) using procedures outlined in the

Long Term 1 Enhanced Surface Water Treatment Rule (LT1ESWTR) Disinfection Profiling and

Benchmarking Technical Guidance Manual (USEPA, 2003). LT1ESWTR classifies hydraulic

disinfection efficiency through the use of a term known as the baffling factor (*BF*), which is

directly used in the calculation of a multiplicative quantity called CT. The *BF* is defined by the

USEPA as t_{10}/TDT, where t_{10} is the time at which ten percent of the inlet concentration is

observed at the outlet under continual injection and TDT is the theoretical detention time

(USEPA, 2003). The TDT of a system can be calculated by dividing the volume of a system by

the system flow rate (V_{system}/Q_{system}).

The USEPA assigns disinfection credit using a generally descriptive table and a series of

exemplary sketches (see Table 1.1). This method is highly imprecise and does not consider

critical components of design, such as inlet size and orientation. Also, the USEPA baffling

descriptions fail to consider the use of small tanks in series or the use of large open surface tanks,

which are commonly used in Colorado. In fact, a wide range of practical research has shown the

use of Table 1.1 to be overly non-conservative (Wilson & Venayagamoorthy, 2010; Taylor, 2012; Barnett, 2013; Barnett *et al*, 2014). The only way to truly determine the *BF* of a given system is to perform physical tracer studies or to conduct three-dimensional numerical simulations (Rauen, 2012).

Table 1.1: Baffling Classification Table from LT1ESWTR Disinfection Profiling and Benchmarking Technical Guidance Manual (USEPA, 2003)

Baffling Condition	*BF*	Baffling Description
Unbaffled (Mixed Flow)	0.1	None, agitated basin, very low length to width ratio, high inlet and outlet flow velocities.
Poor	0.3	Single or multiple unbaffled inlets and outlets, no intra-basin baffles.
Average	0.5	Baffled inlet or outlet with some intra-basin baffles.
Superior	0.7	Perforated inlet baffle, serpentine or perforated intra basin baffles, outlet weir or perforated lauders.
Perfect (plug flow)	1	Very high length to width ratio (pipeline flow), perforated inlet, outlet, and intra-basin baffles.

In addition to the USEPA table, a number of empirical and loosely developed theoretical models have been used to approximate hydraulic disinfection efficiency. Included in these models are First in First-Out (FIFO) Plug Flow models, Last in-First Out Plug Flow (LIFO) models, and compartmental models (Lansey & Boulos, 2005). FIFO and LIFO models operate under the assumption that the system in question is undergoing a phenomena known as "plug-flow." Plug-flow describes an idealized scenario in which a parcel of fluid moves evenly across the entire area of a given system, i.e pure advection. In reality, the presence of viscosity and turbulence introduce local velocity gradients which result in short circuiting and the formation of dead zones. Compartmental models attempt to account for recirculating zones by dividing tanks into compartments which are defined by varying exchange rates. However, detailed knowledge of the internal hydraulics of a given tank would need to be known to successfully apply such a simplified model.

Advances in numerical methods and processing power have made computational fluid dynamics (CFD) an affordable and invaluable tool for understanding the complex flow phenomena that occur within disinfection contactors (Hannoun *et al*, 1998; Wenjun *et al*, 2007; Zhang *et al*, 2011; Zhang *et al*, 2012). The use of Computational Fluid Dynamics for the design and analysis of disinfection contact tanks has been validated by a number of comprehensive studies (Wang *et al*, 1998; Wang *et al*, 2003; Baawain *et al*, 2006; Khan *et al*, 2006; Rauen *et al*, 2008; Amini *et al*, 2011). Resolution of internal velocity fields and scalar transport through numerical modeling can be used to develop beneficial tank modifications and to increase general understanding of relative processes. An increased understanding can be used to re-shape existing guidance and improve future designs.

1.2 Scope of Work and Objectives

Work presented in this thesis represents the final portion of a four phase project for the Water Quality Control Division of CDPHE. The first phase was completed by Qing Xu for her master's thesis titled *Internal Hydraulics of Baffled Disinfection Contact Tanks Using Computational Fluid Dynamics*. The second phase of the project and part of the third phase were complete by Jordan Wilson as part of his master's thesis entitled *Evaluation of Flow and Scalar Transport Characteristics of Small Public Drinking Water Disinfection Systems using Computational Fluid Dynamics*. The remainder of the third phase and a portion of the fourth phase were completed by Zachary Taylor for his master's thesis titled *Towards Improved Understanding and Optimization of the Internal Hydraulics of Chlorine Contact Tanks*. Taylor Barnett worked on the remainder of phase four through his master's thesis entitled *Flow Dynamics and Scalar Transport in Drinking Water Contact Tanks*. The scope of work for the fourth phase of the project for CDPHE includes the following:

1. Phase 4a: Baffle Factor Modeling

    a) Perform computer modeling of tank configurations that simulate poor, average, and superior baffling as described in Table 1.1

        i.   Produce a project plan outlining modeling scenarios.

        ii. Generate computer models for the agreed upon configurations

    b) Provide an oral and written presentation to CDPHE engineers on the findings from Phase 4a.

2. Phase 4b: Small System Disinfection Contact Basin Modification Project

    a) Design, build, and test a rectangular tank that can be physically modified to validate the models proposed in Phase 4a. Tracer studies should be performed at multiple flow rates.

    b) Outreach to participating public water systems to provide tank modifications and baffling factor tracer studies to verify baffling factor conditions before and after tank modifications are made.

    c) Provide an oral and written presentation to CDPHE engineers on the findings from Phase 4b.

3. Phase 4c: Guidance Document

    a) Develop a guidance document to address overall baffling factor issues and provide effective contact basin design guidance. This guidance document will address:

        i.   Assessing the adequacy of the existing baffling factor criteria in Long Term 1 Enhanced Surface Water Treatment Rules (LT1ESWTR) *Disinfection Profiling and Benchmarking Technical Guidance Manual.*

ii. Investigating and evaluating the effect of several factors on the overall disinfection contact time, including, but not limited to:

    A. Basin Geometry

    B. Inlet/Outlet configurations (e.g. location and size)

    C. Inlet/Outlet design (e.g. velocity)

    D. Intra Basin baffling configurations

    E. Other modifications (addition of media, etc.) to increase baffling factors

    F. Water quality parameters (e.g. temperature)

iii. Developing baffling factor determinations for typical basin design configurations

iv. Provide cost effective recommendations of disinfection contact basin design.

The work presented in this thesis involves computational modeling of contact tank configurations, validation of numerical methodology, and physical testing of modified disinfection systems. Material from chapters 3-5 was prepared and incorporated into a final guidance document that was submitted to CDPHE in December of 2013.

1.3 New Contributions

Research presented in this thesis makes the following unique contributions:

- Validated the use of CFD in modeling the transport of a passive scalar within a disinfection contactor using full-scale physical measurements from a 1500 gallon rectangular tank.

- Extended the work of Barnett (2013) in refining the design guidelines for the construction of serpentine baffle contact tanks with sharp inlets by considering tank length, baffle opening width, and baffle channel width for baffles parallel to the long axis of a tank.

- Investigated the local application of random packing material within larger systems for increasing hydraulic disinfection efficiency. CFD was used as an intuitive guide in this endeavor.

1.4 Research Publications

Work presented in this thesis has been accepted for presentation in the Emerging and Innovative Technologies Track at the 2014 World Environmental and Water Resources (EWRI) Congress of the Environmental and Water Resources Institute of the American Society of Civil Engineers (ASCE). A paper entitled "Use of Innovative Techniques to Enhance the Hydraulic Disinfection Efficiency of Drinking Water Contact Tanks" will be published in the conference proceedings. Work found in Chapter 3 is currently being prepared for submission to the ASCE Journal of Environmental Engineering with the title "Residence Time Distribution of Baffled Disinfection Contact Tanks with Sharp Inlets." The contents from Chapters 4-5 has been submitted to the journal *Environmental Science and Technology* under the title "Improving the residence time distribution of baffled and un-baffled drinking water contact tanks through localized application of random packing material."

1.5 Organization of Thesis

Chapter 2 provides the reader with a detailed literature review that consists of a comprehensive background for the entire study. This section discusses methods for quantifying hydraulic disinfection efficiency, which includes the formulation of CT and determination of the baffling factor. It also outlines procedures for the physical testing of disinfection systems, which

includes the step and pulse input methods. In addition to describing theoretical background, chapter 2 defines the term "industrial packing material" and provides common uses and examples. Chapter 2 concludes with a review on the modeling of turbulence and fluid flow, which includes descriptions of commercial software used in this investigation.

Chapter 3 presents and summarizes the results of a parametric baffle study in which the length and number of baffles was varied for a given tank with a set footprint. Baffles were placed parallel to the long axis of the tank with the goal of optimizing hydraulic disinfection efficiency. This section includes a detailed mesh independence study and compares model results with measured data, validating the applied methodology.

Chapter 4 outlines a parametric study that was conducted in order to evaluate the use of random packing material as an inlet modifier in open systems. Packing material was placed in box like structures and fastened over the inlet. The height and length of the inlet-box were systematically varied in order to determine relative effects on gains in disinfection efficiency.

Chapter 5 extends the work presented in chapter 4 into a baffled system by considering the placement of random packing material at the inlet and at baffle turns. Results yielded *BF* values around 0.70, suggesting successful dispersion of the turbulent jet. Overall it appears that the most efficient system can be obtained through a combination of internal baffling and inlet modification.

CHAPTER 2: LITERATURE REVIEW

2.1 Small Public Drinking Water Systems

The USEPA defines a small public water system as serving fewer than 3,300 persons (USEPA, 2012). Although these systems cater to a mere 18% of the U.S. population, they contribute to over 95% of the maximum contaminant level (MCL) violations given by the USEPA (USEPA, 2011). The majority of these violations are directly related to inadequate inactivation of microbiological organisms, which is a sign of a poorly designed contact tank. Small systems exhibit such difficulty in meeting standard disinfection requirements due to a lack of financial and professional resources (USEPA, 2012). Without access to necessary resources, many small systems install inadequately designed contact tanks characterized by poor inlet conditions, severe short circuiting, and recirculating dead zones (Wilson & Venayagamoorthy, 2010; Wilson, 2011). For systems that utilize chlorine as a disinfection agent, this can lead to unanticipated development of cancerous disinfection byproducts (DBP) and reduced disinfection (Kothandaraman, 1974). A number of these issues could be resolved by highlighting fundamental design flaws and eliminating the ambiguity of traditional design practice, which is the purpose of this study.

Without access to finances, services, or the necessary expertise, smalls systems rarely conduct physical tracer studies or perform CFD simulations. A majority of smaller systems visually determine the baffling factor for disinfection calculations using guidelines found in LT1ESWTR (Table 1.1). Not only is this method ambiguous, but it is under-conservative and limited in its applicability. Research presented in this study increases fundamental understanding of flow within these small systems and exposes critical design flaws that are ignored in traditional design methodology.

2.2 Quantifying Disinfection in Chlorinated Systems

Chlorination is the most common method for microbial disinfection in the United States due to its relatively low cost and reliability (Davis & Cornwell, 2008). The USEPA quantifies disinfection for chlorinated systems using a multiplicative quantity known as CT. This methodology assumes that the amount of microbial deactivation is related to the product of the disinfectant concentration (C) and the time that the disinfectant is in contact with contaminants (T) (USEPA, 2003). In addition to chlorine concentration and contact time, inactivation is assumed to be dependent on the ambient temperature and pH. Chlorine has been found to disassociate into hypochlorous acid (HOCl) and hypochlorite (OCl⁻) when placed in water. As the pH of the environment increases, there is an exponential decrease in the fraction of hypochlorous acid available, which is more effective at inactivating harmful organisms (Letterman, 1999).

CT can be empirically approximated using the following relationship (Davis & Cornwell, 2008):

$$CT = 0.9847C^{0.1758}pH^{2.7519}T_o^{-0.1467}, \tag{1}$$

where pH is the system pH, and T_o is the temperature of the water in $°C$. The USEPA has developed tables for determining required values of CT for different levels of log inactivation using Equation 1, inherent safety factors, and empirical observations (USEPA, 2003). Log inactivation is a measurement that indirectly represents the inactivation of micro-organisms achieved through disinfection. Log inactivation is determined as:

$$\text{Log Inactivation} = \log\left(\frac{\text{Influent Contaminant Concentration}}{\text{Outfluent Contaminant Concentration}}\right) \tag{2}$$

Equation 2 implies that a system achieving 3-log inactivation disinfects 99.9% of contaminants and that a system achieving 4-log inactivation disinfects 99.99% of contaminants and so on. An

example of log inactivation regulation can be seen in the Surface Water Treatment Rule, which requires systems to demonstrate 3-log inactivation of giardia. Systems regulated under the Ground Water Rule requires 4-log inactivation for most contaminants (USEPA, 2003).

The USEPA quantifies hydraulic disinfection efficiency through assignment of a term known as the baffling factor (BF). The baffling factor represents the ratio of an approximated contact time to the theoretical detention time (TDT) of a given system. The USEPA's BF formulation approximates the contact time from CT as t_{10}, which is the time it takes for 10% of the inlet disinfectant concentration to be observed at the outlet under continual injection. Systems with baffling factors at or below 0.1 exhibit diffusion dominated flow and are considered poor disinfection contactors while systems that yield a BF close to 1.0 are characterized by advective transport and are considered excellent disinfection contactors.

If the outlet concentration of a continuously injected disinfectant is plotted as a function of time the resulting plot is known as a residence time distribution (RTD) curve. Normalizing the concentration, C, by the maximum observed concentration, $C_{\max}$, and normalizing the time, t, by the TDT allows for direct determination of the baffling factor from a given RTD curve. Examples of normalized RTD curve can be seen in Figure 2.1. RTD curves can be directly obtained from the implementation of physical tracer studies, which utilize conductivity or non-reactive tracers such as fluoride or lithium ions. RTD curves can also be obtained through the use of CFD modeling. All of the RTD curves presented in this study were normalized for ease of comparison.
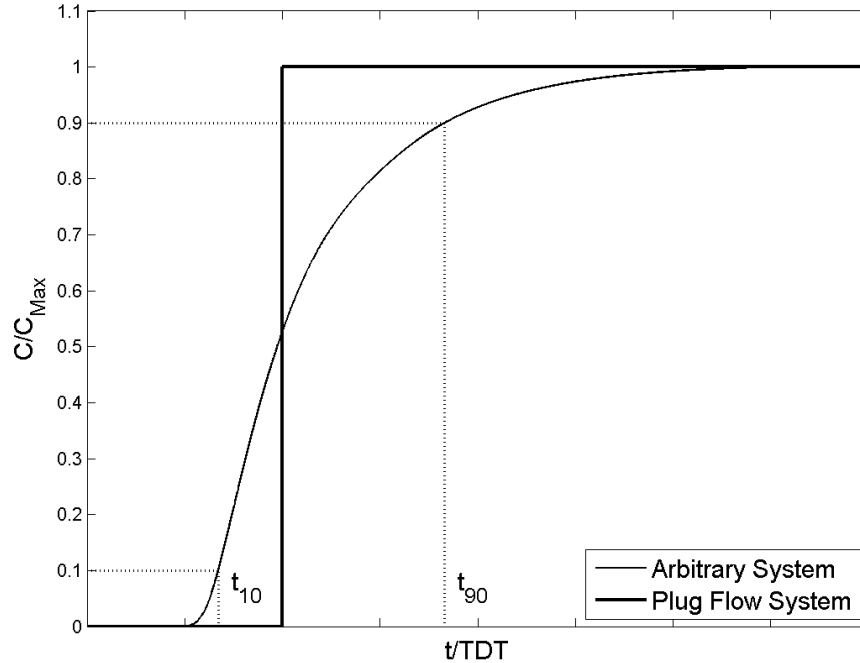
Figure 2.1: Residence Time Distribution Curves for an Arbitrary Disinfection System and an Idealized Plug Flow

In addition to allowing for determination of the baffling factor, RTD curves provide insight into the hydraulics of a given system through their shape. A system with a $BF = 1.0$ is undergoing a phenomena known as plug flow, which describes a purely advective system free of diffusive forces. The square curve in Figure 2.1 represents such a system, which is theoretically unobtainable due to presence of diffusion. Deviations from this behavior are represented by a flattening of the RTD curve, a decrease in slope representing the domination of diffusion.

Since the definition of BF utilizes the TDT of a system, it includes an inherent assumption that plug flow is possible in any reactor. This assumption is unreasonable since the presence of viscosity and turbulence will always promote flow separation, diffusion, and the formation of dead zones. A number of studies have proposed alternate measures of hydraulic disinfection efficiency in order to correct this fundamental oversight. Other indices include t_{10}/t_{90} (see Figure 2.1), Morrill index, dispersion number, and the dispersion index (Wilson &

Venayagamoorthy, 2010; Wols *et. al.*, 2010). However, the BF is the only parameter used in this study because of its direct regulatory role in the United States (USEPA 2003). For more information on alternate methods please refer to the work of Wilson (2011).

2.3 Tracer Studies

The hydraulic disinfection efficiency of a given system can be estimated with the use of a physical conservative tracer study. A conservative tracer study is conducted by introducing a conservative or nonreactive tracer (e.g., fluoride, lithium, sodium chloride) into a system and continually observing changes in tracer concentration at the system outlet. Observations are made until effluent concentration reaches a steady state. Tracer studies should be performed at a variety of flow rates in order to guarantee passivity of the applied tracer and to determine relative effects on system performance.

2.3.1 Pulse Input Method

The pulse input method involves the instantaneous introduction of a known mass of conservative tracer. A large "pulse" of tracer is introduced upstream of a contact tank's inlet and fully mixed into the flow before entering the system. In order for the definition of "instantaneous" to be realistically satisfied, the time required for mixing should be less than one percent of the TDT. If the outlet concentration is plotted as a function of time, both rising and falling limbs can be observed. The resulting curve is known as a flow through curve (FTC), which can be numerically integrated to obtain an RTD curve as shown in Figure 2.1. This is required for the determination of t_{10} and the baffling factor. An example of a normalized FTC for an arbitrary system can be seen in Figure 2.2. The concentration (C) is normalized by the maximum concentration (C_{max}) and the time (t) is normalized by the TDT.
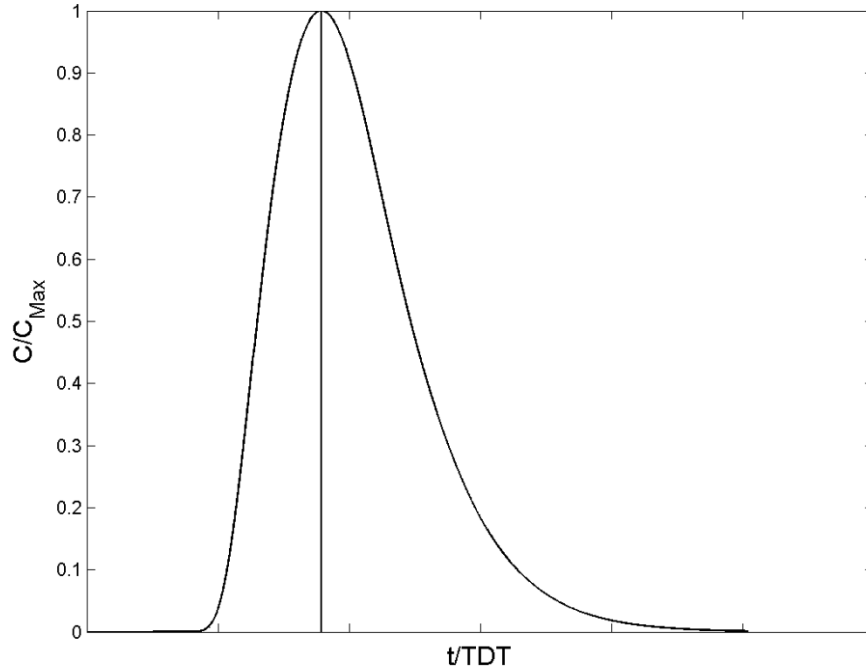
Figure 2.2: FTC Resulting from a Pulse Input Study for an Arbitrary System

2.3.2 Step Input Method

An alternative to using the pulse input method is the application of what is known as the step input method. The step input method involves continual injection of conservative tracer, which is done at a constant rate. Tracer is integrated into the main flow before entering the contact tank and is introduced for the duration of the test. Conservative tracer can be introduced by using existing chemical feed pumps or by constructing temporary input systems. Plotting the outlet concentration as a function of time results in the formation of an RTD curve, which only has a rising limb. Figure 2.1 shows an example of a normalized RTD curve for an arbitrary system.

When compared to the pulse input method the step input method allows for reduced tracer concentrations and fewer sampling intervals, which makes it more reliable. Determination of t_{10} and the baffling factor is simpler when using the step input method because they can be graphically determined from resulting RTD curves. However, mean residence time is more

14

difficult to determine and there is not a reliable way to determine the collected mass of tracer, which can be used to determine steady state. Also, for larger systems, the use of the step input method requires a larger volume of conservative tracer. All of the physical tracer studies conducted for this thesis utilized the step input method for its reliability and ease of *BF* determination.

2.4 Industrial Packing Material

Packing material is traditionally used in vapor separation towers to facilitate the stripping of volatile organic compounds (VOCs) from contaminated liquids. Common areas of industrial application for packing material include frequent use in aeration towers (Kavanaugh & Trussell, 1980), distillation columns (USDOE, 2001; Pilling *et al*, 2001), and trickling filters (Richards & Reinhart, 1986). Column packing material can be classified as either random or structured. Random packing material is designed to be dumped into columns while structured packing material is installed in interlocking units. A number of packing material products are comprised of material that meets National Sanitation Foundation (NSF) Standard 61 criteria and as such are fit for use in drinking water applications.

Despite its use in other areas of water treatment, the application of packing material within contact tanks has not been thoroughly investigated. Research performed by Barnett et al in 2014 suggests that the application of random industrial packing material has the potential to greatly increase the hydraulic disinfection efficiency of small systems. However, this study only considers laboratory scale experiments (up to 50 gallons) (Barnett et al, 2014). Chapters 4 and 5 of this thesis investigate full scale application of packing material in disinfection contactors, making them novel contributions to an evolving field of study.

Packing material is designed by manufacturers to maximize available surface area and minimize induced pressure losses (Jaeger, 2006). This results in material with relatively high porosities (on the order of 0.9). In general, random packing material can be purchased in smaller volumes than structured material and can be used to fill a larger variety of containers, making it appealing for use in drinking water contactors. Following this line of reasoning, all of the studies in this thesis utilized random packing material. Nominally spherical packing material 2" in diameter was the only material considered in this study due to its proven application in drinking water disinfection (Barnett *et al,* 2014). An example of this material can be seen in Figure 2.3. Other available shapes of random packing material include disks, cylinders, saddles, and a variety of other shapes (Jaeger, 2006).

Figure 2.3: Random Industrial Packing Material

CFD has been used to model the internal hydraulics of packing material systems, but the majority of existing studies are limited in scale or scope. The earliest CFD simulations involving packing material were performed during 2003 and focused on single phase flow in individual volume elements of structured packing arrays (Petre *et al*, 2003). Since that time a number of

other simulations involving structured packing material have been performed (Szulczewska *et al*, 2003; Mahr & Mewes, 2007; Wen *et al*, 2007; Owens *et al,* 2013). Experiments performed by Szulczewska et al (2003) used a two-dimensional CFD model to attempt and describe two-phase flow within a single structured canal. Mahr and Mewes (2007) approximated structured packing as a porous media in an attempt to quantify pressure loss over an entire column, and Owens et al (2013) developed a detailed three dimensional model for a complete packing cell. All of these studies focus on either macroscopic variables, such as pressure loss, or describing highly localized flow. Pressure loss within packing columns is a major component of what is known as flooding, which is a major area of study for multi-phase packing systems (Sherwood & Shipley, 1938). Similar studies have been conducted for random packing material, but results from these studies are less accurate and more indeterminate (Yin *et al*, 2000; Fei *et al*, 2003). Therefore, affordable computational modeling of random packing material within large systems relies on grossly macroscopic models for turbulent flow in porous media.

The nature of turbulent flow through porous media is highly debated and difficult to parameterize. Discrepancy between various methods arises from two prevalent problems: determination of a microscopic turbulence model and development of a representative macroscopic model. Turbulence has to be adequately defined within pores, but the pores have to be numerically developed. Approximate methods imply zero-equation turbulence models, which modify existing methods through the introduction of terms that consider "porous eddies" (Chan *et al*, 2007). More complete macroscopic models, like the one developed by Pedras & de Lemos (2007), are based on k-ε closure schemes and utilize periodic circular and elliptic rods to represent porous matrices (Pedras & de Lemos, 2000). Other models, like the v2f model proposed by Kazerooni and Hannani (2009), are closer to LES in formulation and are more

17

computationally expensive (Kazerooni & Hannani, 2009). The mentioned turbulent porous models were designed assuming relatively high porosities and were not validated for three-dimensional flows containing intermittent zones of porosity. The random packing material used in this thesis exhibits porosities of around 0.9. Even if a tank were completely filled with this material, the material's porosity classifies it beyond the application of existing models. The packing material was also locally applied. Any attempt at macroscopic modeling would result in ambiguous velocity fields and incorrect prediction of scalar transport. Numerical knobs of existing models could be adjusted to force agreement with measured data, but this would result in the application of flawed physics. With these considerations in mind, CFD was not used to model systems containing packing material for this study. This is an area that needs further consideration beyond the scope of this thesis.

2.5 Computational Modeling of Fluid Flow

The physics of fluid flows have long been studied through the use of analytical thinking and empirical logic. Theoretical understanding in the form of partial differential equations and dimensional analysis define one of the fundamental fields of fluid dynamics. Analytical solutions to simple problems can be achieved through the use of potential flow, scaling arguments, and simplifying assumptions, but resulting insight is limited and excludes the majority of practical problems (Wilcox, 2007). Experimental methods can be used to extend the limits of theoretical understanding, but physical testing is expensive and is limited in its application due to available measurement devices and the effects of scaling.

The final and most recent field of fluid dynamics has emerged in response to the development of computer science. Computational fluid dynamics (CFD) describes the numerical analysis of systems involving fluid flow and other transport phenomena (Versteeg &

Malalasekera, 2007). Increased availability of processing power, high-end computers, and commercial codes has made CFD one of the most intensely studied topics of the twenty first century. CFD involves the discrete approximation of governing equations on a finite grid or mesh. These approximations are strictly numerical, but they are derived from theoretical understanding. CFD simulations can be used to model full scale systems at reduced costs, but the methods involved are approximate and require experimental validation. Therefore, a complete understanding of a given flow involves theoretical insight, numerical approximation, and experimental validation. These are the three pinnacles of the study of fluid dynamics.

For most fluid dynamic problems, flow characteristics can be described through conservation of mass and conservation of momentum. For flows involving constant-property Newtonian fluids (i.e. incompressible flows under the Boussinesq approximation), these concepts are expressed through the continuity equation and the Navier-Stokes equations (Pope 2000). The continuity equation and Navier-Stokes equations are given by[1]

$$\frac{\partial u_i}{\partial x_i} = 0 \tag{3}$$

and

$$\frac{\partial u_i}{\partial t} + \frac{\partial}{\partial x_i}(u_i u_j) = -\frac{1}{\rho_o}\frac{\partial p}{\partial x_j} + \nu \frac{\partial^2 u_i}{\partial x_j x_j} - \frac{g}{\rho_o}\rho \delta_{i3}, \tag{4}$$

where u_i is the instantaneous velocity field, ρ_o is a reference fluid density which refers to a reference temperature T_o, p is the pressure, ρ is the mass density of the fluid, ν is the kinematic viscosity of the fluid, g is the acceleration of gravity, and δ_{i3} is the Kronecker delta function. The index number 3 refers to the vertical direction, z.

---

[1] Equations are displayed using Einstein's summation notation.

2.6 Turbulence Modeling

Generally speaking, turbulence describes fluid flow that is characterized by "disorder, irreproducible details, mixing, and irregular vorticity in three dimensions" (Stewart, 1968). The state of turbulence is in direct contrast to a laminar state, which is characterized by reproducible details, order, and predictability. Mixing occurs in both laminar and turbulent flows, but in laminar flows mixing is primarily molecular and is not visible at larger scales. Turbulent mixing, on the other hand, occurs both above and at the molecular level. Momentum and other flow properties will be exchanged and mixed on a large scale in turbulent flow. This occurs in part because turbulent flows are dominated by inertial forces. Turbulent flow occurs at higher Reynolds numbers while laminar flow occurs at lower Reynolds numbers. This means that laminar flows are dominated by viscosity and turbulence is dominated by momentum. This domination of momentum helps give turbulence its chaotic structure.

Turbulence within fluid flows is one of the most difficult aspects to capture using numerical models. This difficulty arises from the range of scales present within turbulent flows. Scaling arguments made by Kolmogorov reason that the smallest motions of turbulent flows decrease in both length and timescale as the Reynolds number increases (Pope, 2000). The Reynolds number dependence for the range of scales is represented by:

$$\frac{\eta}{l_o} \sim \text{Re}^{-3/4} \tag{5}$$

where η is the Kolmogorov scale, which is the smallest mean dissipative scale in the flow, and l_o is the turbulent mixing length, which is an approximation of the largest scale in the flow. Scaling relations shown in Equation 5 result from reasoning provided in Kolmogorov's hypotheses, which suggest that energy is produced at larger scales and dissipated at the smallest scales. If this line of reasoning is correct, then the smallest scales of the flow have to be modeled

in order to successfully capture the physics of the flow. If these scales are not resolved, then conservation of energy will not be obtainable and the results will be meaningless (Pope, 2000). Hence for a three dimensional domain the number of cells required for a complete simulation is proportional to $Re^{9/4}$. This limitation is just one of many that makes modeling turbulent flows a significant challenge.

Numerical solution of the Navier-Stokes equations also proves a difficult and expensive task because they are non-linear and exhibit hyperbolic, parabolic, and elliptic characteristics. Non-linearity can be dealt with by using a staggered grid, but parabolic and hyperbolic characteristics result in strict stability requirements for explicit methods. As a result, semi-implicit methods are more common and large systems have to be solved at each time step. Elliptic properties of the pressure increases the cost of simulation because changes in pressure can be felt instantaneously throughout the entire domain and have to be iteratively solved at each time step.

2.6.1 DNS

Direct numerical simulation (DNS) refers to the direct solution of the continuity and Navier-Stokes equations on a finite grid. Full DNS models do not contain a turbulence model, are time dependent, and resolve all scales of the modeled flow (Versteeg & Malalasekra, 2007). The application of DNS is limited to simple problems and low Reynolds number flows due to inherent computational cost. DNS is primarily used by theoretical researchers to attempt and obtain insight about fundamental flow properties and to develop turbulence models. Most DNS systems use higher order spectral methods to obtain solutions (Pope, 2000).

2.6.2 LES

Large eddy simulation (LES) attempts to directly solve the Navier-Stokes equations on a prescribed grid while modeling the motion of sub-grid scales. In other words, LES uses a filtering function to separate larger and smaller scales. Large scales are retained and smaller scales are not resolved, but reconstructed using some sort of model. Finite volume codes solve a time-dependent, space-filtered version of the governing equations that is coupled with a sub-grid-scale stress (SGS) model (Versteeg & Malalasekera, 2007). LES is less computationally expensive than DNS methods, but it still requires larger run times than traditional averaging models (RANS models). Advances in the availability of processing power have increased the use of LES in the solution of practical problems, but it is not widely used in industry.

2.6.3 RANS

The overwhelming range of scales within turbulent flows and the chaotic behavior of turbulent velocity have led to consideration of a statistical approach to modeling turbulence. This approach uses a concept known as Reynolds decomposition. Reynolds decomposition assumes that instantaneous flow quantities can be "decomposed" into average and fluctuating components:

$$u_i(t) = \bar{u}_i + u_i' \tag{6}$$

$$p(t) = \bar{p} + p' \tag{7}$$

where $u_i(t)$ and $p(t)$ are the instantaneous velocity and pressure, $\bar{u}_i$ and $\bar{p}$ are the average velocity and pressure, and u_i' and p' are the fluctuating components of the velocity and pressure.

Applying Reynolds decomposition to the continuity and Navier-Stokes equation yields Equations 8 and 9 respectively, which are known as the Reynolds equations. The averaged

Navier-Stokes equations by themselves are known as the Reynolds averaged Navier-Stokes (RANS) equations.

$$\frac{\partial \bar{u}_i}{\partial x_i} = 0 \tag{8}$$

$$\frac{\partial \bar{u}_i}{\partial t} + \bar{u}_j \frac{\partial \bar{u}_i}{\partial x_j} = \frac{1}{\rho_o}\frac{\partial \bar{p}}{\partial x_i} + \frac{\partial}{\partial x_j}\left(\nu \frac{\partial \bar{u}_i}{\partial x_j} - \overline{u_i' u_j'}\right) \tag{9}$$

The Reynolds equations appear identical to their un-averaged counterparts with the exception of an additional second-order tensor, $\overline{u_i' u_j'}$, whose terms are known as the Reynolds stresses. Representing the covariance of velocity fluctuations, the Reynolds stresses turn the Reynolds equations into an indeterminate system with six degrees of freedom. Determination of the Reynolds stresses defines what is classically known as the closure problem (Pope, 2000).

One of the most common approaches used to model the Reynolds stresses involves the use of the turbulent-viscosity hypothesis. Introduced by Boussinesq in 1877, the turbulent-viscosity hypothesis assumes that the deviatoric Reynolds stress is proportional to the mean rate of strain, which is analogous to the stress-rate-of-strain relation for a Newtonian fluid (Pope, 2000). The turbulent-viscosity hypothesis is mathematically represented as

$$\overline{u_i' u_j'} = \frac{2}{3}k\delta_{ij} - \nu_t\left(\frac{\partial \bar{u}_i}{\partial x_i} + \frac{\partial \bar{u}_j}{\partial x_j}\right), \tag{10}$$

where ν_t is the turbulent eddy viscosity. The only unknown value in Equation 10 is ν_t. By using the turbulent-viscosity hypothesis, the degree of indeterminacy for the Reynolds equations is reduced from six to one. A number of turbulence models have been developed to prescribe ν_t, which include zero and two equation models.

2.6.4 RNG k-ε Model

The Re-Normalization Group (RNG) k-ε model was developed by Yakhot & Orszag in 1986 using a variety of statistical methods. The RNG k-ε model belongs to a group of turbulence models known as two-equation models. Two equation turbulence models solve two additional partial differential equations (PDEs) in addition to the Reynolds equations in order to prescribe ν_t. For the RNG k-ε model, these additional PDEs are transport equations for the turbulent kinetic energy (k) and the turbulent kinetic energy dissipation (ε). The turbulent kinetic energy is defined as

$$k = \frac{1}{2}\left(\overline{u_1'^2} + \overline{u_2'^2} + \overline{u_3'^2}\right) \tag{11}$$

Other two equation models include the standard k-ε turbulence model and the shear stress transport (SST) k-ω turbulence model (Versteeg & Malalasekera, 2007). All modeling studies performed for this thesis used the RNG k-ε model to prescribe ν_t based on its ability to handle swirling and low Reynolds number flows (ANSYS, 2010; Yakhot & Orszag, 1986). Transport equations for the RNG k-ε model are outlined below where Equation 12 is the modeled k equation and Equation 13 is the modeled ε equation (ANSYS, 2010).

$$\frac{\partial}{\partial t}(\rho k) + \frac{\partial}{\partial x_i}(\rho k u_i) = \frac{\partial}{\partial x_j}\left(a_k \mu_{eff}\frac{\partial k}{\partial x_j}\right) + G_k + G_b - \rho\varepsilon + S_K \tag{12}$$

$$\frac{\partial}{\partial t}(\rho\varepsilon) + \frac{\partial}{\partial x_i}(\rho\varepsilon u_i) = \frac{\partial}{\partial x_j}\left(a_\varepsilon \mu_{eff}\frac{\partial\varepsilon}{\partial x_j}\right) + C_1\frac{\varepsilon}{k}(G_K + C_{3\varepsilon}G_b) - C_2^*\rho\frac{\varepsilon^2}{k} \tag{13}$$

Where

$$C_{2\varepsilon}^* = C_{2\varepsilon} + \frac{C_\mu \eta^3(1 - \eta/\eta_0)}{1 + \beta\eta^3} \tag{14}$$

and

$$v_t = C_\mu \frac{k^2}{\varepsilon} \qquad (15)$$

With related constants being:

$$C_\mu = 0.0845, a_k = a_\varepsilon \approx 1.393, \eta = \frac{Sk}{\varepsilon}, \eta_0 = 4.38, \beta = 0.012, C_{1\varepsilon} = 1.42, C_{2\varepsilon} = 1.68 \qquad (16)$$

G_k is a term that accounts for generation of k from mean velocity gradients, G_b accounts for generation of k through buoyancy, and S_k and S_ε are user-defined source terms (ANSYS, 2010).

2.7 Modeling Scalar Transport

RTD curves were obtained from simulations by modeling a disinfectant as a passive conservative scalar. A passive conservative scalar is an unreactive species that does not have any influence on the existing flow field. Hence chemical and biological reactions of the disinfectant were not considered (due to relatively small retention times of modeled systems). The Reynolds averaged equation for a conservative passive scalar can be written as:

$$\frac{\partial C}{\partial t} + \bar{u}_j \frac{\partial C}{\partial x_j} = \frac{\partial}{\partial x_i}\left(\left(\kappa + \frac{v_t}{Sc_t}\right)\frac{\partial C}{\partial x_i}\right), \qquad (17)$$

where C is the average tracer concentration, κ is the molecular diffusivity of the tracer, and Sc_t is the turbulent Schmidt number. This formulation uses the gradient diffusion hypothesis, which assumes that transport occurs down the mean scalar gradient (Pope, 2000). Use of the gradient diffusion hypothesis models the scalar flux as

$$\overline{u_j' C'} = -\kappa_t \frac{\partial C}{\partial x_j} \qquad (18)$$

where k_t is the turbulent diffusivity and can be recast as

$$k_t = \frac{v_t}{Sc_t} \qquad (19)$$

Substitution of Equations 18 and 19 into the original transport equation for a passive scalar yields Equation 17. The turbulent Schmidt number was taken as 0.7, which is a generally accepted value for neutrally stratified flows (Venayagamoorthy & Stretch 2010).

2.8 Commercial Software

A number of different software packages are available for pre-processing, developing, running, and post processing computational models. Commercial CFD codes include but are not limited to COMSOL, CFX, FLUENT, FLOW-3D, STAR-CD, PHOENICS, and OpenFOAM (Versteeg & Malalasekera). OpenFOAM is an open source code that has been growing in popularity due to its transparency and customizability. OpenFOAM does not contain standard graphical user interface (GUI) modules and is mainly text based, so it is more difficult to use than other packages. Other packages, such as FLUENT and FLOW-3D, contain extensively developed GUIs and organized structures. However, industrial CFD packages require expensive licenses and offer limited amounts of customization. All of these codes have been thoroughly tested and applied in industry, but each contains its own strengths and weaknesses.

ANSYS FLUENT v.13.0.0 was used exclusively for all CFD computations and partially for all post processing procedures. FLUENT was chosen for its proven robustness, adaptive meshing abilities, and support for user defined functions. FLUENT has also been validated for modeling scalar transport within disinfection contact tanks (Wilson & Venayagamoorthy, 2010; Wilson, 2011; Taylor, 2012; Barnett, 2013; Barnet *et al*, 2014). Imbedded geometry and meshing software in ANSYS workbench v.13.0.0 were used to create and mesh all simulation geometries.

2.8.1 ANSYS Workbench

ANSYS Workbench is a sophisticated GUI that provides access to a number of different programs. Workbench references and passes data in-between software packages that can model

multiphysics, structural analysis, fluid flow, and a number of other phenomena. Workbench is capable of importing geometric files from industrial CAD packages such as SolidWorks or AutoCAD, but an integrated package labeled ANSYS DesignModeler was used to create the geometry for each simulation. Creation of geometry within Workbench avoids continuity errors like missing facets or inadequately defined edges, which can occur with imported geometry. After geometry was created, it was discretized using ANSYS Meshing, which is another program inside Workbench. ANSYS Meshing automatically fits an un-structured mesh to a given geometry using a wide range of settings, tools, and local controls. All meshes are body fitted and can implement tetrahedral, hexahedral, polyhedral, pyramid, wedge, or cut (rectangular) cells. This means that the input geometry is preserved in FLUENT. Other software packages, such as FLOW-3D, use structured meshes where the resolution of geometry is mesh dependent. All of the meshes used in simulations for this thesis were cutcell meshes. Reasoning for this decision is presented in Chapter 3.

2.8.2 ANSYS FLUENT

ANSYS FLUENT is a commercial CFD code that implements the finite-volume method. Use of the finite-volume method involves integration of governing equations over discrete control volumes. Therefore, imposing a computational "mesh" over a given domain divides that domain into a series of interacting volumes. By taking an integral approach, the finite-volume method guarantees conservation of mass for fluid flows, which is not guaranteed under other methods like the finite-difference or finite-element methods. In addition to guarantying conservation of mass, FLUENT guarantees preservation of geometry through the use of unstructured meshes. FLUENT also allows for the use of user-defined functions, which can be

written in the C computing language. These aspects make FLUENT an attractive CFD package for modeling scalar transport.

2.8.2.1 Numerical Solvers

FLUENT's pressure-based segregated solver was used to numerically approximate the RANS and averaged scalar transport equations. This algorithm belongs to a general class of methods known as the projection method (Chorin, 1968). The pressure-based segregated solver decouples the governing equations and iteratively solves for each variable until resulting residuals fall below some specified tolerance. FLUENT's user manual states that this method applies a pressure correction, which can be formulated using a variety of methods. A flow chart of FLUENT's pressure-based segregated algorithm can be seen in Figure 2.4.
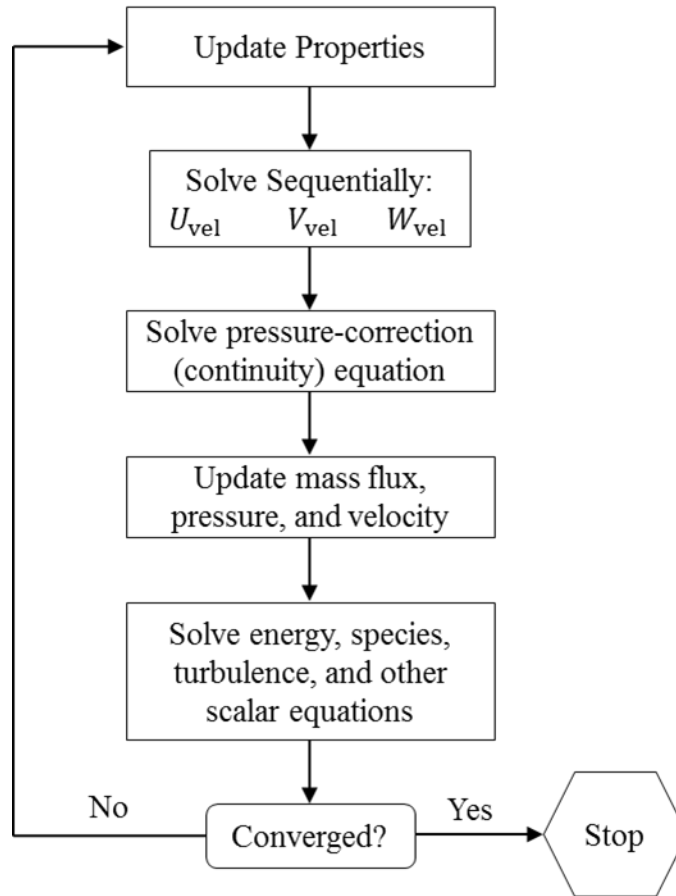
Figure 2.4: Flow Chart Outlining FLUENT's Pressure-based Segregated Algorithm (ANSYS, 2010)

FLUENT also has a pressure-based coupled algorithm, which couples the momentum and pressure-based continuity equations. This method runs faster than the decoupled method because it converges faster, but it uses almost twice the memory because it stores larger systems. The segregated algorithm was chosen for use in this study to conserve memory.

FLUENT offers several pressure-velocity coupling algorithms for use in its solver. Options include SIMPLE, SIMPLEC, PISO, Fractional Step, and Coupled methods. The SIMPLE, or Semi-Implicit Method for Pressure-Linked Equations, algorithm was used for

pressure-velocity coupling within the simulations of this thesis. The SIMPLE algorithm can be simply described using four generic steps:

1. Gradients of the velocity and pressure are determined from values at the previous time step. (FLUENT uses a co-located scheme, so both the velocity and pressure are stored at cell centers. Pressure is interpolated to cell faces using momentum equation coefficients and velocity is interpolated using momentum weighted averaging).

2. An intermediate velocity field is then obtained through the solution of the discretized momentum equations with an "approximated" pressure.

3. A postulated flux correction based off of pressure corrections is inserted into the discrete continuity equation to create a pressure correction equation. This equation is iteratively solved using the Algebraic Multigrid method.

4. The pressure is corrected and resulting changes in the velocity field are determined, forming a new set of fluxes which satisfy continuity.

Spatially varying convective terms were discretized using a first-order upwind scheme. This scheme simply assumes that the face value of a quantity is the same as the cell-center value of an upstream cell. This simplistic method has been validated for use in modeling the transport of a passive scalar (Taylor, 2012; Barnett, 2013). Diffusive terms are discretized using a central difference scheme, which is second order accurate.

Spatial gradients were evaluated using the least squares cell-based gradient evaluation method. Given the scenario shown in Figure 2.5, the change in cell values between $c0$ and ci along the vector δr can be represented as:

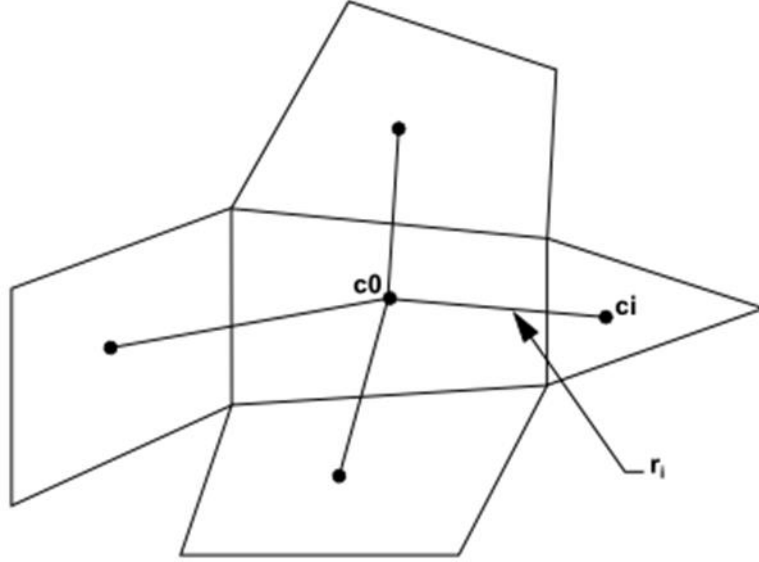$$(\nabla \phi)_{c0} \cdot r = (\phi_{ci} - \phi_{c0}),$$

(20)

Figure 2.5: Cell Centroid Evaluation Example (ANSYS, 2010)

where $(\nabla \phi)_{c0}$ is the cell gradient of the current cell, r_i is the displacement vector from the upstream cell centroid to the face centroid, and ϕ_{ci} and ϕ_{c0} are cell centered values. This formulation assumes that the solution varies linearly. If similar expressions are written for each surrounding cell near $c0$ an over-determined linear system is obtained:

$$[J](\nabla \phi)_{c0} = \Delta \phi \tag{21}$$

where $[J]$ is a coefficient matrix obtained from geometry. Decomposing $[J]$ using the Gram-Schmidt process yields a matrix of weighting factors for each cell. The gradient for the given cell can be obtained by multiplying respective weighting factors by each difference vector and summing the results. The least squares cell-based method refers to this process in its entirety (ANSYS, 2010).

A first order implicit scheme was used to facilitate time advancement. Known as backward Euler, this scheme approximates integration of a temporal derivative as follows:

$$\phi^{n+1} = \phi^n + \Delta t F(\phi^{n+1}) \tag{22}$$

where ϕ is some scalar and $F(\phi^{n+1})$ is some function of the scalar at a future time step (discretized versions of spatial gradients). The use of a fully implicit method allows for the stability of the solution to be independent of the chosen time step. FLUENT uses multigrid methods in the solution of linear systems that develop from implicit methods. These methods include algebraic multigrid (AMG) and full-approximation storage (FAS) (ANSYS, 2010).

2.8.2.2 Wall Functions

Modeling of near wall turbulence within wall bounded flows is one of the most important and difficult parts of any CFD simulation. The existence of a no-slip condition on walled surfaces results in significant velocity gradients and intensive shear. Therefore, walls are a major source of vorticity and turbulence, which means that the majority of turbulent kinetic energy production happens near the wall. This means that incorrect modeling of flows near walls affects the entire simulation and can lead to erroneous results (Pope, 2000).

Experiments have shown that the near-wall region can be divided into three different sections or layers. The region closest to the wall is dominated by viscous forces and is almost laminar in its behavior. This region is known as the viscous sublayer. At the end of the viscous sublayer there is a transitional region known as the buffer layer where the dominance of viscosity slowly gives way to the effects of turbulence. Beyond the buffer layer the flow is dominated by turbulence in a layer known as the fully turbulent region. The extent of each of these layers can be described using a dimensionless wall unit, y^+, which is defined as

$$y^+ = \frac{u_\tau y}{\nu},$$

(23)

where u_τ is the friction velocity ($\sqrt{\tau_w/\rho}$), τ_w is the wall shear stress, y is the distance from the wall, ρ is the fluid density, and ν is the kinematic viscosity (Pope, 2000). The viscous sublayer

exists in the region $y^+ < 5$, the buffer layer exists in the region $5 \leq y^+ \leq 50$, and the fully turbulent region exists in the region $y^+ > 50$.

Wall functions within FLUENT use an alternate dimensionless parameter known as y^* to handle near-wall treatment of flows. The parameter y^* is defined as

$$y^* = \frac{C_\mu^{1/4} k_P^{1/2} y_P}{\nu} \tag{24}$$

where k_P is the turbulent kinetic energy at the near-wall node P and y_P is the distance from the wall to the node P. The standard wall function applies the log-law when $y^* > 11$ and applies a viscous stress relationship when $y^* < 11$, which means that near-wall cells are generally assumed to be in the outer turbulent region. FLUENT's enhanced wall functions assume that near wall flow is within the viscous sublayer and applies more detailed equations for the formulation of the boundary layer. If y^* is too large, FLUENT will revert to standard wall functions. y^+ values for near wall cells should be less than 5 to use the enhanced wall functions. For the standard wall functions the first cell should ideally satisfy $30 \leq y^+ \leq 60$, but the log-law approximation can be applicable for y^+ up to 1,000 for high Reynolds number flows (ANSYS, 2010; Pope, 2000).

2.8.2.3 Study Methodology

Rigid lid models were used for all 49 CFD simulations in order to limit computational cost. Free surface elevation was estimated for all simulations from measurements in a corresponding prototype. Boundary conditions were defined for all simulations as follows: velocity inlet, pressure outlet, standard no slip walls, and symmetry rigid lid. Default solver options were selected and shown to be adequate through experimental validation. Each simulation was run towards convergence using the steady state solver. Resulting flow fields were then run without the presence of a passive conservative tracer for one TDT using transient

solvers. After this, a non-dimensional scalar concentration of 1.0 was introduced at the inlet and

a monitor was placed at the outlet. Simulations were run until convergence (around 3.5 TDTs).

Scalar transport was modeled with a user-defined diffusivity coefficient as defined

below:

$$\kappa_{eff} = \kappa + \frac{\nu_t}{Sc_t} \tag{25}$$

where κ_{eff} is the effective diffusivity, κ is the molecular diffusivity (taken to be that of water),

and Sc_t is the turbulent Schmidt (or Prandtl) number. A user-defined function was written in the

C programming language to prescribed this diffusivity at each time step (see Appendix A).

CHAPTER 3: PARAMETRIC BAFFLE STUDY

3.1 Introduction

Internal baffling is one of the most widely accepted methods for increasing the hydraulic disinfection efficiency of drinking water contact tanks (USEPA, 2003). The introduction of interior walls within open tanks helps to channelize flow and prevents the formation of dead zones, eddies, and short circuiting. The existence of these turbulent structures creates significant problems for systems that utilize chlorine as a disinfection agent. Chemical transport within recirculating dead zones is dominated by the process of diffusion, which leads to increased residence time and the development of cancerous disinfection byproducts (DBP). Short circuiting poses the opposite problem, reducing local residence times and providing inadequate duration for disinfection. Poorly baffled systems exhibit both of these extremes, resulting in significant hazards regarding public health.

The majority of studies that investigate internal baffling concern tanks with a rectangular foot print, which is one of the most common system designs. Given the inherent complexity of hydraulics within these systems, researchers have relied on physical models and CFD to gain fundamental insight regarding internal baffling. Two of the earliest studies involving CFD were conducted by Wang and Falconer in 1998, which modeled an 1:8 Froude scale model of the Embsay Water Treatment Plant in Yorkshire England. Wang and Falconer validated the use of a 2D depth averaged model through the comparison of velocity profiles and a measured FTC using a variety of numerical methods (Wang & Falconer, 1998). A similar study was conducted by Shiono and Teixeira in 2000, which involved classification of turbulent characteristics within the same scaled model of the Embsay Water Treatment Plant. Shiono and Teixeira used a laser Doppler anemometer to measure velocity fields and classify turbulent characteristics within the

model. These measurements were used to further validate the numerical model of Wang and Falconer (Shiono & Teixeira, 2000). Results from these studies suggested that the use of a two dimensional standard k-ε model could adequately reproduce flow quantities within the later channels of a seven chamber system. Inconsistencies were attributed to the amount of turbulence introduced by the inlet, which was a channel inlet with a width equal to that of the baffle channel. Hence the hydrostatic assumption broke down near the inlet and a three dimensional model would have been required for adequate resolution of flow features.

In 2003 Khan et al developed and validated a three-dimensional CFD model of the scaled Embsay tank studied by Shiono and Teixeira. This 3D model resolved flow patterns within a RANS framework using the standard k-ε turbulence model and modeled disinfectant as a passive conservative scalar. Results from this study provided excellent agreement for both three dimensional velocity fields and resulting FTCs. (Khan *et al*, 2006). Similarly Baawain et al (2006) validated the k-ω turbulence model for predicting FTCs using tracer studies from two existing prototypes (Baawain *et al*, 2006). The standard k-ε model has also been validated for predicting scalar transport by Wilson (2011) and Taylor (2012), and the RNG k-ε model has been validated by Barnett (2013).

Extensive validation of CFD for resolving scalar transport has led to a number of parametric studies involving rectangular baffled systems. In 2007 Wejun et al attempted to quantify resulting effects from the addition of baffles to rectangular systems with sharp inlets. Baffles were varied in number from zero to nine and the baffle length was varied for several systems. However, descriptions of this study fail to describe applied numerical methodology and do not clearly define modeled geometry. Wejun et al claim to have conducted 2D simulations using FLUENT v 6.1, but applied turbulence models and scalar transport methods are not

discussed. The inlet orientation within the studied systems was not described and a grid independence study was not completed. The use of a sharp inlet introduces significant amounts of turbulence and flow separation when compared to a channel inlet, so a two-dimensional model is not adequate for resolving important flow features within the systems studied by Wejun et al (Shiono & Teixeira, 2000). Due to the uncertainties involved in this study, its results must be brought into question (Wejun *et al*, 2007).

More reliable and well documented parametric studies have been performed by Xu (2010), Amini et al (2011), Taylor (2012), and Barnett (2013). Xu investigated the effect of varying the number of baffles within the foot print of the scaled Embsay tank using a 2D model (Xu, 2010). Amini et al reproduced Xu's work using a three-dimensional RANS simulation and investigated the application of an original baffle design (Amini *et al*, 2011). Taylor extensively expanded the work of Amini et al by varying both the number and length of baffles. Taylor also investigated the effects of original dimensionless parameters on disinfection efficiency and designed optimal baffling configurations based on numerical observations (Taylor, 2012). Research conducted by Barnett considered the variation of baffle length and number within a 1500 gallon rectangular tank utilizing a sharp inlet. Barnett investigated similar dimensionless parameters to those described by Taylor (Barnett, 2013).

With the exception of Barnett (2013), all of the previous parametric studies consider tanks with a channelized inlet. In practice, a majority of small systems make use of sharp inlets to reduce cost and allow for integration of contactors into existing pipe networks (USEPA, 2003; Baawain, 2006; Barnett, 2013). Use of a sharp inlet results in the formation of a turbulent jet, promoting larger amounts of flow separation than a channel inlet. Barnett quantified this

difference for baffles placed along the short axis of a tank, but a complete parametric study that considers the placement of baffles parallel to the long axis of a tank is yet to be undertaken.

Research presented in this chapter summarizes the results of 49 different CFD simulations in an attempt to optimize the hydraulic disinfection efficiency of a rectangular contact tank through internal baffling. Complementing the work of Barnett (2013), this study considers placement of baffles parallel to the long axis of a 1500 gallon rectangular tank with a sharp inlet. In addition to optimizing tank performance, this study seeks to quantify the detrimental effects of using a sharp inlet and to display the importance of inlet orientation.

Organization of this chapter is as follows: Section 3.2 outlines applied numerical methodology, Section 3.3 provides a description of the studied system and its modeled counterpart, Section 3.4 validates model results against experimental data and summarizes a grid independence study, Section 3.5 describes the parametric study, Section 3.6 presents parametric study results and accompanying discussion, and Section 3.7 summarizes resulting conclusions.

3.2 Numerical Methodology

The finite-volume code ANSYS FLUENT v 13.0.0 was used to conduct three-dimensional simulations of the studied systems. Imbedded geometry and meshing software in ANSYS workbench v.13.0.0 were used to create and mesh all simulation geometries. All geometries were meshed using an unstructured cutcell mesh with local sizing controls. FLUENT was chosen for its proven robustness, adaptive meshing abilities, and support for user defined functions. Rigid lid models were used for all CFD simulations in order to limit computational cost. Free surface elevation was estimated for all simulations from measurements in a corresponding prototype. Small changes in free surface elevation were shown to have little effect on simulation results.

All simulations were performed in a RANS frame work using the RNG k-ε closure scheme. The RNG k-ε turbulence model was used for its ability to handle swirling and low Reynolds number flows (ANSYS, 2010; Yakhot & Orzag, 1986). Disinfectant was modeled as a passive conservative scalar using the relationship shown in Equation 26:

$$\frac{\partial C}{\partial t} + \bar{u}_j \frac{\partial C}{\partial x_j} = \frac{\partial}{\partial x_i}\left(\left(\kappa + \frac{v_t}{Sc_t}\right)\frac{\partial C}{\partial x_i}\right), \tag{26}$$

where C is the average tracer concentration, κ is the molecular diffusivity of the tracer, and Sc_t is the turbulent Schmidt number, which was taken as 0.7 (See Venayagamoorthy & Stretch, 2010 for justification).

Boundary conditions were defined for all simulations as follows: velocity inlet, pressure outlet, standard no slip walls, and symmetry rigid lid. Default solver options were selected and shown to be adequate through experimental validation (see Section 3.4). This means that a pressure-based segregated solver was used and that the SIMPLE algorithm was used to couple velocity and pressure. Spatial quantities were interpolated using a first-order upwind scheme and temporal derivatives were discretized using backward or implicit Euler. Spatial gradients were approximated using the least-squares based gradient method. Standard wall functions were used due to difficulties associated with resulting y^+ values. Resulting y^+ values for near wall cells varied between 0.4 and 270 for the modeled resolution. Use of enhanced wall functions would adequately model the lower end of this range but would misappropriate shear for the upper end. Average y^+ values were within an appropriate range for standard wall functions.

Each simulation was initially run towards convergence using the steady state solver. Resulting flow fields were then run without the presence of a conservative tracer for one TDT using transient solvers. After this a non-dimensional scalar concentration of 1.0 was introduced at the inlet and a monitor was placed at the outlet. Simulations were run until convergence,

which was defined by minimal changes in scalar concentration at the outlet (around 3.5 TDTs). The intermediate running of transient solutions before the introduction of conservative tracer was deemed necessary in order to bring solutions into a quasi-steady state. Average velocities within the tank would not stabilize until the transient solver was run for around one TDT. An example of this can be seen in Figure 3.1.
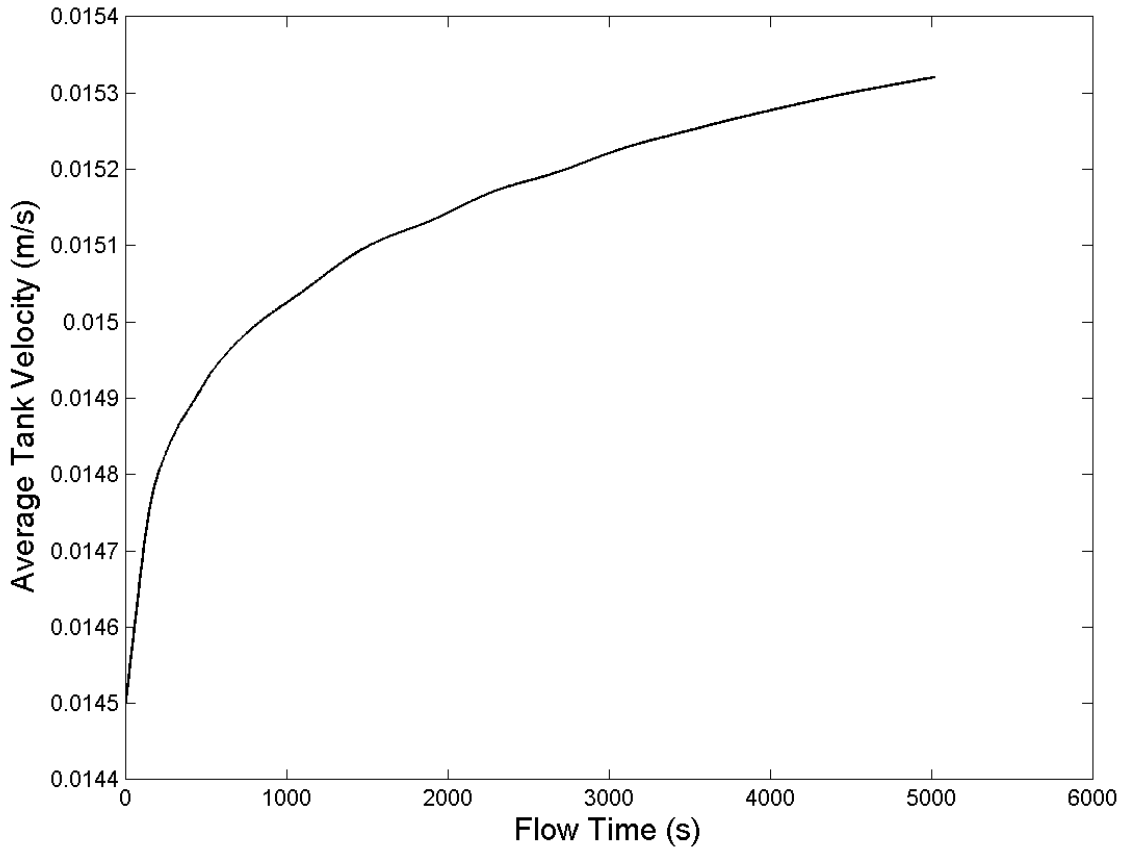

Figure 3.1: Example of Average Velocity Magnitude Convergence for an Arbitrary System

3.3 Tank Geometry and System Description

The rectangular concrete tank shown in Figure 3.2(a) served as a base system for the entire study. Built from 6" reinforced concrete, this tank currently resides at Colorado State University's (CSU) Engineering Research Center (ERC). As shown in Figure 3.2(b), the tank interior is 4 feet wide, 11 feet long, and 6 feet deep. Fluid enters at the bottom of the tank

through a 2" inlet and exits at the top through a 4" outlet. At a flow rate of 20 gallons per minute (GPM) the tank has an approximate volume of 1500 gallons and a depth of 5.23 ft.
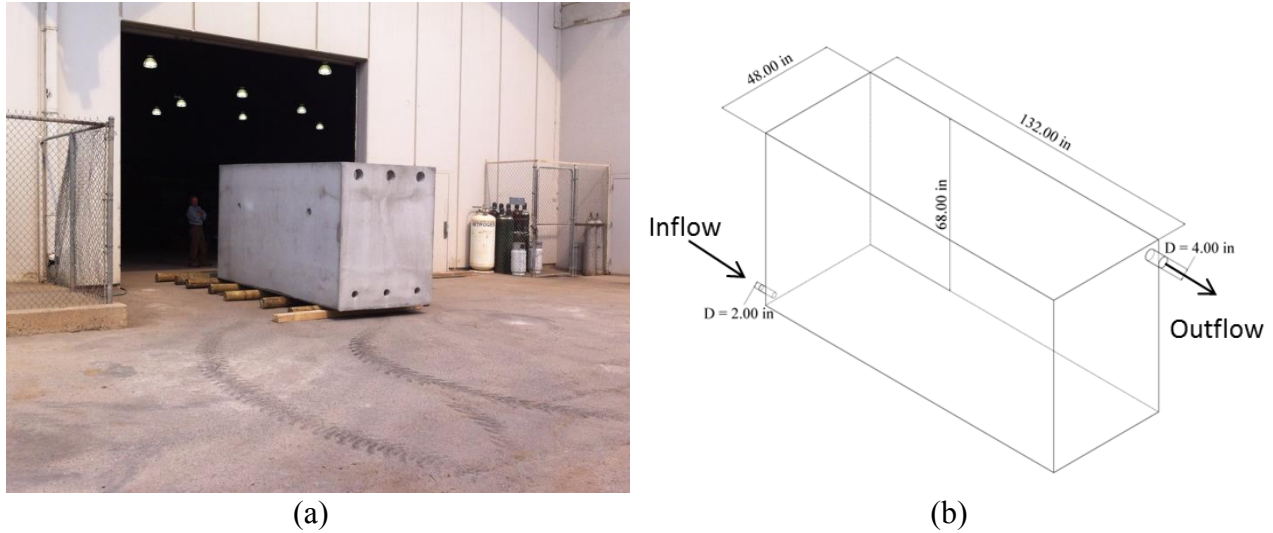

<div align="center">(a)   (b)</div>

Figure 3.2: (a) Photograph of 1500 Gallon Prototype, (b) Interior Volume of 1500 Gallon Prototype

Digitized geometry shown in Figure 3.2(b) was vertically truncated using Boolean operations in order to account for the free-surface level.

      The base system outlined in Figure 3.2(a) and (b) is representative of a number of existing disinfection contactors. These concrete tanks are relatively inexpensive and can be designed to fit a variety of plumbing configurations. The physical prototype used in this thesis was set up so that a number of different inlet and outlet configurations could be achieved. Three 2" inlets were placed on the bottom of each side of the tank and three 4" outlets were placed at the top of each side of the tank. This was done to allow for the potential installation of different baffle configurations. Without any modification rectangular tanks like the base system perform poorly, obtaining BF values of 0.1.

3.4 CFD Model Validation

Two separate scenarios were physically constructed and tested within the prototype in order to validate the applied numerical methodology. One scenario considered the base case shown in Figure 3.2(a) and (b) at a flow rate of 20 GPM. For the second scenario the base system shown in Figure 3.2(a) and (b) was modified using internal baffling. A total of two baffles were used to limit cost and allow for ease of construction. Baffles were constructed using 48" X 74" X ¾" treated plywood sheets. Before baffles were installed, 1" X 4" wooden planks were fastened around the perimeter of the tank bottom and around the tank rim. These wooden frames were attached using a hammer drill and 2" bolts. Two 2" X 4" wooden planks were attached to each frame to facilitate baffle placement. Baffles were attached to these guide planks using wood screws and resulting gaps were filled with water tight silicon. Baffle orientation, spacing, and length were selected based off of recommendations from previous studies (Taylor, 2012; Barnett, 2013). Figure 3.3(a) shows a plan-view schematic of the baffled system and Figure 3.3(b) shows the fully constructed prototype.
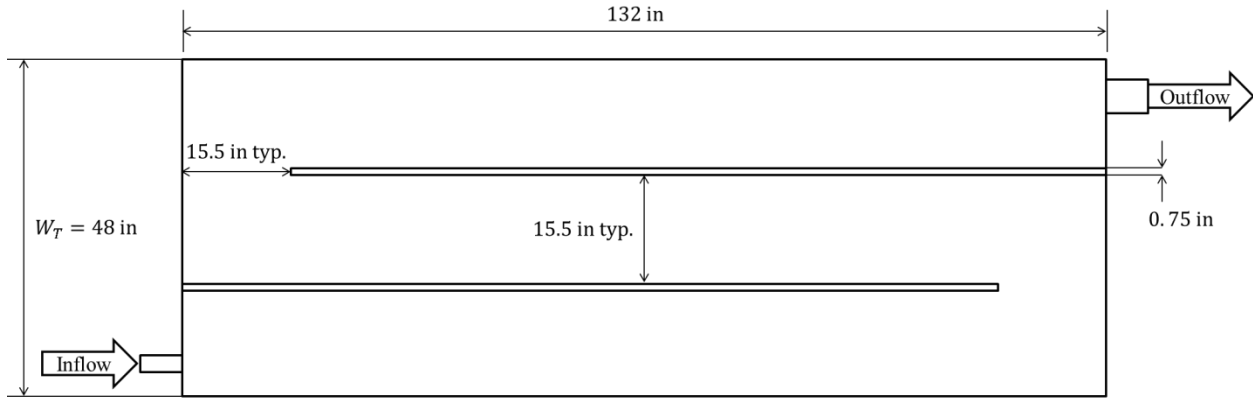
(a)

(b)

Figure 3.3: (a) Geometric Plan View of Two Baffle System and (b) Corresponding Physical Prototype

3.4.1 Tracer Study Results

Step-wise tracer studies were performed on system prototypes to quantify hydraulic disinfection efficiency. Both the base system and the two baffle system were investigated using sodium-chloride as a conservative tracer. One of these studies was redone using lithium-chloride solution in order to further validate applied methodology. Lithium-chloride is generally considered a more accurate tracer than conductivity due to the existence of low background levels in un-modified influent and the ability of methods to accurately detect small concentrations. Using lower tracer concentrations reduces the risk of introducing buoyancy

43

effects and violating the assumption of a passive scalar. Tests were conducted a minimum of two times in order to ensure consistency. Prior to testing, solution was mixed in a plastic container with the use of an electric paint mixer. Solution was then injected into the main flow using a constant displacement pump and integrated via a static mixing tube. The concentration of sodium-chloride solution was selected to increase the conductivity of the existing system between 50-100 $\mu S/cm$. Similarly, the concentration of lithium-chloride solution was selected so that the maximum observed concentration would be around 0.4 mg/l, which is an MCL drinking water standard. During sodium chloride testing conductivity was monitored at the outlet in a fabricated flow through device using a YSI EcoSense EC300A conductivity meter, which was calibrated using manufacturer specifications (see Appendix B). For tests using lithium chloride, samples were taken at predetermined time intervals using a tap (at the same location as the flow through device). All lithium samples were analyzed in the Soil, Water, and Plant testing laboratory at CSU using inductively coupled plasma-atomic emission spectroscopy. Photographs of testing equipment can be seen in Figure 3.4(a-d).
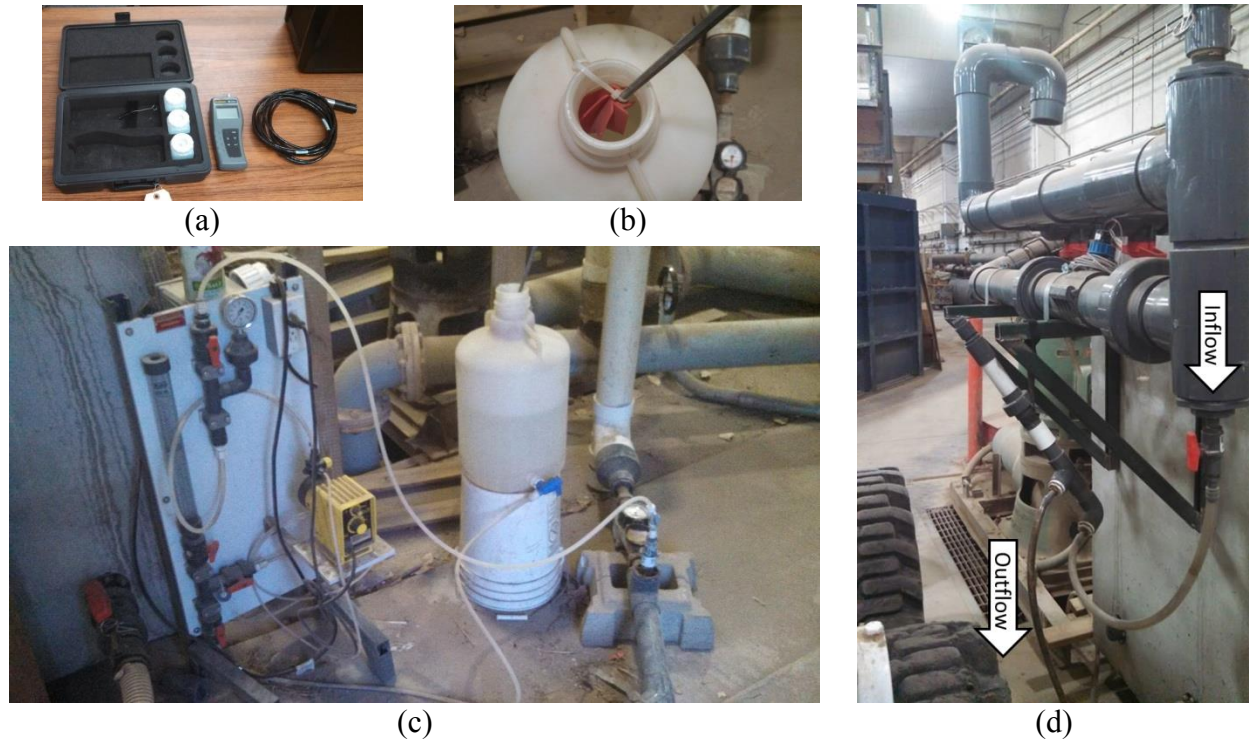
Figure 3.4: Photographs of the (a) EC300A Conductivity Meter, (b) Paint Mixer, (c) Constant Displacement Pump and Injection System, and (d) Fabricated Flow through Cell

Experimental results from physical tracer studies were compared against numerically derived RTD curves. Figure 3.5(a) and (b) show comparisons of resulting RTD curves for the base and two baffle systems respectively. For both cases CFD model, lithium tracer, and sodium chloride tracer results varied by less than 1% of C_{max} within the region of interest (t_{10}) and less than 5% of C_{max} overall, validating applied methodology. Results suggest that the base system exhibited a baffling factor of 0.05 and that the baffled system exhibited a baffling factor of 0.35.
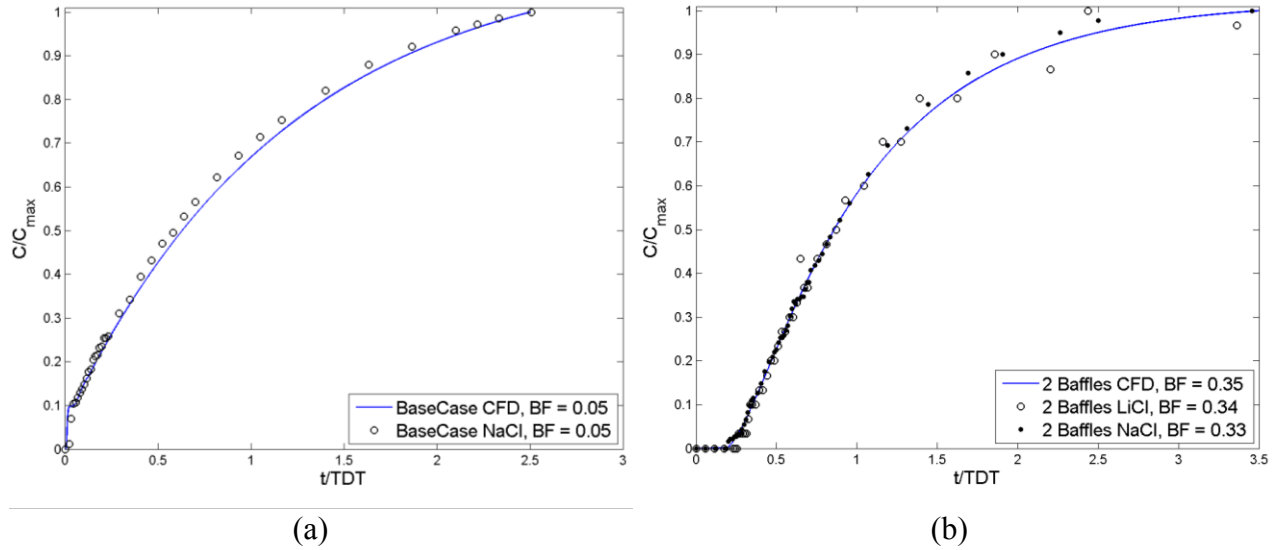
(a)	(b)

Figure 3.5: Comparison of CFD and Physical Tracer Results for the (a) Base System and the (b) Two Baffle System

Additional tracer studies were conducted within the baffled system at 40 GPM to determine if resulting disinfection efficiencies were dependent on flow rate. Doubling the flow rate resulted in negligible changes regarding scalar transport, as shown in Figure 3.6. Similar results have been discovered by Taylor (2012) and Barnett (2013). Based on this observation, remaining CFD simulations were conducted at 20 GPM and effects of flow rate were not investigated further. Barnett (2013) showed that at lower flow rates (5 GPM) disinfection systems could enter the laminar flow regime and lose contact volume. These effects were not considered or investigated in the current study under the assumption that this range of flows was unlikely to occur in practice for systems like the studied prototype (systems with poorly oriented sharp inlets).
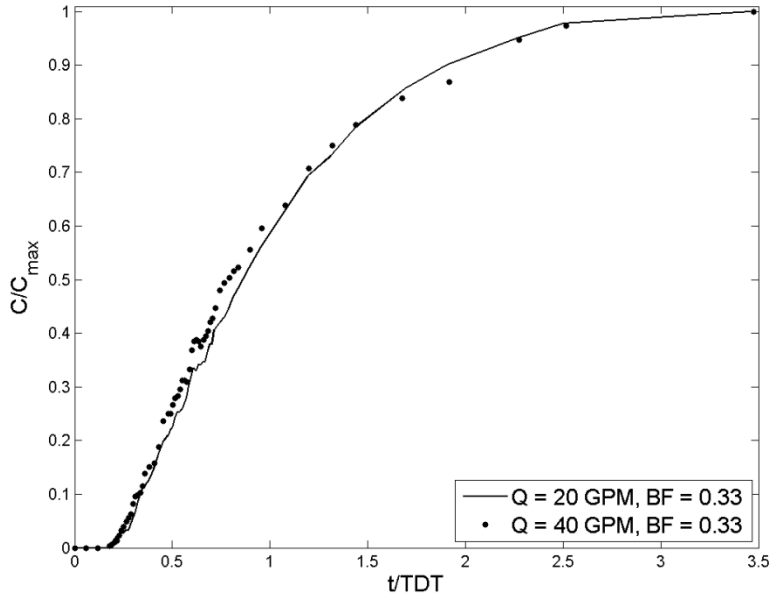
Figure 3.6: RTD Curves for the Two Baffle System at Various Flow Rates

3.4.2 Grid Independence Study

Two different types of spatial grids were initially investigated for discretization of system geometry. The first set of tested grids applied the use of tetrahedral cells while the second set used rectangular cells or cutcells. In total four different tetrahedral meshes and seven different cutcell meshes were tested for resolving the baffled system shown in Figure 3.3(a) and (b). Optimal grid generation settings were then used to develop tetrahedral and cutcell meshes for the base system shown in Figure 3.2(a) and (b).

The coarsest tetrahedral mesh contained approximately 460,000 cells while the finest tetrahedral mesh contained approximately 890,000 cells. Increasing the resolution of the tetrahedral mesh caused the baffling factor of the baffled system to converge on a value of 0.23, yielding a reasonable amount of error when compared to experimental results (See Figure 3.7). Error increased with resolution and iterative solutions did not readily converge for each time step, suggesting the presence of systematic flaws and issues regarding mesh quality. Review of resulting velocity profiles suggested excess diffusion of momentum and poor resolution near the

47

boundaries of flow features, which are both numerical artifacts (See Figure 3.8(a) and (b)). These artifacts can be attributed to inappropriate values of orthogonal quality and skewness within the mesh. Due to the rectangular nature of the system, flow within each channel is predominantly in the lengthwise direction. Unlike rectangular cells, tetrahedral cells do not directly line up with the predominant direction of flow and volumes are not always perpendicular to each-other. These geometric inconsistencies introduce numerical physics that result from spatial interpolation schemes. Therefore, in order for a tetrahedral mesh to perform as well as a cutcell mesh, higher order methods would have to be used, which increases computational cost.
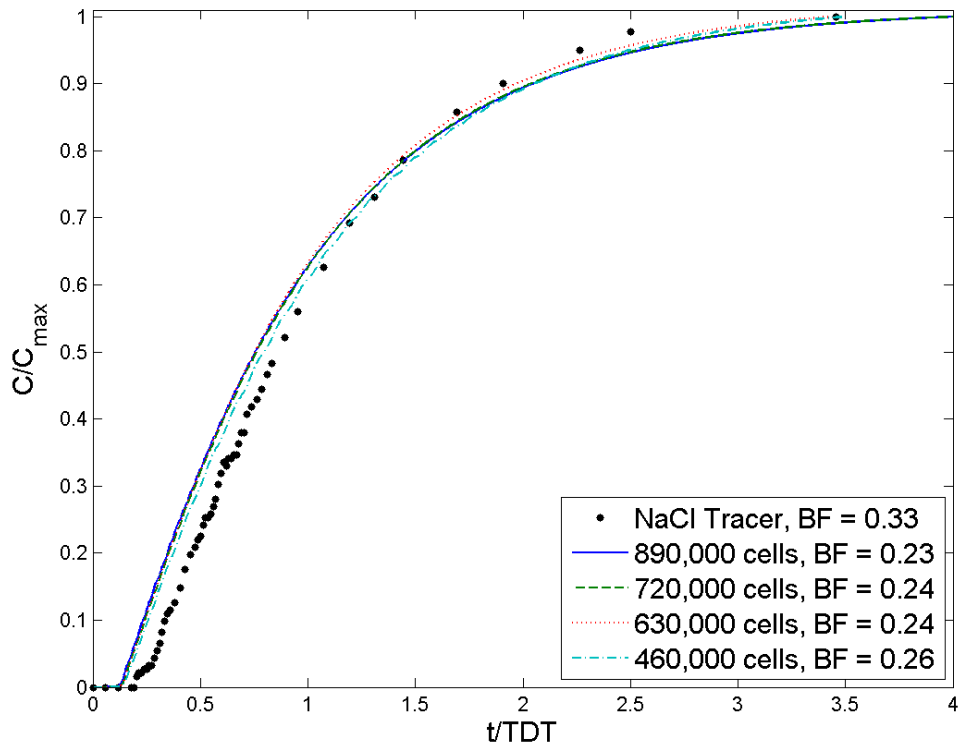

Figure 3.7: Resulting RTD Curves from using Tetrahedral Meshes to Resolve a Two Baffle System
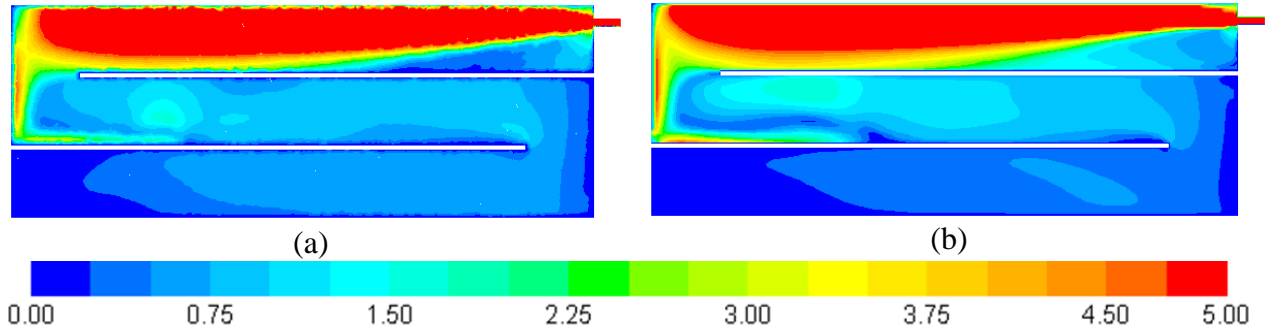
Figure 3.8: Contours of Normalized Velocity (V/V_{average}) at the inlet for a Two Baffle System using a (a) Tetraheydral Mesh and a (b) Cutcell Mesh using $\Delta t = 2\mathbf{s}$.

The coarsest cutcell mesh contained around 350,000 cells and the finest mesh contained approximately 1,600,000 cells. One mesh containing 1,000,000 cells was modified with the use of controlled inflation around the exterior of the tank wall. Effective inflation was difficult to implement without overall grid refinement due to resulting increases in cell aspect ratios, which caused instability. Increasing mesh resolution resulted in convergence of the solution towards experimental results. Discrepancies between experimental and numerical RTD curves can be attributed to experimental error (see Appendix C) and inaccurate modeling of near wall turbulence. Examples of different meshes can be seen in Figure 3.9(a-c) and resulting RTD curves can be seen in Figure 3.10. All simulations were run with a time step of $\Delta t = 2s$.
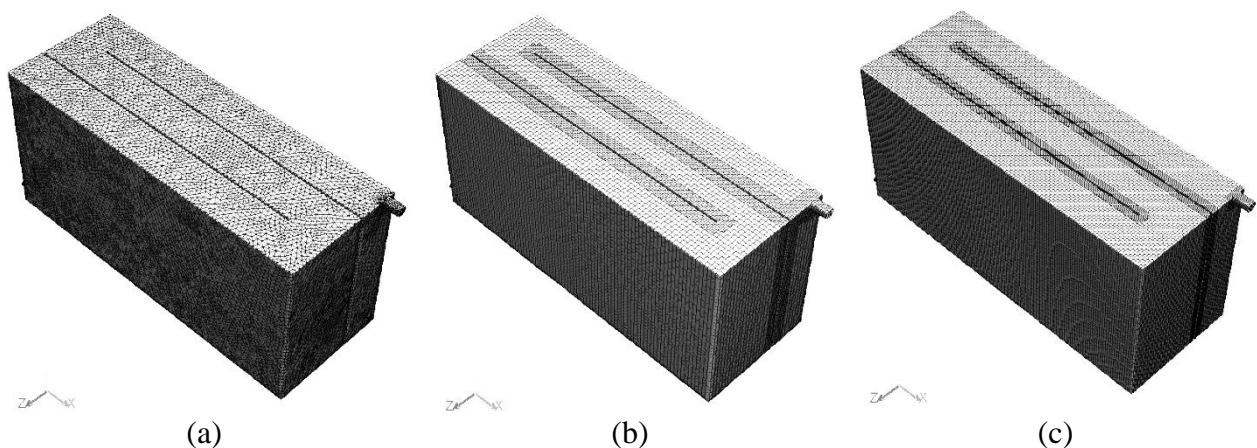

Figure 3.9: (a) 860,000 Cell Tetrahedral Mesh, (b) 350,000 Cell Cutcell Mesh, and (c) 1,000,000 Cell Cutcell Mesh

49
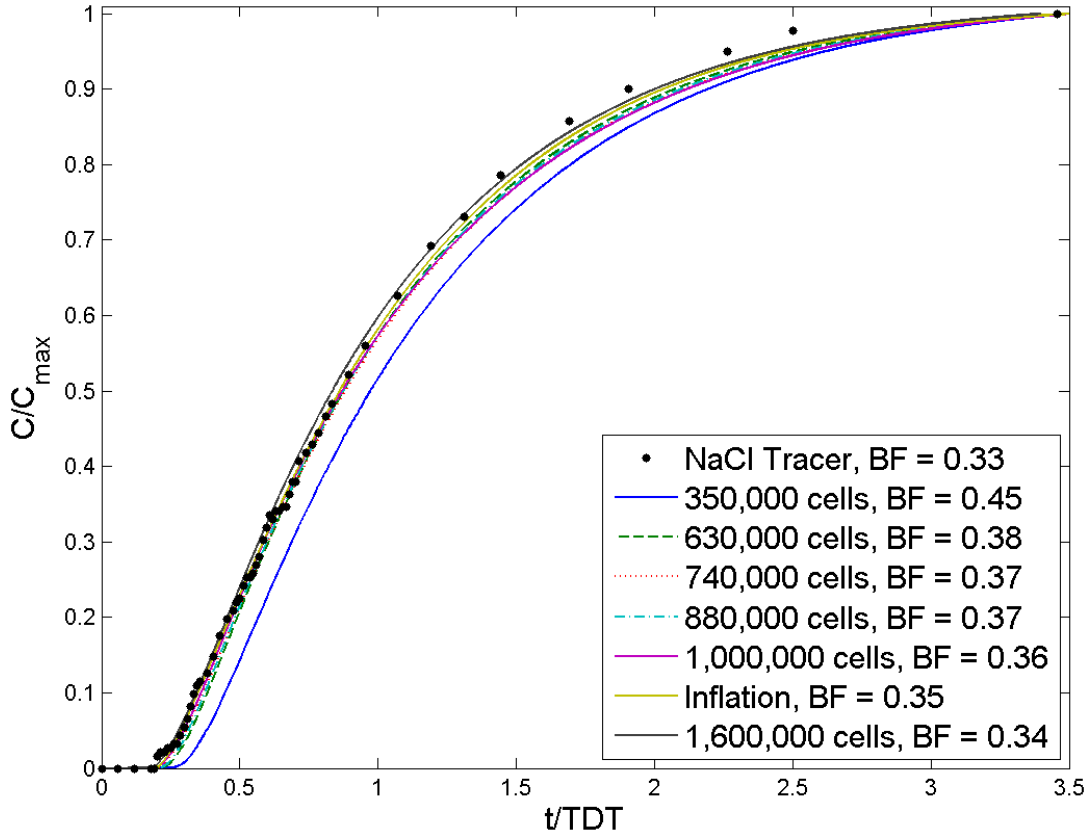
Figure 3.10: Resulting RTD Curves from using Cutcell Meshes to Resolve a Two Baffle System

Application of tetrahedral and cutcell meshes in the approximation of scalar transport within the base system yielded similar results to the two baffle system. Tetrahedral meshes did not readily converge and showed signs of numerically induced physics in the form of oscillating RTD curves. On the other hand, cutcell meshes converged at each time step in three iterations or less and matched experimental data. Figure 3.11 exemplifies these observations. It was therefore decided that cutcell meshes would be used to discretize the remaining systems. Based on Figure 3.12 and the use of *BF* as a convergence factor, it was determined that grid independence was achieved at 1,000,000 cells. Respective settings from this mesh were used to discretize geometries in the parametric study.

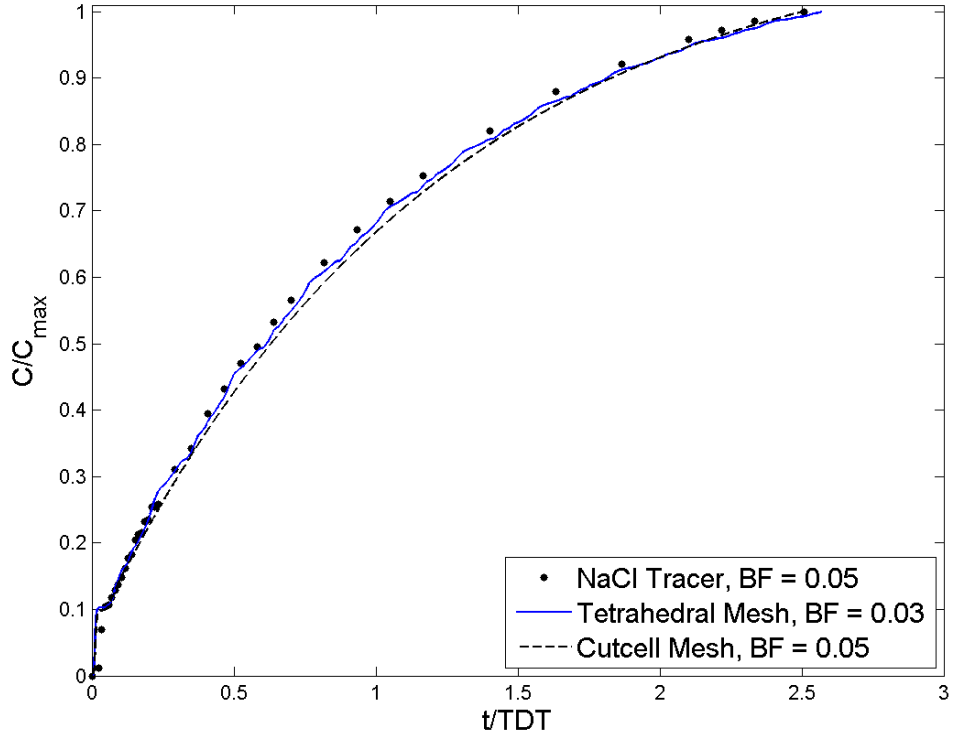**Figure 3.11:** Resulting RTD Curves for the Base System using Tetrahedral and Cutcell Meshes
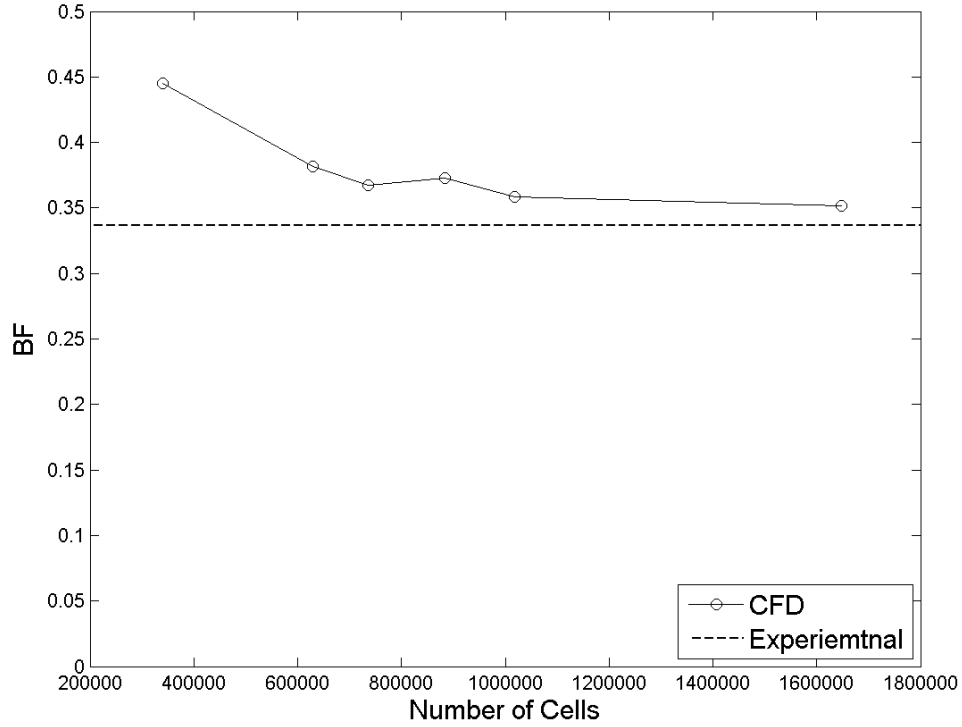
Figure 3.12: Grid Convergence for Cutcell Meshes within a Two Baffle System

In addition to determining spatial convergence, temporal convergence was investigated by varying the time step, Δt. Time steps of $\Delta t = 2s, 4s, 6s, 8s,$ and $10s$ were used to asses effects of temporal resolution on solution results. As shown in Figure 3.13, coarsening Δt had no significant effect on the region of interest (t_{10}) and only affected later portions of resulting RTD curves. A time step of $\Delta t = 2s$ was chosen for the remainder of the study as a conservative measure.

Figure 3.13: Effect of Δt on RTD Curve Shape for a Two Baffle System

3.5 Parametric Study

Once the proposed numerical model was validated, a parametric study was conducted to investigate the effect of placing baffles parallel to the long axis of the studied system. This study differs from past studies in terms of baffle orientation and inlet condition. Taylor (2012)

investigated baffles in a system with a channel inlet and Barnett investigated a system with a sharp inlet and baffles placed parallel to the short axis. CFD was used as opposed to physical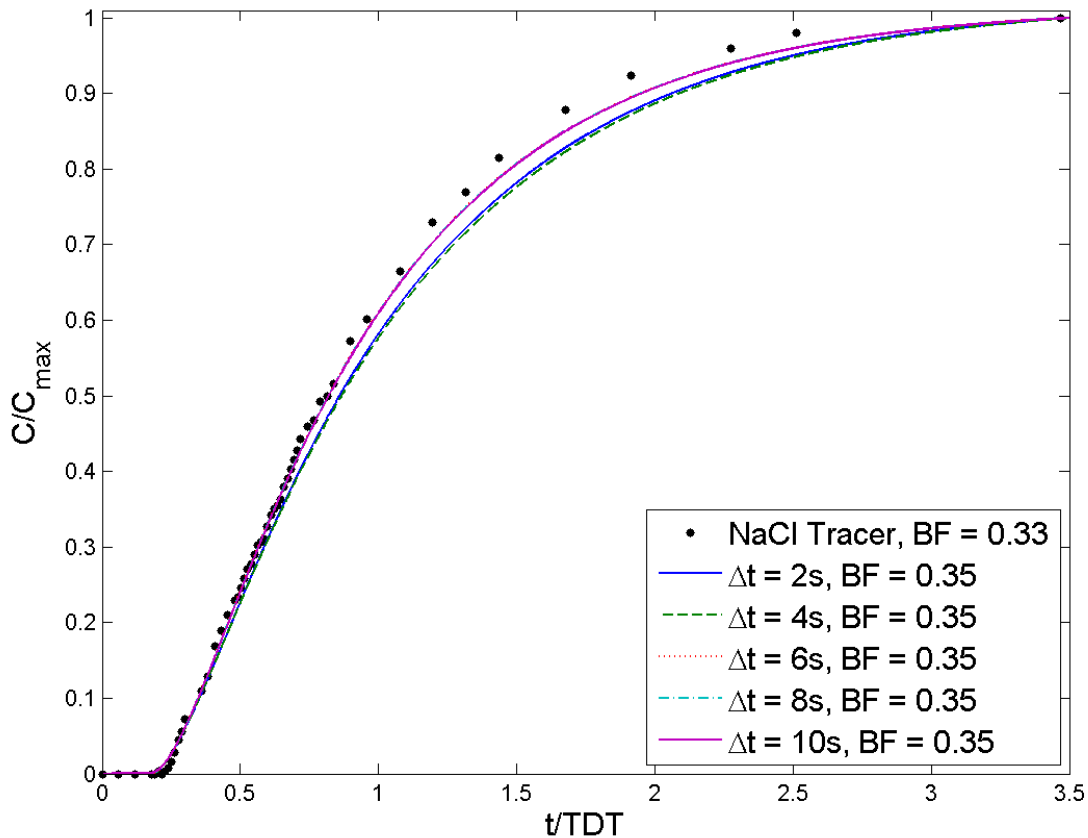 modeling based on economic considerations. Implementing computational models is not only more cost-effective than physical modeling, but is more time-effective. CFD also provides detailed resolution of internal flow characteristics, offering additional insight regarding system performance.

3.5.1 Parameters of Interest

Dimensionless geometric parameters similar to those studied by Taylor (2012) and Barnett (2013) were investigated in this study. A general schematic of a baffled system can be seen below in Figure 3.14, which defines geometric nomenclature. Investigated parameters include L_T/W_{ch}, L_{bo}/W_{ch}, L^*, and the number of baffles (N_B), where L^* and L_{bo} are defined by Equations 27 and 28.

$$L^* = \frac{L_{bo}}{L_T} \tag{27}$$

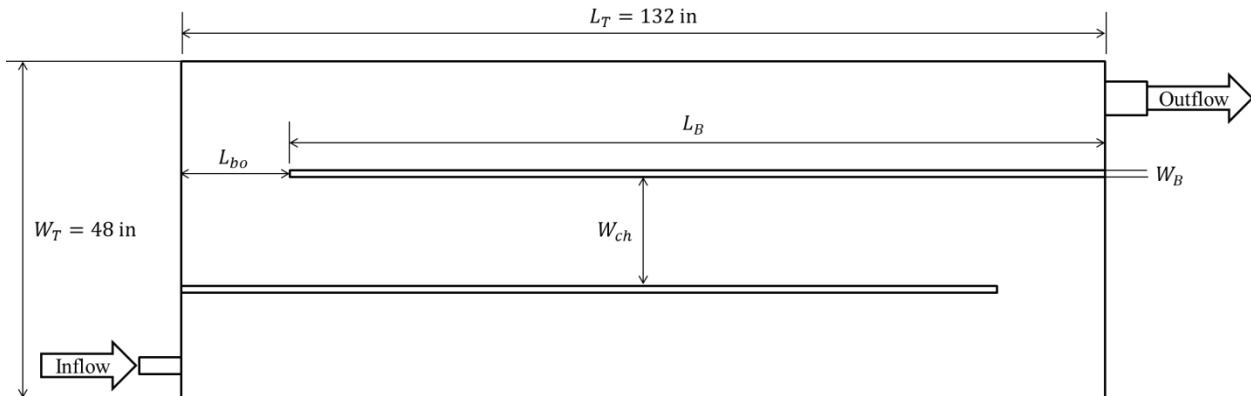$$L_{bo} = L_T - L_B \tag{28}$$

Figure 3.14: Geometric Parameters of an Arbitrary Baffled System

Hydraulic disinfection efficiency was measured through determination of the baffling factor and a quantity known as mean residence time (T_m). Barnett (2013) introduced T_m in order to extend Taylor's discussion of system performance and better explain observed trends. Mean residence time represents an approximation of the average time that a given parcel of fluid spends inside a contact volume. In a system undergoing plug flow T_m is theoretically equivalent to TDT. Under this assumption the amount of contact time that is lost (T_d) can be approximated from T_m and TDT. T_d represents the amount of contact time lost from non-plug flow anomalies such as short circuiting, dead zones, and turbulent eddies. Both T_m and T_d were approximated using formulations presented by Xu (Equations 29 and 30). (Xu, 2010). Integrals were numerically determined using the trapezoidal rule.

$$T_m = \int_0^{C_{max}} t\,dC \approx \sum_{i=1}^{N-1} \frac{1}{2} T_i (C_i + C_{i+1}) \tag{29}$$

$$T_d = TDT - T_m \tag{30}$$

3.5.2 Parameter Space Manipulation

Thirty-seven different baffled scenarios were investigated using CFD. Baffles were placed parallel to the longest axis of the tank and varied in number and length. The number of baffles was varied between zero and six, all channel widths were calculated using Equation 31, and the length was varied according to the parameter L^*. For each number of baffles, L^* was set at 0.10, 0.20, 0.40, 0.60, and 0.80 in addition to one scenario where $L_{bo} = W_{ch}$. All tests were conducted at a flow rate of 20 GPM.

$$W_{ch} = \frac{W_T - N_B W_B}{N_B + 1} \tag{31}$$

3.6 Results and Discussion

Results from this parametric study offer additional insight regarding the internal hydraulics of serpentine baffled contact tanks by challenging traditional lines of thinking. In established design practice the term "length to width ratio" is commonly referred to as a design parameter (USEPA, 2003; Wejun, 2007). Using the terminology of this study, "length to width ratio" can either refer to L_T/W_{ch} for systems with low values of L^* or to L_{ch}/W_{ch}, where L_{ch} is an estimate of the entire system length (i.e. the combined length of all channels). Given the USEPA's reference to pipe-loop contactors, it is likely that the second definition takes precedence. For constant values of L^*, both L_T/W_{ch} and L_{ch}/W_{ch} are directly related to the number of evenly spaced baffles placed within a tank by Equations 32 and 33.

$$\frac{L_T}{W_{ch}} = \frac{L_T(N_B + 1)}{(W_T - N_B W_B)} \tag{32}$$

$$\frac{L_{ch}}{W_{ch}} = \frac{L_T(N_B + 1) + N_B W_B}{W_{ch}} = \left(\frac{(N_B + 1)}{W_T - N_B W_B}\right)[L_T(N_B + 1) + N_B W_B] \tag{33}$$

Results from the study conducted by Taylor (2012) showed that gains obtained by manipulating the length to width ratio were dependent on both L^* and L_{bo}/W_{ch}, modifying traditional ideology. Barnett showed that optimal values of L^*, L_{bo}/W_{ch}, and L_T/W_{ch} were also dependent on the type of inlet used (Barnett, 2013). Results from this study not only validate the concepts tested by Taylor and Barnett, but extend them by showing that inlet and baffle orientation significantly impact gains in hydraulic efficiency.

Table 3.1-Table 3.7 summarize results for all thirty seven tested baffle configurations. Following subsections describe observed trends for each of the studied parameters.

Table 3.1: Design Parameters and Efficiency Quantifiers for $L^* = 1.00$

Number of Baffles	Design Parameters				Efficiency				
	L^*	L_{bo}/W_{ch}	L_T/W_{ch}	L_{ch}/W_{ch}	Volume, Gallons	TDT (s)	BF	T_m	T_d
0	1.00	NA	NA	NA	1722	5165	0.05	3441	1724

Table 3.2: Design Parameters and Efficiency Quantifiers for $L^* = 0.80$

Number of Baffles	Design Parameters				Efficiency				
	L^*	L_{bo}/W_{ch}	L_T/W_{ch}	L_{ch}/W_{ch}	Volume, Gallons	TDT (s)	BF	T_m	T_d
1	0.80	4.47	5.59	11.21	1716	5149	0.09	3573	1576
2	0.80	6.81	8.52	25.65	1711	5133	0.25	3918	1215
3	0.80	9.23	11.54	46.36	1706	5117	0.17	3509	1608
4	0.80	11.73	14.67	73.67	1700	5101	0.24	3705	1395
5	0.80	14.32	17.90	107.90	1695	5085	0.19	3700	1385
6	0.80	16.99	21.24	149.41	1690	5069	0.22	3656	1413

Table 3.3: Design Parameters and Efficiency Quantifiers for $L^* = 0.60$

Number of Baffles	Design Parameters				Efficiency				
	L^*	L_{bo}/W_{ch}	L_T/W_{ch}	L_{ch}/W_{ch}	Volume, Gallons	TDT (s)	BF	T_m	T_d
1	0.60	3.35	5.59	11.21	1711	5133	0.09	3574	1559
2	0.60	5.11	8.52	25.65	1700	5101	0.22	3801	1300
3	0.60	6.92	11.54	46.36	1690	5069	0.27	3872	1196
4	0.60	8.80	14.67	73.67	1679	5036	0.17	3429	1607
5	0.60	10.74	17.90	107.90	1668	5004	0.29	3967	1038
6	0.60	12.74	21.24	149.41	1657	4972	0.36	3826	1146

Table 3.4: Design Parameters and Efficiency Quantifiers for $L^* = 0.40$

Number of Baffles	Design Parameters				Efficiency				
	L^*	L_{bo}/W_{ch}	L_T/W_{ch}	L_{ch}/W_{ch}	Volume, Gallons	TDT (s)	BF	T_m	T_d
1	0.40	2.23	5.59	11.21	1706	5117	0.10	3588	1529
2	0.40	3.41	8.52	25.65	1690	5069	0.31	4016	1053
3	0.40	4.62	11.54	46.36	1673	5020	0.49	4288	732
4	0.40	5.87	14.67	73.67	1657	4972	0.56	4336	635
5	0.40	7.16	17.90	107.90	1641	4923	0.52	4241	682
6	0.40	8.50	21.24	149.41	1625	4875	0.49	4017	857

Table 3.5: Design Parameters and Efficiency Quantifiers for $L^* = 0.20$

Number of Baffles	Design Parameters				Efficiency				
	L^*	L_{bo}/W_{ch}	L_T/W_{ch}	L_{ch}/W_{ch}	Volume, Gallons	TDT (s)	BF	T_m	T_d
1	0.20	1.12	5.59	11.21	1700	5101	0.09	3345	1756
2	0.20	1.70	8.52	25.65	1679	5036	0.34	4031	1005
3	0.20	2.31	11.54	46.36	1657	4972	0.53	4296	676
4	0.20	2.93	14.67	73.67	1636	4907	0.61	4307	600
5	0.20	3.58	17.90	107.90	1614	4843	0.64	4250	593
6	0.20	4.25	21.24	149.41	1593	4778	0.65	4172	607

Table 3.6: Design Parameters and Efficiency Quantifiers for $L^* = 0.10$

Number of Baffles	Design Parameters				Efficiency				
	L^*	L_{bo}/W_{ch}	L_T/W_{ch}	L_{ch}/W_{ch}	Volume, Gallons	TDT (s)	BF	T_m	T_d
1	0.10	0.56	5.59	11.21	1698	5093	0.10	3513	1580
2	0.10	0.85	8.52	25.65	1673	5020	0.40	4106	914
3	0.10	1.15	11.54	46.36	1649	4948	0.57	4320	628
4	0.10	1.47	14.67	73.67	1625	4875	0.65	4259	616
5	0.10	1.79	17.90	107.90	1601	4802	0.73	4472	330
6	0.10	2.12	21.24	149.41	1577	4730	0.74	4217	513

Table 3.7: Design Parameters and Efficiency Quantifiers for $L_{bo} = W_{ch}$

Number of Baffles	Design Parameters				Efficiency				
	L^*	L_{bo}/W_{ch}	L_T/W_{ch}	L_{ch}/W_{ch}	Volume, Gallons	TDT (s)	BF	T_m	T_d
1	0.18	1.00	5.59	11.21	1700	5099	0.09	3527	1572
2	0.12	1.00	8.52	25.65	1674	5023	0.35	3979	1043
3	0.09	1.00	11.54	46.36	1648	4944	0.58	4330	615
4	0.07	1.00	14.67	73.67	1622	4865	0.67	4297	567
5	0.06	1.00	17.90	107.90	1595	4784	0.77	4488	296
6	0.05	1.00	21.24	149.41	1568	4704	0.79	4256	448

3.6.1 L^* and Number of Baffles Vs. BF

Figure 3.15 shows the baffling factor as a function of the number of baffles where curves are grouped by L^*. Increasing the number of baffles does not yield a systematic increase in hydraulic efficiency for $L^* > 0.4$, which is consistent with the findings of Taylor (2012) and Barnett (2013). However, the findings of this study differ from those conducted by both Taylor and Barnett in terms of the rate at which efficiency is gained with an increase in the number of baffles and optimally observed values of L^*.

For the system studied by Taylor it was found that optimal values of L^* were dependent on the number of baffles. Barnett's results disagreed with this observation, suggesting an optimal L^* value of 0.2. Figure 3.15 from this study suggest that for $N_b > 3$, L^* is optimum when $L_{bo} = W_{ch}$. If the baffling factor is plotted as a function of L^*, as in Figure 3.16, then it can be seen that for $N_B < 3$, $W_{ch} > 0.1 L_T$ and that the baffling factor systematically increases with a decrease in L^*. This means that optimal values of L^* correspond to minimal values of L_{bo}, making the observation of $L_{bo} = W_{ch}$ being ideal a coincidence. Discrepancies in the behavior of L^* across parametric studies can be attributed to differences regarding inlet conditions and baffle orientation.

In the parametric study presented here baffles are placed parallel to a sharp inlet. It is apparent from Figure 3.17(a-g) that this results in the formation of a turbulent jet. This jet causes significant amounts of short circuiting and flow separation, leading to the formation of dead zones. Comparing Figure 3.17(a-g) shows that the addition of baffles reduces short circuiting by forcing the flow through a directed path, but flow separation induced by the inlet persists for over two channels and is exaggerated at baffle turns. Figure 3.17(a-g) also suggest that contraction of initial baffle openings provides additional head-loss, which helps to normalize the

flow. Volume deficit resulting from the inlet is so large that excessive contraction of baffle openings leads to system improvement even though it causes separation in later channels. This effect is what causes observed differences in the behavior of L^*, N_B, and BF across parametric studies.

The study implemented by Taylor (2012) considered systems with channeled inlets sized to match the widths of resulting contact chambers. Use of a variable and uniform inlet results in initialized flow which contains less kinetic energy and has a shorter development length than flow resulting from a sharp or contracted inlet. Contraction of L_{bo} for these scenarios introduces head-loss into systems that are nearly developed and contain varying levels of kinetic energy, making optimal values of L^* dependent on N_B.

Systems studied by Barnett contained baffles placed perpendicular to a sharp inlet, allowing for the use of baffle walls in diffusion of excess momentum. For this scenario increasing the number of baffles increases the amount of head-loss occurred from collision, decreasing the amount of head-loss required for distribution of remaining velocity gradients. This explains why optimal values of L^* converge near 0.2. At this point additional head-loss incurred by contraction of L_{bo} becomes counterproductive. Dispersion of the inlet jet also prevents increases in BF with N_B from leveling off for optimal values of L^*.

Variability in the behavior of BF with respect to L^* between parametric studies demonstrates that L^* is not a suitable design variable. The effect of L^* on system performance is dependent on initial system geometry, inlet type, inlet orientation, and baffle orientation, making it difficult to optimize. However, all three parametric studies show that the condition $L^* \leq 0.4$ must be satisfied in order for the addition of baffles to be productive. If L^* is too low channeling

occurs between the tips of baffles, resulting in the loss of contact volume. This effect is exemplified in Figure 3.18 (a-g).
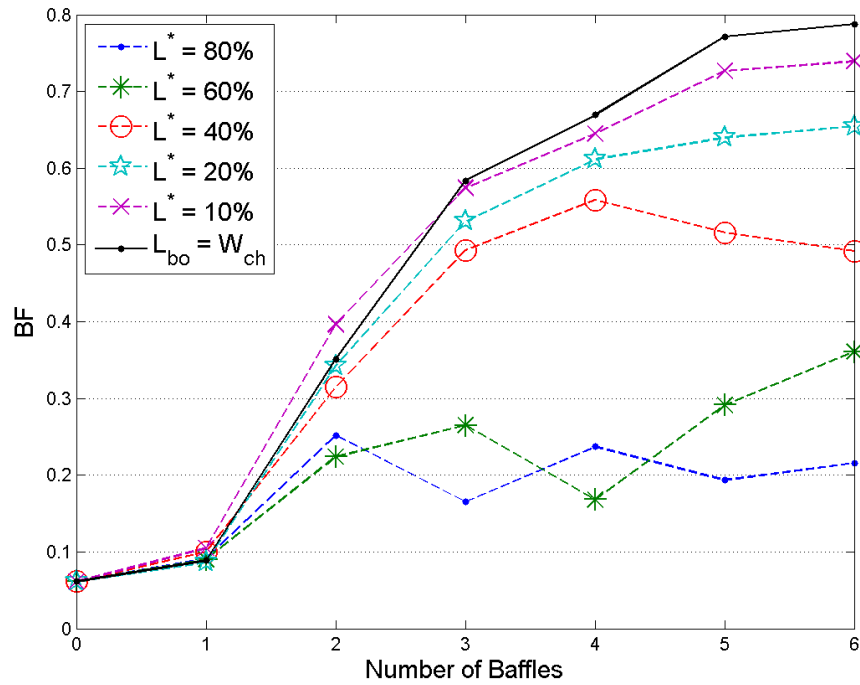
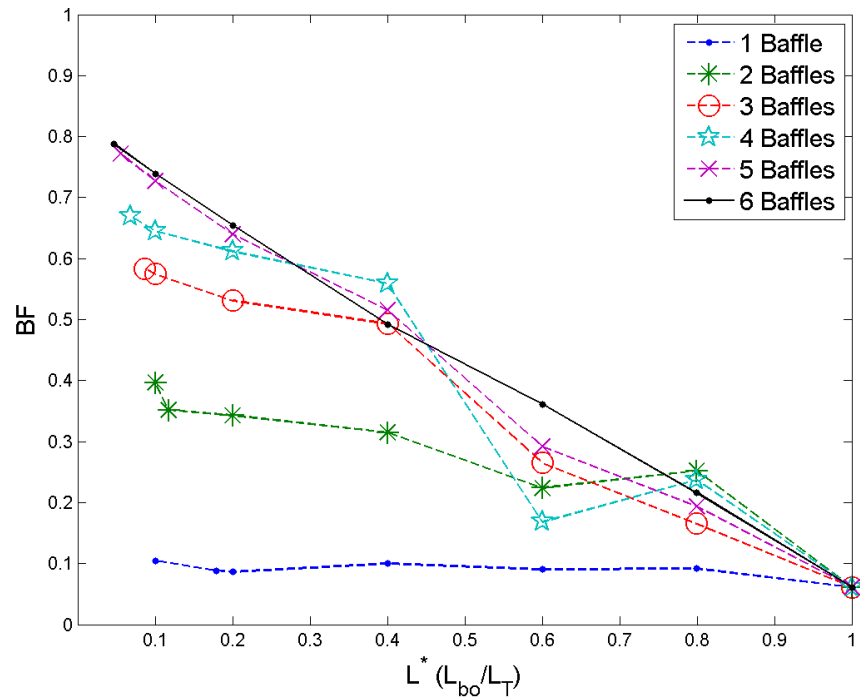

Figure 3.15: Number of Baffles Vs. Baffling Factor

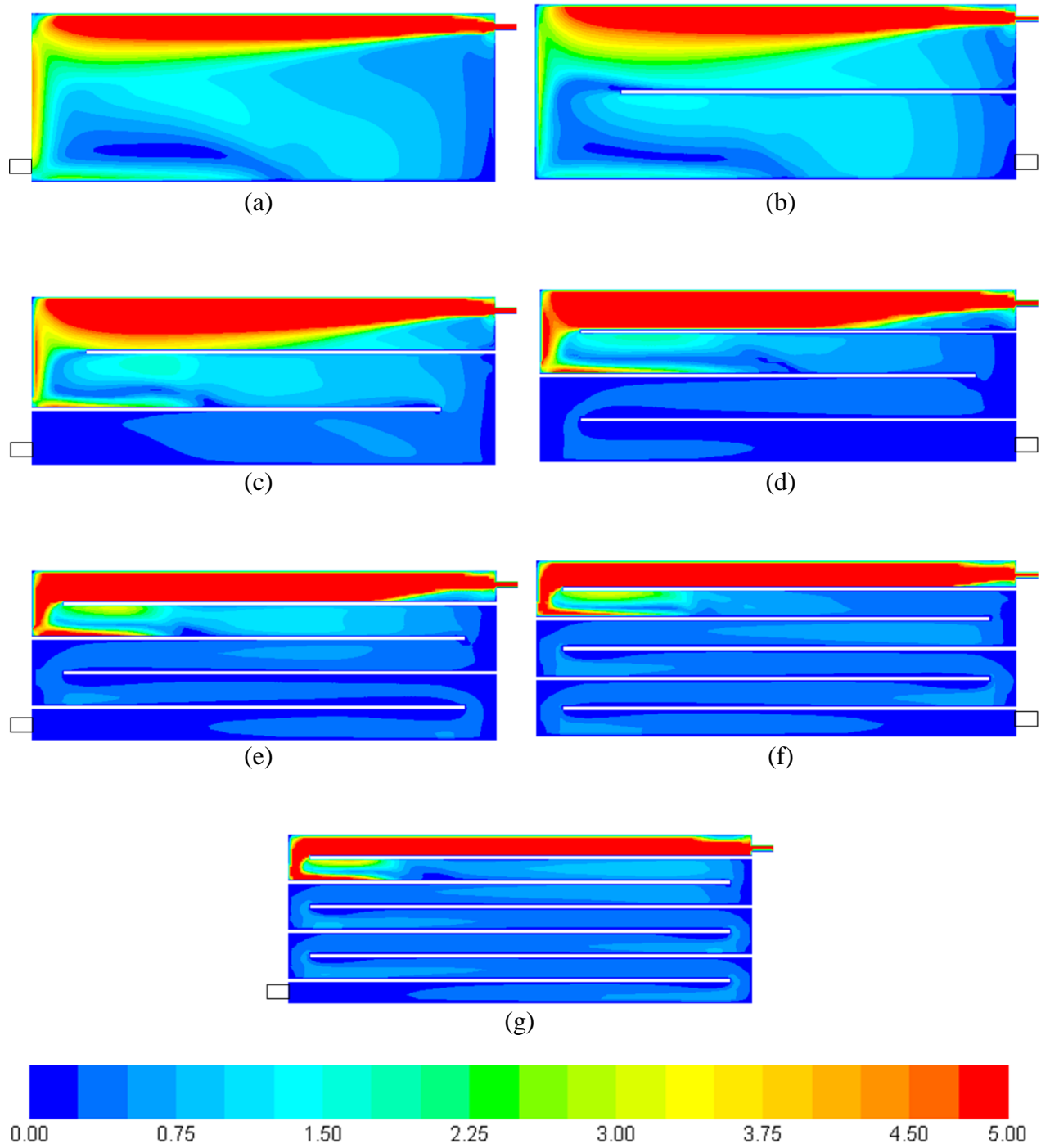**Figure 3.16:** L^* Vs. Baffling Factor

Figure 3.17: Normalized Contours of Velocity Magnitude $\left(V/V_{\text{average}}\right)$ at a Plane Intersecting the Inlet in Systems with $L_{bo} = W_{ch}$ using (a) No Baffles, (b) One Baffle, (c) Two Baffles, (d) Three Baffles, (e) Four Baffles, (f) Five Baffles, and (g) Six Baffles
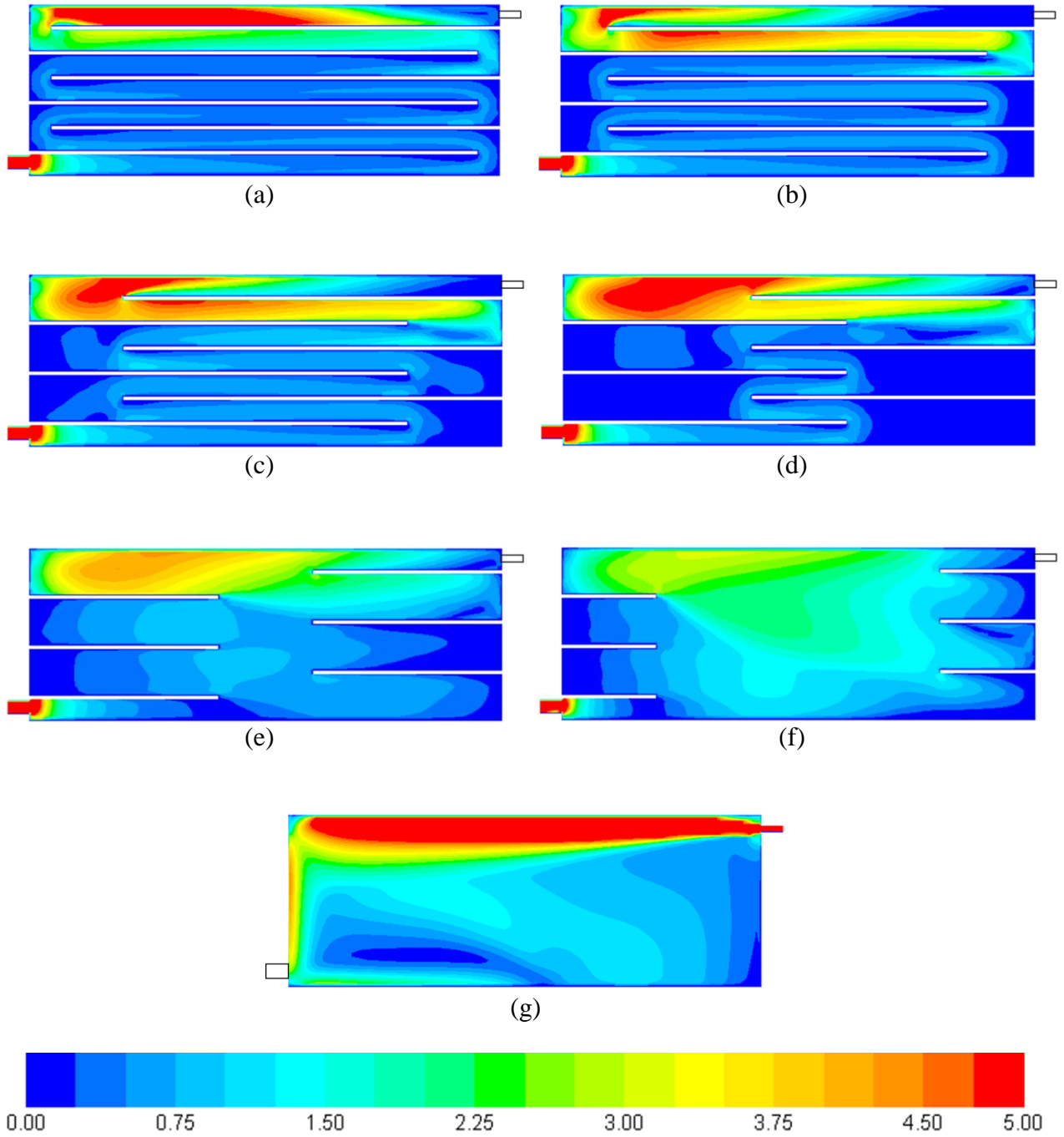
Figure 3.18: Normalized Contours of Velocity Magnitude $\left(V/V_{\text{average}}\right)$ at a Plane Intersecting the Outlet in Systems using Six Baffles with $L^{*} =$ (a) 0.05, (b) 0.10, (c) 0.20, (d) 0.40 (e) 0.60, (f) 0.80, and (g) 1.00

3.6.2 L_{bo}/W_{ch} Vs. Baffling Factor

The ratio L_{bo}/W_{ch} is an insightful parameter because it provides a relative measure of contraction or expansion at baffle turns. Values of $L_{bo}/W_{ch} > 1$ represent an expansion of flow while values of $L_{bo}/W_{ch} < 1$ represent a constriction of flow. As shown in Figure 3.18(a-g), expansive geometry can lead to channeling of the flow near baffle tips and creation of recirculating dead-zones near channel corners. In contrast to expansive geometry, constrictive geometry causes flow to separate from the tip of baffles and lightly recirculate on the opposite side. Also, as discussed in Section 3.6.1, constrictive geometry introduces additional head loss, which can be beneficial for tanks employing sharp inlets.

Figure 3.19 shows the baffling factor as a function of L_{bo}/W_{ch}. Results suggest that minimizing L_{bo}/W_{ch} will maximize disinfection efficiency, enforcing the conclusions drawn in Section 3.6.1. Since this effect has been attributed to the beneficial effects of constricting the initial jet, it is likely that optimal values of L_{bo}/W_{ch} for the studies systems lies in the interval $0.1 \leq L_{bo}/W_{ch} \leq 0.6$, which is outside of the tested range. This statement agrees with observations made in the study by Barnett (2013). However, if the incoming turbulent jet were dispersed in some way, the optimal value of L_{bo}/W_{ch} would approach unity, which was the conclusion drawn by Taylor (2012).

Taylor found that energy loss resulting from contraction and sharp turns reduced the baffling factor for systems with a channel inlet. These systems can reach fully developed flow conditions in approximately one baffle reach, so additional head-loss at baffle turns causes unwanted separation and loss of effective volume. Therefore, the ratio L_{bo}/W_{ch} can be prescribed for design, but its optimum value depends on the inlet condition.
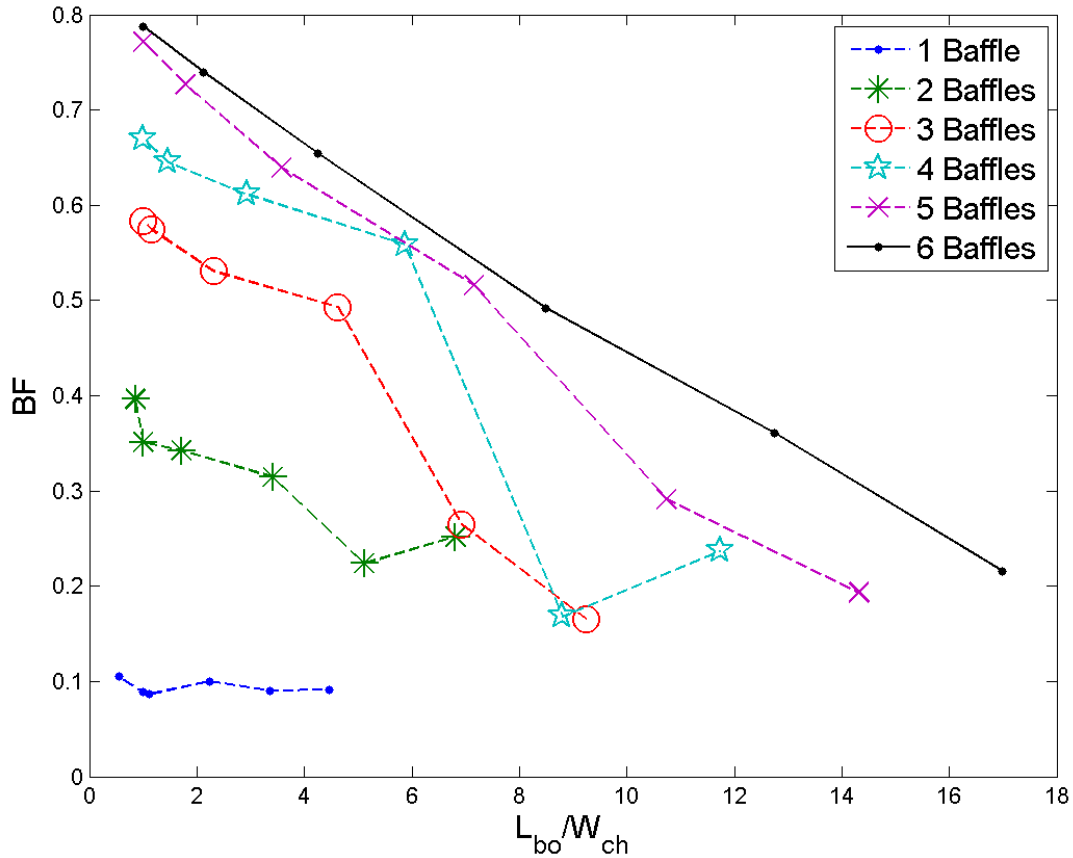
Figure 3.19: L_{bo}/W_{ch} Vs. Baffling Factor

3.6.3 L_T/W_{ch} and L_{ch}/W_{ch} Vs. Baffling Factor

The parameters L_T/W_{ch} and L_{ch}/W_{ch} represent length to width ratios that are linearly related to the number of baffles, implying that resulting relationships will appear exactly like the one shown in Figure 3.15. However, the maximum obtainable values of each of these ratios directly depend on baffle orientation and system geometry. Traditional design guidance only considers these parameters without the effects of L^* and L_{bo}/W_{ch}, suggesting that the "length to width ratio" should be maximized (USEPA, 2003). Earlier parametric studies considered the ratio L_{ch}/W_{ch}, but the importance of this parameter solely relies on L_T/W_{ch} (Wenjun *et al*, 2007). If L_T/W_{ch} is significantly small, then flow within each channel will not have sufficient length in between baffle turns to fully develop, diminishing efficiency through the loss of

effective volume (Taylor, 2012). This makes L_T/W_{ch} a more effective parameter since it represents a localized length to width ratio.

For this study the largest values of L_T/W_{ch} and L_{ch}/W_{ch} were obtained in six-baffle systems. The six-baffle system with optimal values of L^* and L_{bo}/W_{ch} exhibited a baffling factor of 0.79 as well as length to width ratios of $L_T/W_{ch} = 21.2$ and $L_{ch}/W_{ch} = 149.4$. In comparison the optimum baffling configuration from Barnett's study used ten baffles and exhibited a baffling factor of 0.80. This system exhibited length to width ratios of $L_T/W_{ch} = 4.6$ and $L_{ch}/W_{ch} = 51.5$ and used around 57% of the material as the optimal six-baffle system. Barnett's system exhibits length to width ratios less than one-fourth of the six-baffle system, but it performs in a similar matter. This disproves traditionally accepted concepts and displays the detrimental effects of using a poorly oriented sharp inlet. Effects of length to width ratios on gains in efficiency are therefore dependent on L^*, L_{bo}/W_{ch}, and most importantly the inlet condition, which has serious implications regarding design of practical systems. For instance, consider results for the most efficient 2-baffle, 3-baffle, and 4-baffle systems shown in Figure 3.15. All of these systems would easily be classified as Average or Superior using USPEA guidelines (Table 1.1), suggesting baffling factors of 0.5 to 0.7. This range is significantly above observed values, which could result in overestimation of disinfection and resulting outbreaks of disease.

Additional studies conducted by Taylor show that the use of baffles in the long direction can more than double the baffling factor of a system using a channelized inlet (Taylor, 2012). Similar gains should be obtainable for systems using sharp inlets, but the inlet would have to be either re-directed or diffused.

3.6.4 T_m and T_D

Figure 3.20 (a-f) show plots of TDT, T_m, and T_d for different values of L^*. Investigation of T_m and T_d offer additional insight into tank hydraulics by providing a quantitative measurement of lost contact time. It is clear from Figure 3.20 (a-f) that for values of $L^* < 0.4$ an increase in the number of baffles yields an increase in T_m and a decrease in T_d. For lower values of L^*, increasing the number of baffles increases L_T/W_{ch}, further directing the flow and reducing the formation of short-circuiting and dead zones, which increases the mean residence time (See Figure 3.17). For higher values of L^*, flow separates at baffle turns and moves through the center of the tank, resulting in recirculating zones in between the short baffles and reducing residence time (See Figure 3.18). Flattening of T_m and T_d curves in Figure 3.20 (d) and (e) are indicative of this channeling effect.

Results in Figure 3.20 (a-f) show agreement with discussion from Sections 3.6.1, 2.6.2, and 3.6.3. Results indicate that increasing the number of baffles results in improved hydraulic disinfection efficiency, but the behavior of gains is directly dependent upon L^*, L_{bo}/W_{ch}, and the inlet condition. Leveling off of T_d curves in Figure 3.20 (a), (b), (c), and (f) indicate that increasing the number of baffles further would not yield significant gains in efficiency, which is in agreement with Figure 3.15.
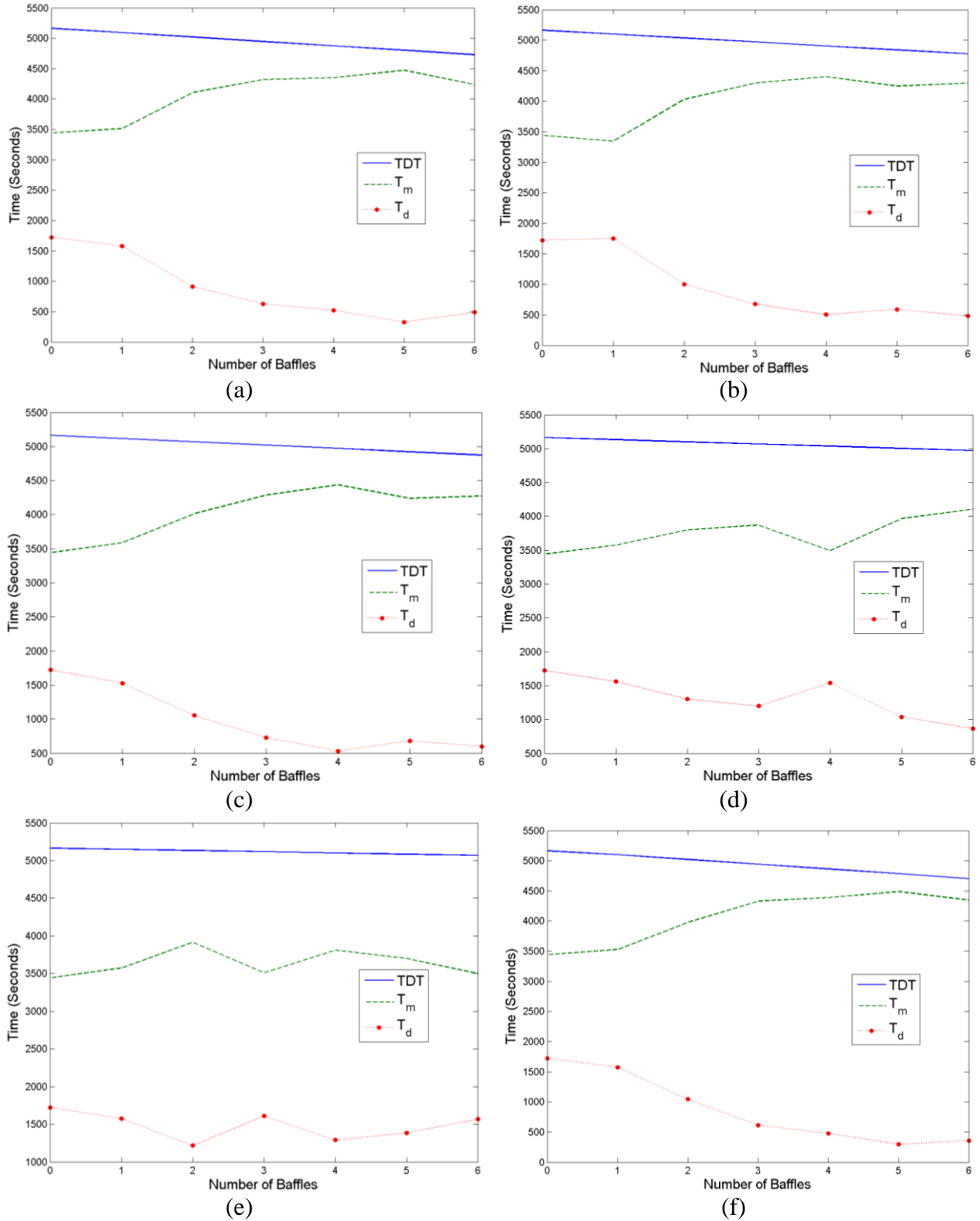
Figure 3.20: Plots of TDT, T_m, and T_d for L^* Values of (a) 0.10, (b) 0.20, (c) 0.40, (d) 0.60 (e) 0.80, and the Case Where (f) $L_{bo} = W_{ch}$

3.7 Conclusions

Overall it was found that inlet type and orientation significantly affect potential gains in hydraulic disinfection efficiency through the use of internal baffling. Comparison of results to previous parametric studies exemplified varying trends regarding the parameters L^*, L_{bo}/W_{ch}, and the number of baffles, which were related back to inlet conditions. For design of a baffled system with a channelized inlet, it is recommended that $L_{bo}/W_{ch} \approx 1$, that L_T/W_{ch} be maximized, and that the number of turns be minimized. For design of systems involving sharp inlets, it is recommended that the inlet be diffused or oriented perpendicular to the direction of baffle placement. From here, if baffles are placed parallel to the short axis of a tank, L^* should be set between 0.1-0.2 and the number of baffles should be chosen to obtain $L_{bo}/W_{ch} \approx 1$. If baffles are oriented parallel to the long axis of a tank, L_{bo}/W_{ch} should be set somewhere between 0.4 and 1. The variables T_m and T_d provided useful insight regarding internal hydraulics of the studied system, but were not recommended for design due to difficulties regarding determination. T_m and T_d can only be determined from CFD model results or physical tracer studies.

Even though internal baffling is one of the most widely accepted methods for improving hydraulic efficiency, results suggest that traditional design considerations are inappropriately non-conservative. Estimation of baffling factors from Table 1.1 resulted in overestimation of values by as much as 42%, suggesting dominance of inlet orientation over L_T/W_{ch} and L_{ch}/W_{ch}. Additional studies need to be conducted in order to fully quantify detrimental effects of inlet size and orientation. Such studies would investigate localized head-loss and dimensionless ratios involving inlet and channel areas.

CHAPTER 4: RANDOM PACKING MATERIAL INLET MODIFICATION STUDY

4.1 Introduction

CFD results from the parametric study in Chapter 3 showed that the presence of a sharp inlet induces significant amounts of short circuiting and flow separation, resulting in the formation of recirculating dead zones and a loss of effective volume. While the use of internal baffling provides an effective method for counteracting these effects, purchase and installation of baffle walls is often beyond the budget of most small systems (USEPA, 2011). In order to propose a more cost-effective option, research presented in this chapter investigates the innovative application of industrial packing material as an inlet modification.

4.2 Issues with the Inlet

The system of interest for this study is the base system from Chapter 3, which is a rectangular concrete tank with an approximate volume of 1500 gallons (See Section 3.3). Normalized velocity contours $\left(V/V_{\text{average}}\right)$ from a validated simulation of this system can be seen below in Figure 4.1(a-f). Two particularly insightful contours are Figure 4.1(a) and (b), which show contours of normalized velocity on horizontal and vertical planes intersecting the inlet. Both of these figures clearly display the development of a turbulent jet resulting from the use of a sharp inlet. The diameter of this jet does not exceed 25% of the tank width (W_T) or the tank length (L_T), resulting in excessive velocity deficits. Once the jet hits the back wall it spreads over a thin section and short circuits, moving directly to the outlet and spreading over the water surface. This results in the formation of a large recirculating dead zone. The extent of this recirculating zone is exemplified by Figure 4.1(c-f), which show velocity contours at different percentages of the free surface depth. In contrast, a three-dimensional representation of effective

volume can be seen in Figure 4.2(a) and (b), which show an iso-surface encompassing velocities greater than twice the average.

CFD results clearly show that the use of a sharp inlet induces short circuiting which results in the formation of significant dead zones, yielding a baffling factor of 0.05 and an RTD curve dominated by molecular diffusion (See Figure 3.5). For chlorinated systems this would result in inadequate disinfection and the development of cancerous DBPs. Results suggest these detrimental effects could be reduced by re-distributing the incoming flow over a larger area. Research in this study provides a means of re-distributing flow through investigating the local application of random packing material as an inlet modification.
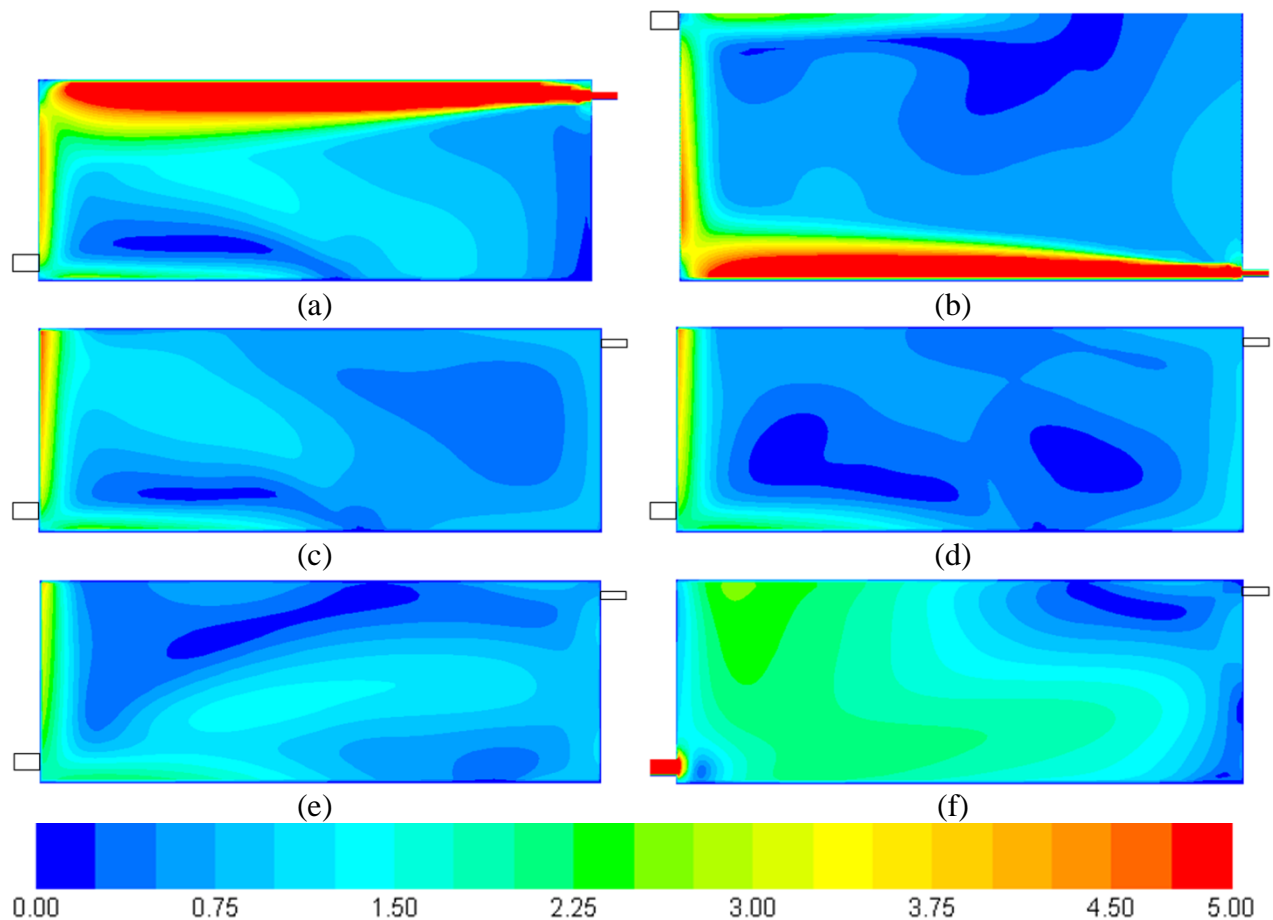

Figure 4.1: Contours of Normalized Velocity Magnitude ($V/V_{average}$) within the Base System for (a) a Horizontal Plane at the Inlet, (b) a Vertical Plane at the Inlet, and Planes at (c) 25%, (d) 50%, (e) 75%, and (f) 100% of the Free Surface Depth
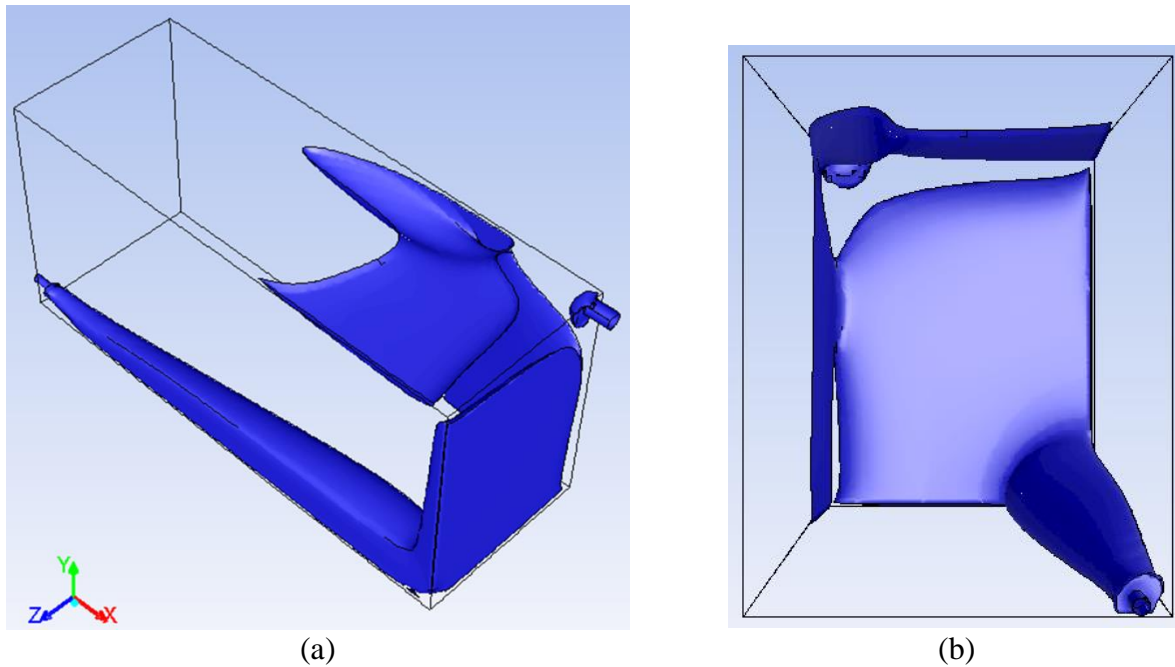
(a)   (b)

Figure 4.2: (a) Isometric View and (b) Back View of a 3D Iso-Surface of Velocity Magnitude Corresponding to $V \geq 2V_{\text{average}}$

4.3 Random Industrial Packing Material

As discussed in Section 2.4, previous research suggests that the application of random industrial packing material has the potential to greatly increase the hydraulic disinfection efficiency of small contact tanks (Barnett *et al,* 2014). Originally designed for use in vapor separation towers, column packing material is traditionally used in aeration towers, trickling filters, and distillation towers (Kavanaugh & Trussell 1980, Richards & Reinhart 1986, USDOE 2001). Research in this study considers the use of random packing material as a localized diffuser of kinetic energy through inlet modification and strategic placement. Spherical packing material 2" in diameter was the only material considered in this study due to its proven application in drinking water disinfection (Barnett *et al,* 2014). Previous research involving the application of industrial packing material to disinfection contact tanks has only considered laboratory scale studies (Barnett *et al,* 2014). Therefore, research presented in this chapter and in

Chapter 5 extends existing literature through investigating the application of packing material to full scale prototypes.

4.4 Inlet Box Design

Random packing material was implemented as an inlet modification based on inferences from CFD results. Packing material was organized into box like structures and fastened over the inlet using wooden guide frames. Referred to as inlet boxes, these structures were constructed using 1" X 4" wooden boards and chicken wire. Materials were chosen based on economic considerations and to allow for ease of installation. Construction of similar structures within an operational contact tank would require the use of NSF 61 certified building materials. Acceptable materials include plastic grating, fiberglass grating, or plastic coated wire mesh, which are readily available from a number of distributers. Examples of constructed packing material structures can be seen in Figure 4.3 (a-c). Figure 4.4 shows an arbitrary inlet box and outlines applied nomenclature. Inlet boxes are classified using the notation $H_{Bx} \times L_{Bx}$, where H_{Bx} is the box height and L_{Bx} is the box length.
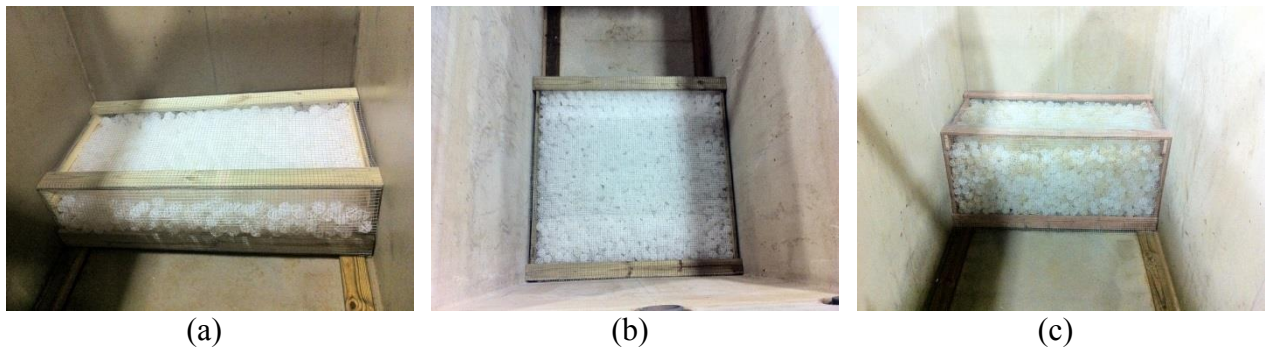

| (a) | (b) | (c) |

Figure 4.3: Inlet Box Prototypes with Dimensions (a) 1ft X 2ft, (b) 1ft X 4ft, and (c) 2ft X 2ft Respectively
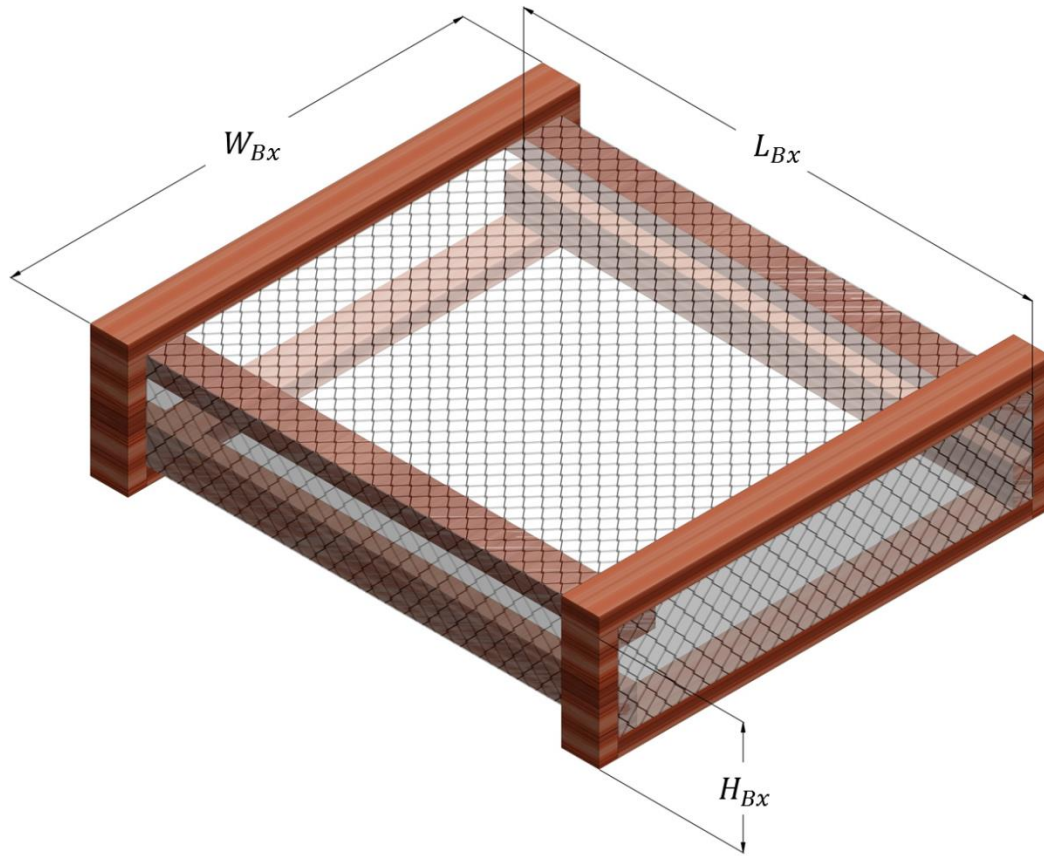
Figure 4.4: Schematic Showing Geometric Parameters of a Generic Inlet Box

4.5 Methodology

Step-wise tracer studies were performed on system prototypes to quantify hydraulic disinfection efficiency. Similar procedures were used as are described in Section 3.4.1. A total of thirty-seven tracer studies were performed using sodium-chloride as a conservative tracer in order to investigate eighteen different inlet box designs. Three of these studies were redone using lithium-chloride solution in order to validate applied methodology. Lithium ions are usually considered a more reliable tracer than conductivity due to low background levels in existing systems. Figure 4.5 (a-c) show a comparison of RTD curves obtained using sodium chloride tracer and lithium chloride tracer for a 1ft X 2ft box ($H_B \times L_B$) at 10 GPM, 20 GPM, and 40 GPM respectively. Good agreement between lithium ion and conductivity results validates the use of sodium chloride as a tracer.
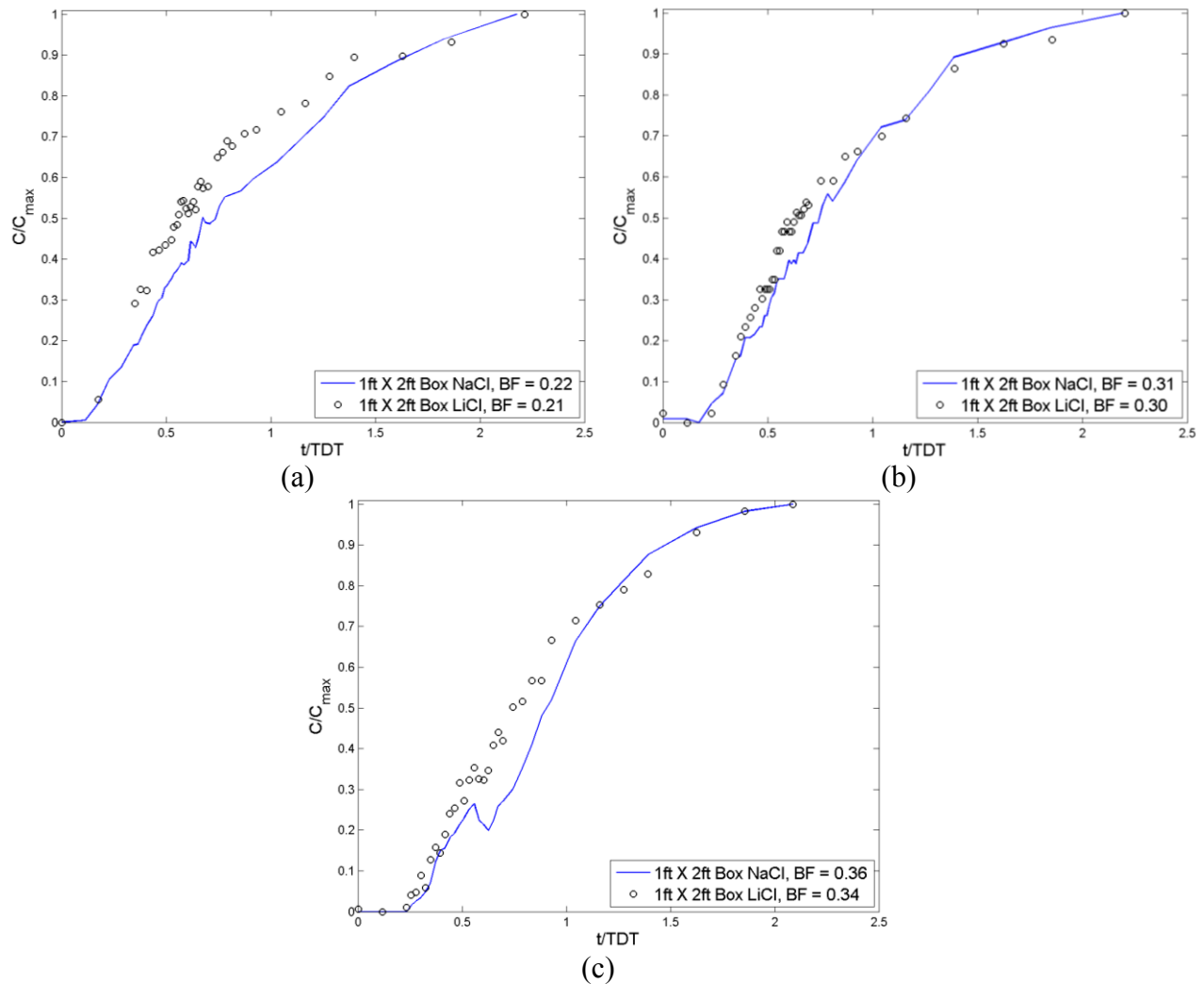
74

Figure 4.5: Comparisons of Resulting RTD Curves for a 1ft X 2ft Inlet Box using LiCl and NaCl Tracers at Flow rates of (a) 10 GPM, (b) 20 GPM, and (c) 40 GPM

Tracer studies were conducted at separate times and performed independently of each-other. For each physical tracer study flow rate was calibrated using an adjustable ball valve and a cumulative flow meter. Systems were allowed to come into steady state before testing was commenced. Prior to testing, solution was mixed in a plastic container with the use of an electric paint mixer. Solution was then injected into the main flow using a constant displacement pump and integrated via a static mixing tube. During sodium chloride testing conductivity was monitored at the outlet in a fabricated flow through device using a YSI EcoSense EC300A conductivity meter. For tests using lithium chloride, samples were taken at predetermined time

intervals using a tap (at the same location as the flow through device). All lithium samples were analyzed in the Soil, Water, and Plant testing laboratory at CSU using inductively coupled plasma-atomic emission spectroscopy.

4.6 Parametric Study

Inlet box dimensions were varied in order to determine the effects of geometric characteristics on BF formation. Investigated dimensions included box length, L_{Bx}, box height, H_{Bx}, and box width, W_{Bx}, which are labeled in Figure 4.4. L_{Bx} was varied between 1 and 4 feet, H_B was varied between 1 and 2 feet, and W_B was set equal to the tank width (4 feet) for all tested configurations. Each system was tested at flow rates of 10, 20, and 40 GPM in order to determine relative effects on gains in efficiency. Figure 4.6 shows generalized schematics of system setup.
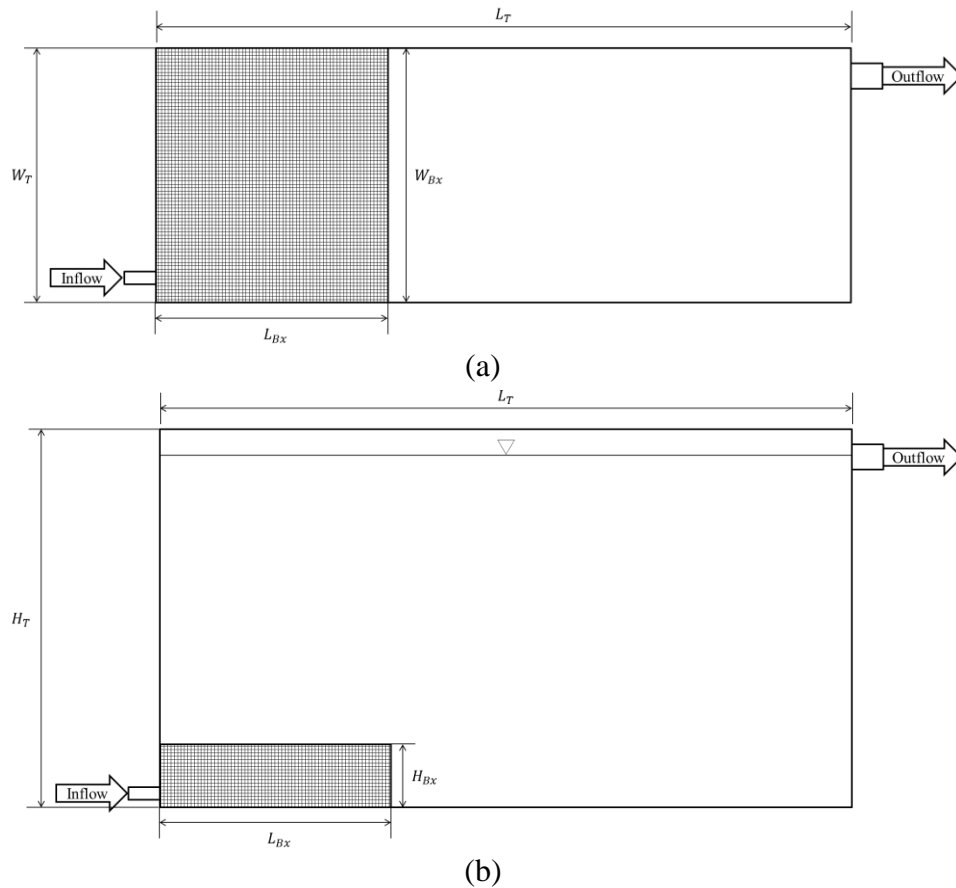

(a)

(b)

Figure 4.6: (a) Plan View and (b) Side View of a Generalized Inlet Box System

4.7 Results and Discussion

It was initially postulated that increasing L_{Bx} would be more beneficial than increasing H_{Bx} due to the orientation of the inlet. As show in Figure 4.6, L_{Bx} is parallel to the trajectory of inlet jet. This means that the majority of momentum resulting from the inlet is oriented along the direction of L_{Bx}. Therefore, as long as H_{Bx} is sufficient to cover the jet shown in the CFD results of Figure 4.1(a-f), increases in L_{Bx} should result in significant spreading of momentum. As shown in Table 4.1, results agree with this reasoning, but increases in hydraulic disinfection efficiency are highly dependent on flow rate.

Table 4.1: Inlet Box Parametric Study Results

Flow Rate, Q ft^3/s	Box Dimensions ($H_B \times L_B$) and BF					
	Base Case (No Box)	1ft X 1ft	1ft X 2ft	1ft X 4ft	2ft X 1ft	2ft X 2ft
10	0.05	0.19	0.21	0.26	0.25	0.22
20	0.05	0.21	0.30	0.33	0.25	0.28
40	0.05	0.24	0.34	0.36	0.28	0.15

4.7.1 L_{Bx} and H_{Bx} Vs. Baffling Factor

The geometric parameter L_{Bx} is not a useful design parameter by itself because it is dimensional and specific to the studied rectangular tank. In order to generalize resulting analysis, it is beneficial to normalize L_{Bx} by some other representative length. Two possible lengths are the length of the tank, L_T, and the diameter of the inlet, D_{inlet}. Since L_T is also system specific, it is not beneficial to use L_T as a comparative length scale. However, comparing L_{bx} to D_{inlet} provides a more insightful comparison because it corresponds to traditional literature regarding turbulent jets (Pope, 2000). The development length of turbulent jets, boundary layers, pipe flows, and even channel flows have been experimentally found to depend on ratios similar to x/D_{inlet}. For a free turbulent jet, the development length (l_d) is independent of the Reynolds

number and occurs at approximately $x/D_{\text{inlet}} = 30$. For wall bounded flows the development length is positively correlated with the Reynolds number due to the effects of shear introduced by the no slip condition (Pope, 2000).

Plots of L_{Bx}/D_{inlet} Vs. BF can be seen in Figure 4.7(a) and (b). Figure 4.7(a) shows the dependence of BF on L_{Bx}/D_{inlet} for $H_{Bx} = 1$ft, and Figure 4.7(b) shows the dependence of BF on L_{Bx}/D_{inlet} for $H_{Bx} = 2$ft. For the case where $H_{Bx} = 1$ft, there is a clear trend between the baffling factor and L_{Bx}/D_{inlet}. As L_{Bx} increases the rate of gain in the baffling factor decreases and starts to level out. In addition to increasing with L_{Bx}, gains in the baffling factor are positively dependent on flow rate, suggesting efficient disinfection rates at larger Reynolds numbers.

Sharply contrasting the first set of observations, results for the case where $H_{Bx} = 2$ft show no apparent trend regarding increases in baffling factor for either L_{Bx} or Q (See Figure 4.7(b)). Resulting systems performed poorly when compared to their $H_{bx} = 1$ft counterparts, converging on a baffling factor of around 0.25. This can be explained by plotting BF as a function of H_{Bx}/D_{inlet} for $L_{Bx} = 2$ft($12D_{\text{inlet}}$), which shows that increasing H_{Bx} beyond one foot($6D_{\text{inlet}}$) is detrimental to system performance (See Figure 4.8(a)). Similarly, if L_{Bx} is decreased to 1ft($12D_{\text{inlet}}$), increases in H_{bx} are only beneficial at lower Reynolds numbers and do not provide optimal performance (See Figure 4.8(b)).

In summary, optimal performance of inlet box structures occurs at low values of H_{Bx}/D_{inlet}, high values of L_{Bx}/D_{inlet}, and high Reynolds numbers. These observations can be explained by considering classical analysis of turbulent jets. As mentioned above, the development length of a free turbulent jet is approximately $30D_{\text{inlet}}$ and is independent of the inlet Reynolds number (Pope, 2000). For a partially wall bounded jet, the development length

should decrease below $30D_{\text{inlet}}$ as a result of shear induced from the no-slip condition. Based on fundamental analysis of wall bounded flows, the amount that l_d deviates from the free jet maximum will be dependent on the inlet Reynolds number. This implies that as the Reynolds number approaches infinity l_d should approach $30D_{\text{inlet}}$. Optimal performance of inlet box structures occurred at $L_{Bx}/D_{\text{inlet}} \approx 24$, suggesting that the maximum possible BF corresponds to $L_{Bx} = l_d$ given that $H_{Bx} \approx 6D_{\text{inlet}}$. This desirable height can be related to the developed diameter of the turbulent jet. For a free turbulent jet the spreading rate of the jet radius past the development length is approximately 0.1 (Pope, 2000). If this spreading rate were taken from the inlet, then the resulting diameter, $D_{\text{developed}}$, at a length of $30D_{\text{inlet}}$ would be approximately $6D_{\text{inlet}}$, which corresponds to the optimally observed value of H_{Bx}. Since a wall bounded jet is affected by boundary layer shear, the rate of spreading should be larger than for a free jet. It can therefore be argued that the 1ft X 4ft box exhibited $L_{Bx} \approx l_d$ and $H_{Bx} \approx D_{\text{developed}}$ and that an optimally shaped inlet box would follow the developing length of a turbulent jet.
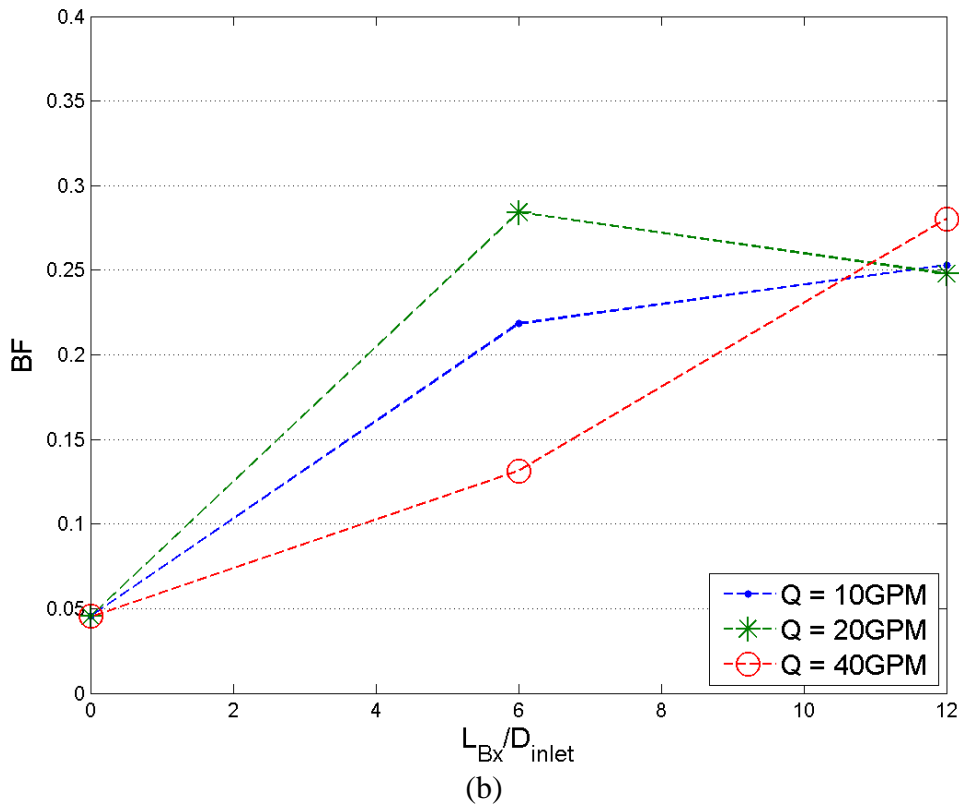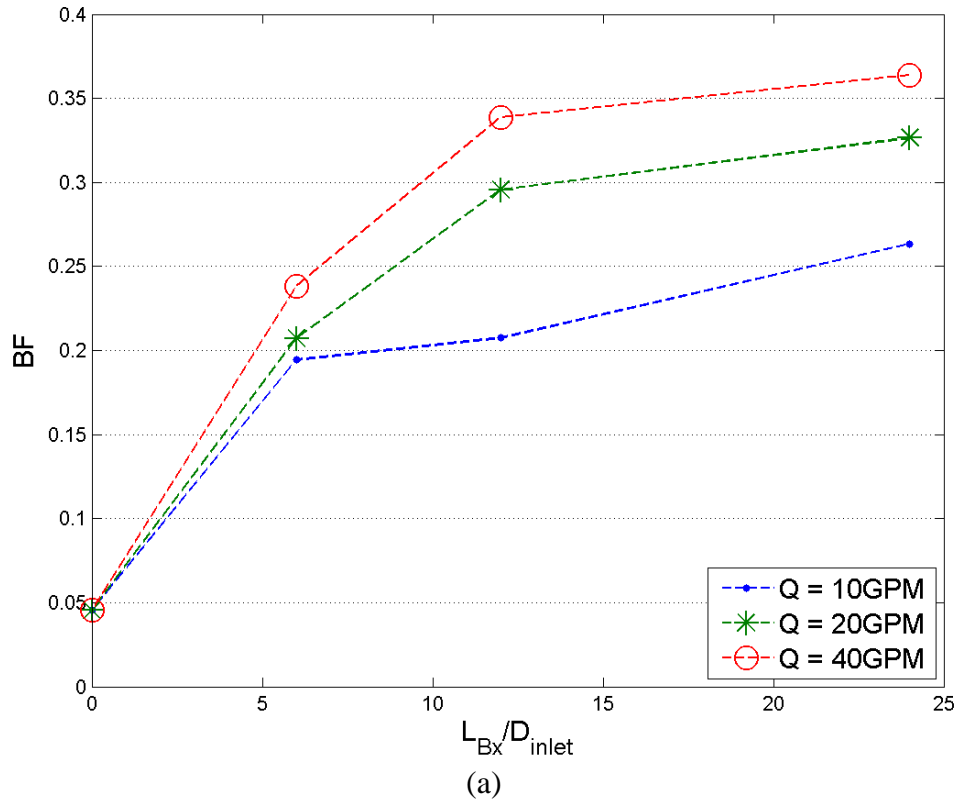
Figure 4.7: L_{Bx} Vx. Baffling Factor for (a) $H_{Bx} = 6D_{inlet}$ and (b) $H_{Bx} = 12D_{inlet}$
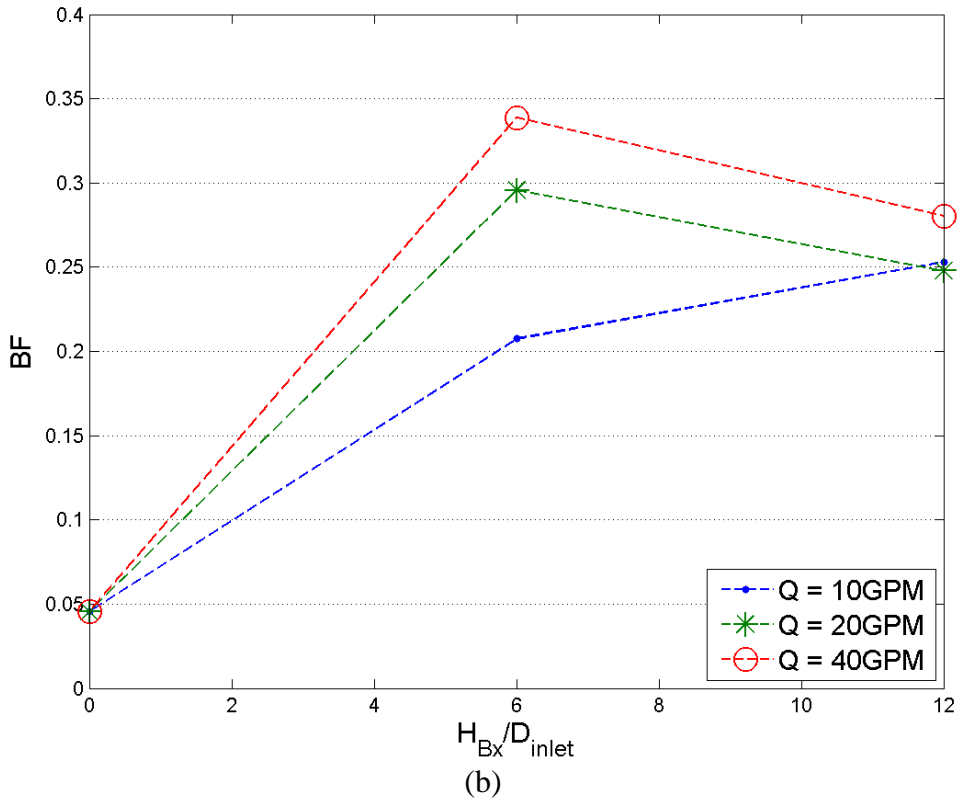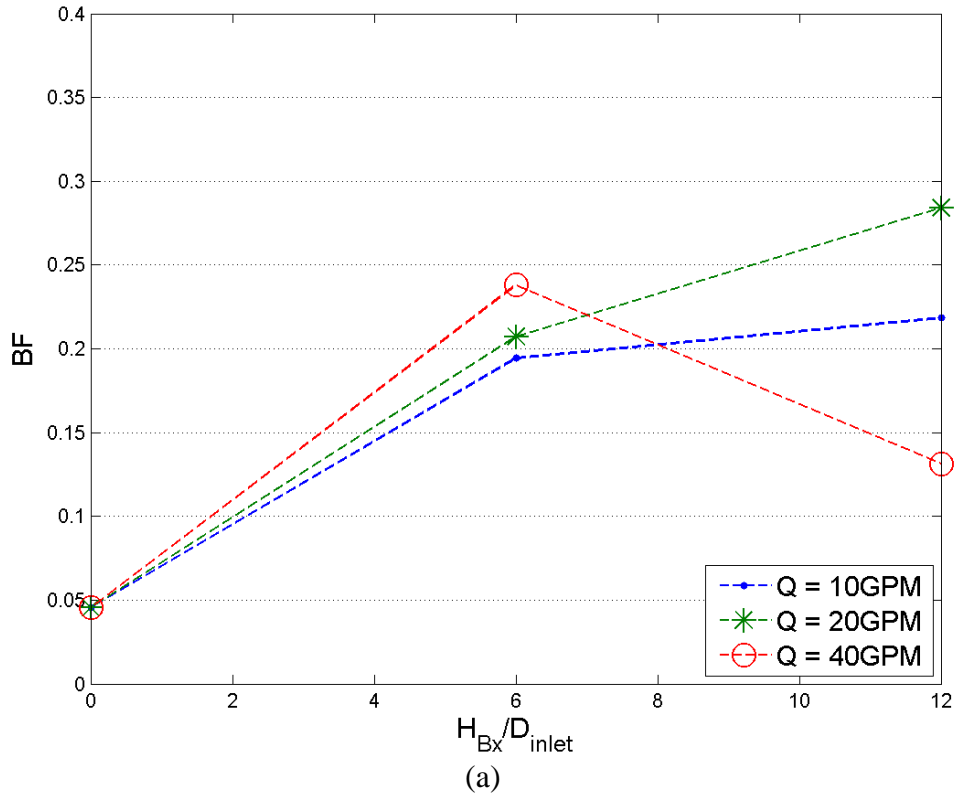
Figure 4.8: H_{Bx} Vs. Baffling Factor for (a) $L_{Bx} = 6D_{inlet}$ and (b) $L_{Bx} = 12D_{inlet}$

4.7.2 L_{Bx}/H_{Bx} Vs. Baffling Factor

By considering the ratio L_{Bx}/H_{Bx}, arguments from Section 4.7.1 can be reinforced and extended. Figure 4.9 shows the baffling factor as a function of L_{Bx}/H_{Bx}. Results suggest that the dispersive action of packing material is dependent on the incoming flow rate or Reynolds number. For low values of L_{Bx}/H_{Bx}, there is not a sufficient amount of packing material in the direction of the resulting jet to effectively re-distribute the flow, resulting in low baffling factors. This is particularly true at higher Reynolds numbers. It may even be that at lower values of L_{Bx}/H_{Bx} packing material forces the flow upwards towards the inlet, promoting short circuiting. When $L_{Bx}/H_{Bx} = 1$ it is more beneficial to have larger values of L_{Bx} and H_{Bx}, but resulting baffling factors are not as high as those obtained using lower values of H_{Bx}.
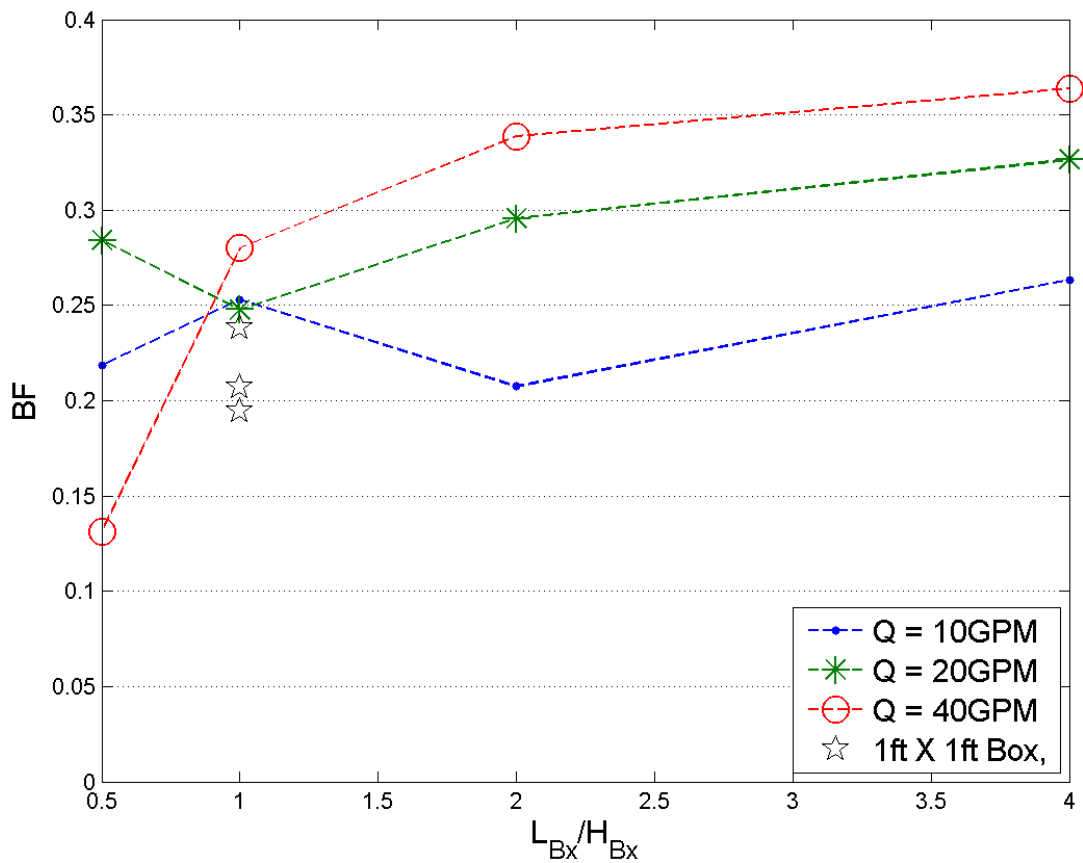

Figure 4.9: L_{Bx}/H_{Bx} Vs. Baffling Factor

As the flow rate increases so do the beneficial effects of increasing L_{Bx}/H_{Bx}. This can be attributed to the Re dependent l_d discussed in Section 4.7.1. As the Reynolds number increases, so does the development length and momentum of the inlet jet. Results suggest that values of L_{Bx} or H_{Bx} beyond the geometry of the inlet jet inhibits vertical and lateral mixing, which results in larger amounts of short circuiting and lower baffling factors. The use of packing boxes should increase the spreading rate of the resulting jet, diverting axial momentum to radial momentum and reducing short circuiting. However, too much packing material could dampen this effect, streamlining the flow.

It can be observed from results shown in Figure 4.10 that as L_{Bx} increases only the initial part of RTD curves are significantly affected. This supports the idea that the use of packing material reduces the severe short circuiting shown in the base system. However, the later portion of resulting RTD curves are comparable, suggesting that the system still exhibits significant amounts of recirculation. Potential gains in hydraulic disinfection efficiency through the use of packing material is therefore limited in an open system. Flow would have to be channelized in order to gain additional benefits.
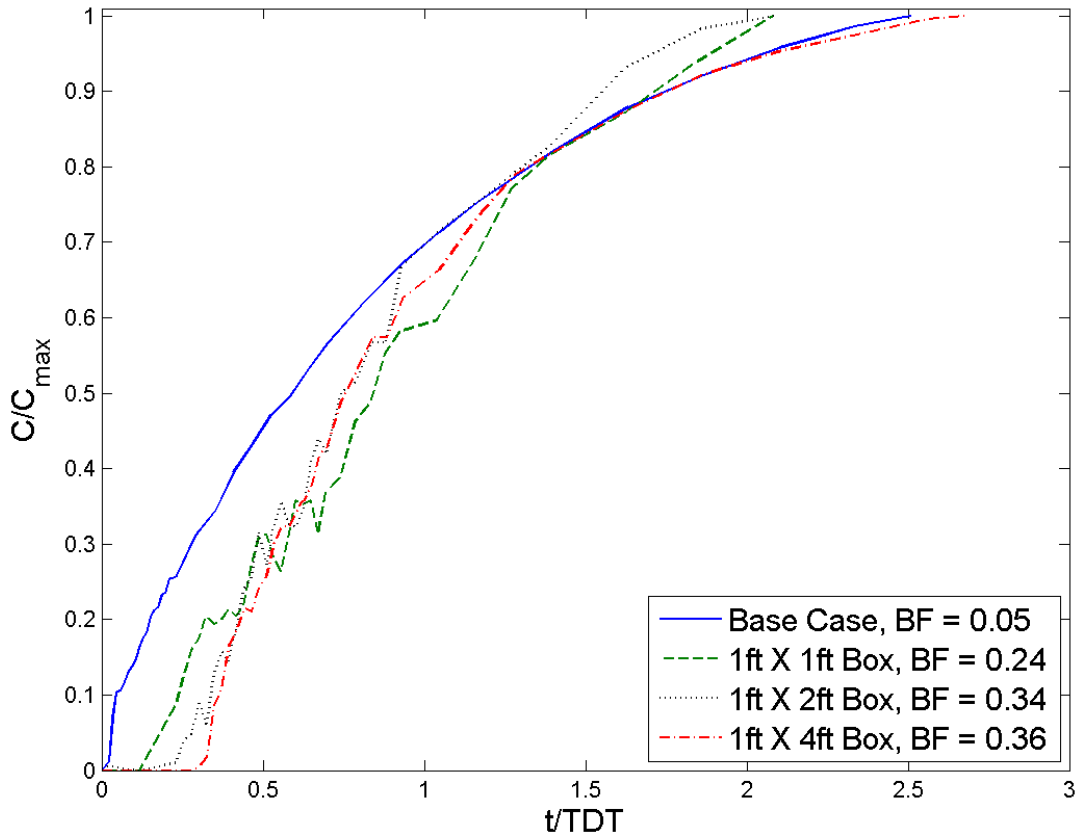
Figure 4.10: Resulting RTD Curves for Inlet Box Systems at a Flow Rate of 40 GPM

4.8 Conclusions

Use of random industrial packing material as an inlet modification can lead to significant gains in hydraulic disinfection efficiency for drinking water contact tanks. An open system with a baffling factor of 0.05 was successfully modified to achieve a baffling factor of 0.36, representing a 600% increase is disinfection capacity. Comparing this gain to results from Chapter 3 shows that inlet modification can be as effective as internal baffling for simple cases. However, increases in disinfection efficiency were highly dependent on flow rate. Use of lower flows resulted in baffling factor gains of less than half that of higher flows. In addition to this, resulting RTD curves exhibited signs of excessive re-circulation, which is not observed in baffled systems. Therefore, use of packing material as an inlet modification would be more beneficial in channelized or baffled systems.

Results from a parametric study suggest that gains in efficiency from the use of inlet boxes can be maximized by mimicking the geometry of a turbulent jet. Based off of classical arguments and observed data, the recommended ratios for design are $20 \leq L_{Bx}/D_{\text{inlet}} \leq 30$ and $H_{Bx}/D_{\text{inlet}} \approx 6$. Values of L_{Bx}/D_{inlet} should be lower for smaller flow rates and higher for larger flow rates. The purpose of these design guidelines is to divert momentum within the developing region of a resulting jet.

Additional research is required to tests the hypothesis of inlet box performance based on turbulent jet geometry. In addition to varying L_{Bx} and H_{Bx}, effects of varying the inlet box width, W_{Bx}, should also be considered. Similarly, research is required to determine the potential for bacterial growth on the surface of porous media within chlorinated disinfection tanks. Research mentioned by Barnett et al (2014) suggests that packing material plastics were unreactive with chlorine, but this has not been extensively tested within the environment of a disinfection contact tank. Other types of packing material should also be investigated for use as inlet and system modifiers.

CHAPTER 5: APPLICATION OF RANDOM PACKING MATERIAL IN BAFFLED CONTACTORS

5.1 Introduction

Research presented in Chapter 4 showed that the use of random packing material as an inlet modifier could significantly reduce short circuiting induced by a turbulent jet. Application of this technique to an open rectangular contact tank yielded baffling factors of around 0.36. Similar gains in disinfection efficiency were observed for a two-baffle system studied in Chapter 3. However, velocity contours within this baffled system showed significant amounts of short circuiting resulting from the use of a sharp inlet, causing flow to bypass the first two channels. In contrast to this issue, measured RTD curves from packing material systems suggested excessive amounts of recirculation, which resulted from the lack of channeling.

Research presented in this chapter seeks to reduce both short circuiting and recirculation by investigating the application of random packing material within a baffled system. Combining these two methods provides an innovative solution which reduces the number of baffles and maximizes potential gains. CFD was used as a guide in this endeavor, facilitating the placement of random packing material at areas of high velocity and flow separation (at the inlet and at baffle turns). Results suggest the creation of a highly efficient system ($BF \approx 0.70$).

5.2 Issues with the Inlet

Proposed modifications were applied to a rectangular system employing the use of two elongated baffles. For the considered system L_{bo} was set equal to W_{ch} and baffles were placed parallel to the long axis of the tank. Velocity contours from a validated simulation of this system can be seen below in Figure 5.1(a-f). The presence of a sharp inlet results in the formation of a turbulent jet, inducing significant amounts of short circuiting and vertical recirculation in the first and second baffle channels (See Figure 5.1(a-d)). Fully developed flow does not occur until the

third channel, suggesting losses of up to two-thirds of potential contact volume (See Figure 5.1(e-f)). A three-dimensional region of influence from the turbulent jet can be seen in Figure 5.2(a) and (b). This region is similar in shape and size to the region observed without the use of baffles, but it is blocked from the outlet by a baffle wall and has a greater vertical extent (See Section 4.2). In addition to short circuiting caused by the inlet, Figure 5.1(a-f) show flow separation at baffle turns. Reducing these effects could increase hydraulic disinfection efficiency.
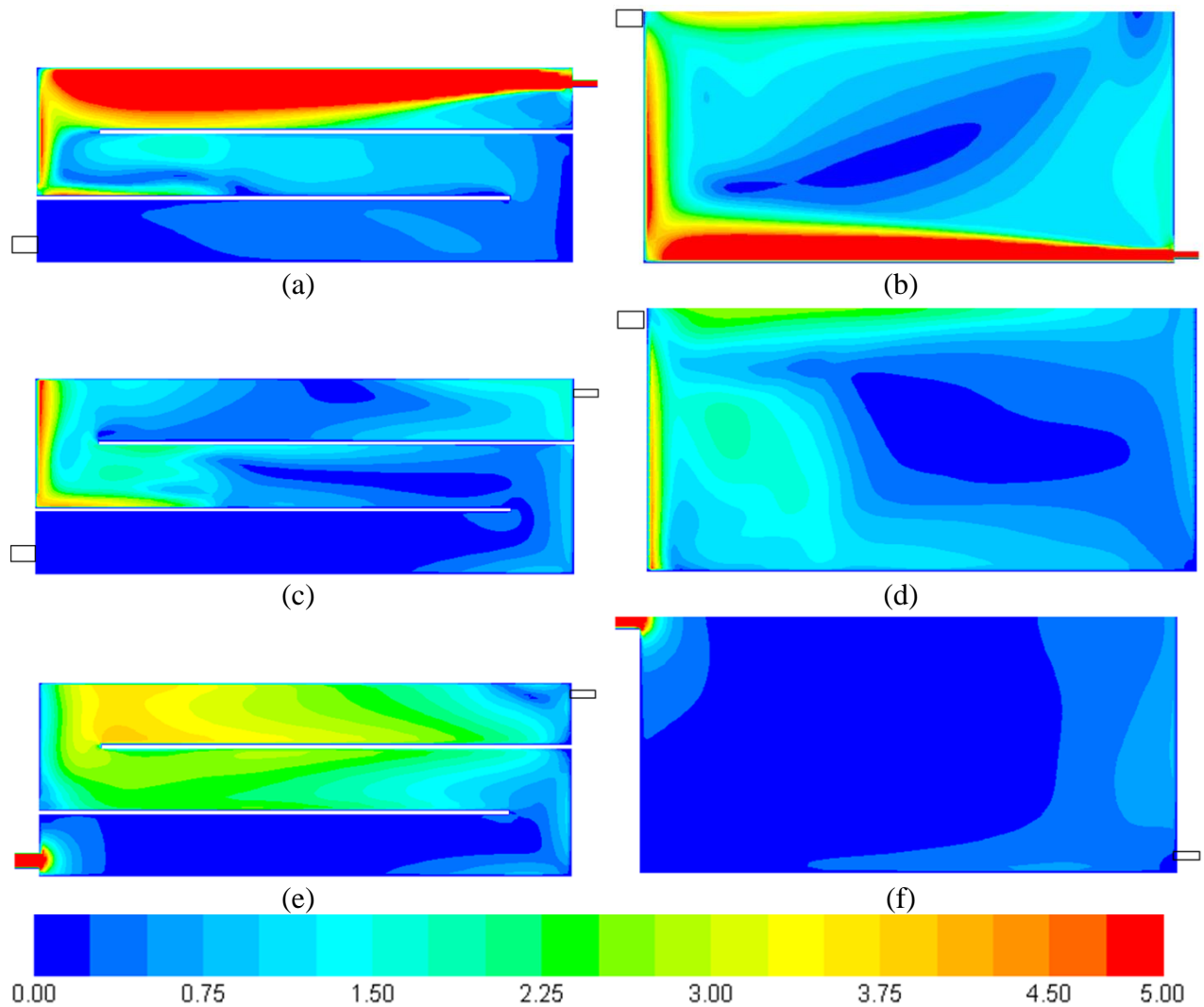

(a)   (b)

(c)   (d)

(e)   (f)

Figure 5.1: Normalized Contours of Velocity Magnitude ($V/V_{average}$) on (a) a Horizontal Plane Intersecting the Inlet, (b) a Vertical Plane Intersecting the Inlet, (c) a Horizontal Plane Intersecting the Center of the Tank, (d) a Vertical Plane Intersecting the Center of the Tank, (e) a Horizontal Plane Intersecting the Outlet, and (f) a Vertical Plane Intersecting the Outlet
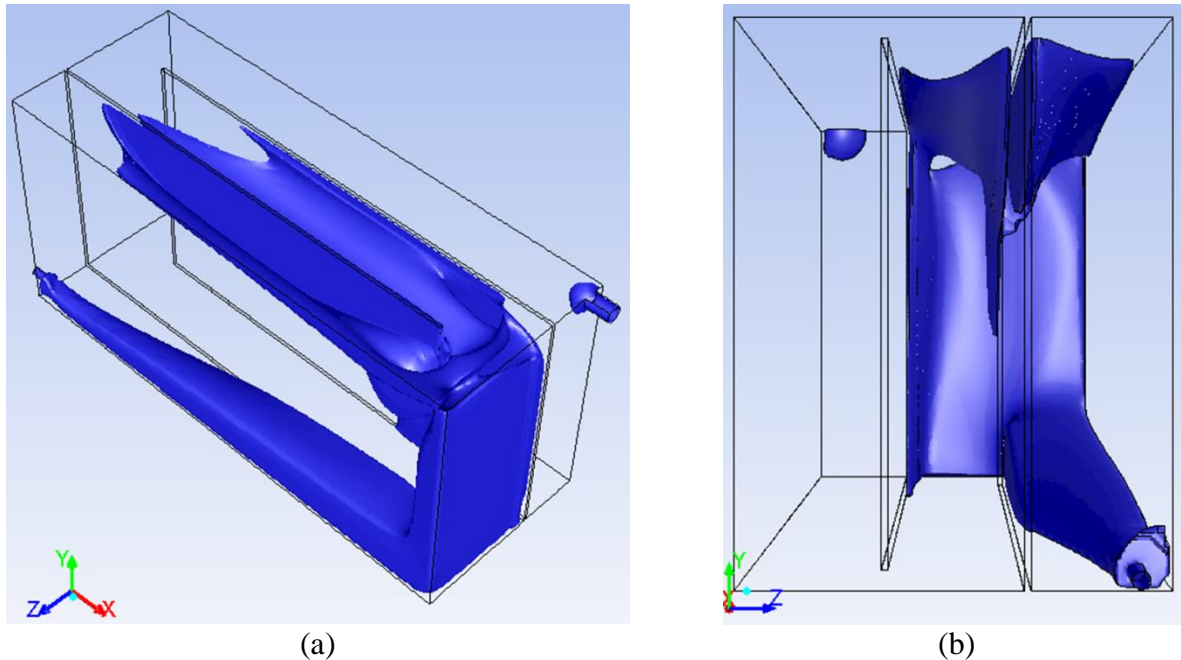
<div align="center">(a)   (b)</div>

Figure 5.2: (a) Isometric View and (b) Back View of a 3D Iso-Surface of Velocity Magnitude Corresponding to $V \geq 2V_{\text{average}}$

5.3 Turn Box Design

Review of CFD results for the baffled system revealed that significant amounts of flow separation and short circuiting occurred at the inlet and at baffle turns. Packing material was placed at these locations within the prototype and gains in efficiency were measured at flow rates between 10 and 50 GPM. For the first modified system a 1ft X 4ft ($H_B \times L_B$) packing material box was placed over the inlet. Inlet box dimensions were chosen based on results from Chapter 4. The inlet box was constructed and installed in a similar manner to those studied in Chapter 4. A photograph of the constructed inlet box within the baffled prototype can be seen in Figure 5.3(a). The second modified system made use of 6" wide structures to fully cover each baffle turn. The purpose of these structures was to promote uniform flow and reduce the formation of circulatory currents within the second baffle channel. Labeled turn boxes, these structures were constructed out of chicken wire mesh. Photographs of the final turn box system can be seen in Figure 5.3 and a general schematic of the final system can be seen in Figure 5.4.

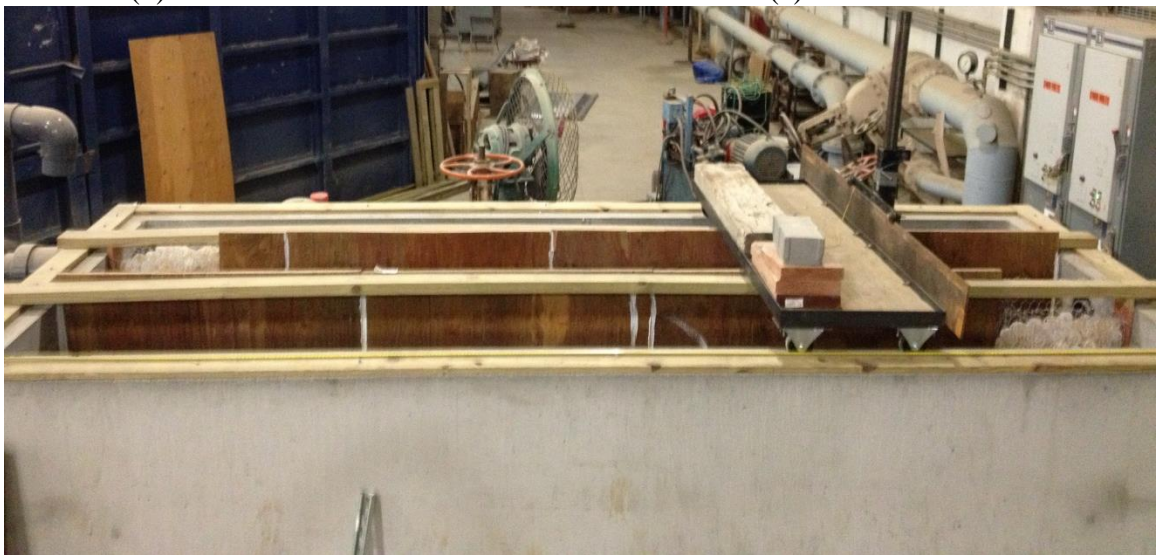<div align="center">88</div>

(a)   (b)   (c)

(d)   (e)

(f)

Figure 5.3: Photographs of (a) Inlet box and (b-f) Turn Box Structures in a Baffled Prototype
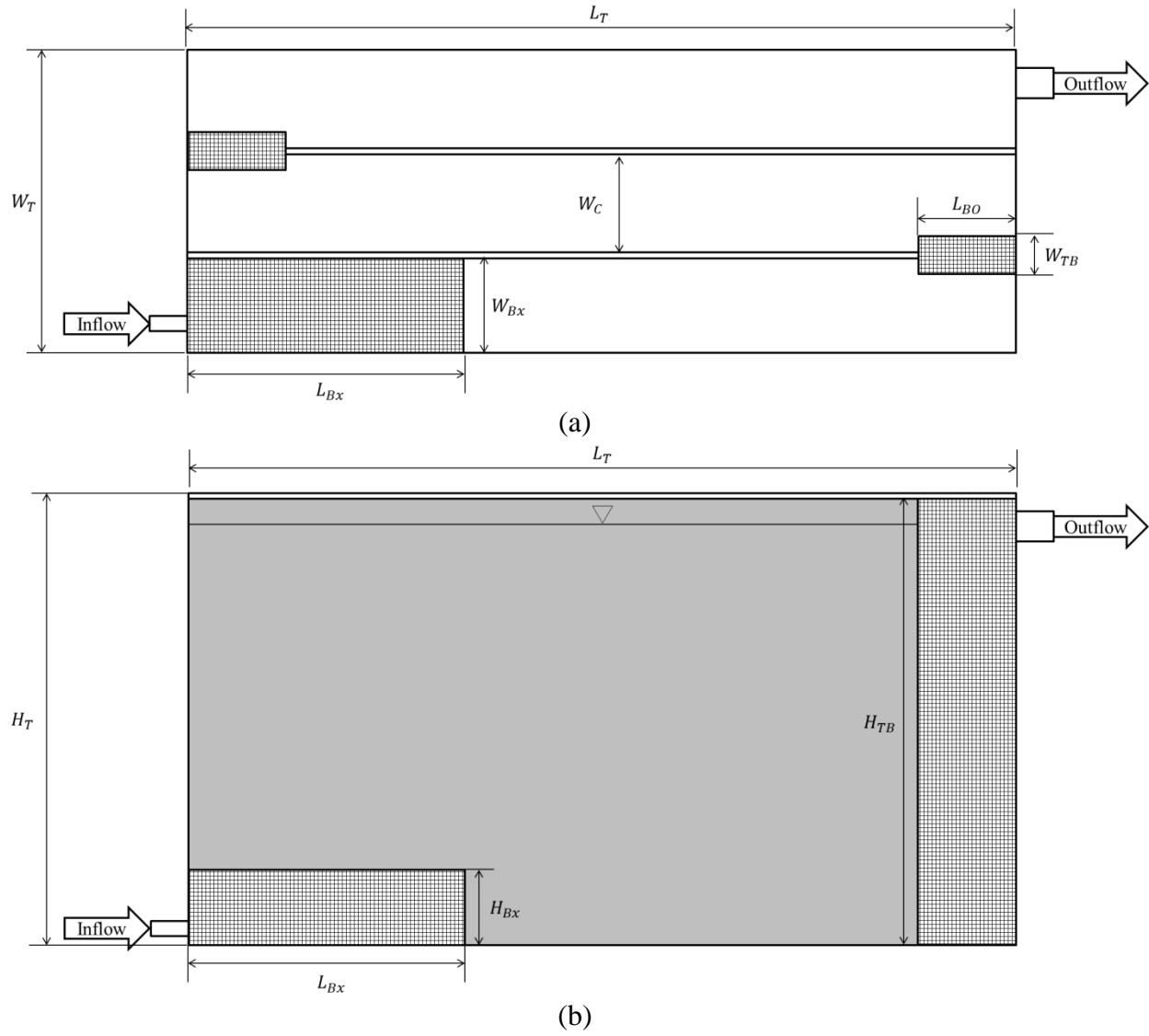
Figure 5.4: (a) Plan View and (b) Side View of a Generalized Turn Box System

5.4 Methodology

Step-wise physical tracer studies were conducted to determine the hydraulic disinfection efficiency of system prototypes. Tracer studies were conducted using the steps outlined in Sections 3.4.1 and 4.5. A total of twenty separate tests were performed using sodium-chloride as a conservative tracer. Two of these tests were redone using lithium-chloride in order to validate the use of conductivity and sodium-chloride in the development of RTD curves. Lithium

validation for this study was already presented in Chapter 3, so it is not reciprocated here (See Figure 3.5(b)).

In total, three different systems were tested for this study. The first system that was tested was the baffled system shown in Figure 3.3(b), which did not contain any packing material modifications. The second studied system considered the modification of the first with a 1ft X 4ft inlet box. The third, and last system that was studied contained a 1ft X 4ft inlet box and two 6" turn boxes. Photographs and schematics of baffled packing box systems can be seen in Figure 5.3 and Figure 5.4. The first system was tested at flow rates of 20 and 40 GPM, the second system was tested at 20 GPM, and the final system was tested at flow rates of 10, 20, 30, 40, and 50 GPM in order to determine relative effects on gains in hydraulic disinfection efficiency.

Once physical tracer studies were completed, a Nortek Vectrino Acoustic Doppler Velocimeter (ADV) was used in an attempt to construct three-dimensional velocity profiles within the final turn-box system. The purpose of this exercise was to obtain qualitative insight regarding observed increases in system performance. Initial testing suggested that a sampling rate of 75 Hz with a nominal velocity range of ± 0.03 m/s and a sampling time of 2 minutes yielded reproducible results. Remaining velocities were collected using these settings. A total of 342 point measurements were taken across four different elevations of the tank. Measured elevations included 6 in., 12 in., 24 in., and 36 in. from the channel bottom. Measurements 6 in. from the bottom were not completed due to observation of inappropriate sound to noise ratios (SNRs) and excessive interference. ADV measurements were conducted with the use of a fabricated point-gauge and measurement cart, which are shown in Figure 5.5(a-c).
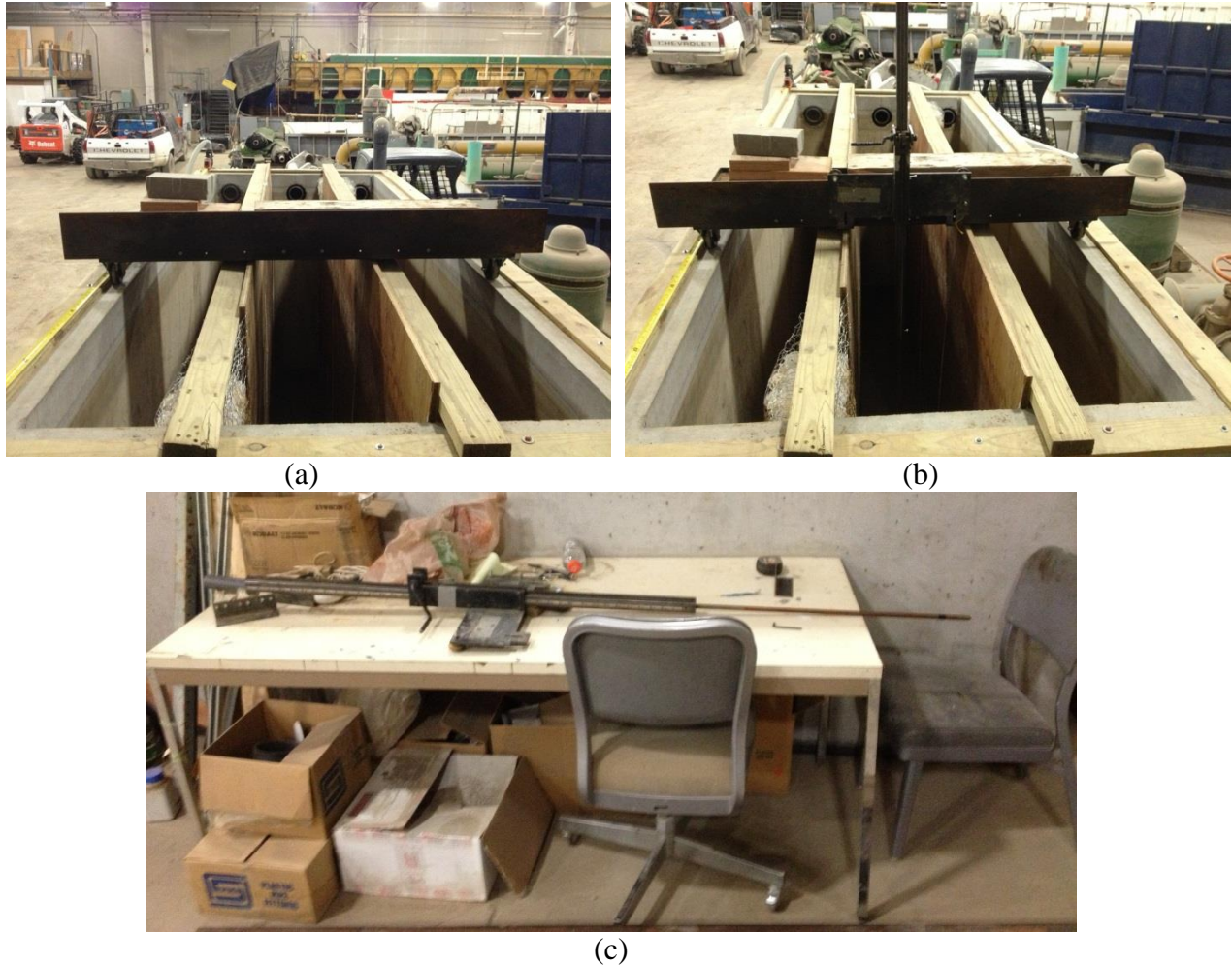
(a)   (b)

(c)

Figure 5.5: Photographs of Fabricated (a) Measurement Cart and (b-c) Point Gauge Used to facilitate ADV Measurements

5.5 Results and Discussion

RTD curves for all physically tested baffled systems can be seen in Figure 5.6(a) and (b). Results displayed in Figure 5.6(a) clearly show that localized application of random packing significantly increases the hydraulic disinfection efficiency of baffled systems, validating applied methodology. As discussed in Chapter 4, use of packing material at the inlet promotes residence time by diffusing the momentum of the incoming jet, reducing short circuiting. Velocity vectors in Figure 5.7(d) demonstrate this by showing vertical redirection of flow caused by the presence of packing material over the inlet. Benefits obtained through the introduction of turn boxes are

92

more difficult to attribute. Review of CFD results for the unmodified baffle system suggests two possible reasons for efficiency gain through the use of turn boxes: (1) additional diffusion of the turbulent jet at the first baffle turn or (2) reduction in flow separation around baffle tips. Results from the parametric study in Chapter 3 showed that lower values of L_{bo} resulted in more efficient systems due to additional choking of separated flow at baffle turns. This makes the first mode of increase more likely. Resulting ADV measurements support this theory. Figure 5.7(a-f) show resulting velocity vectors from ADV analysis. Reversed flow can be observed in the center channel, suggesting the presence of a circulating structure. A similar structure was observed in CFD simulations of the un-modified baffle system, suggesting that the effects of the jet have not been completely eliminated. In addition to this, the largest lateral velocities occur in the third channel, suggesting vertical mixing in the first two channels. These observations support the idea that turn boxes are only beneficial due to the dispersive action of the first baffle turn. Additional research is needed in order to determine if the second turn box has any effect.

Figure 5.8 displays a plot of flow rate against BF for the most efficient case (baffles, inlet box, and turn boxes). As flow rate increases the use of inlet and turn boxes becomes exceedingly beneficial. The baffling factor peaks at around 0.7 for flow rates greater than 40 GPM, but observed benefits diminish at flow rates less than 20 GPM. The introduction of packing material increases hydraulic disinfection efficiency by dispersing kinetic energy and redistributing the flow. Therefore, if the Reynolds number of flow through the inlet is very low (approaching the transitional regime) the packing material will not effectively distribute velocity and may even constrict the flow. This may be related to the range of scales occurring in the flow decreasing compared to the pore size of the packing material.
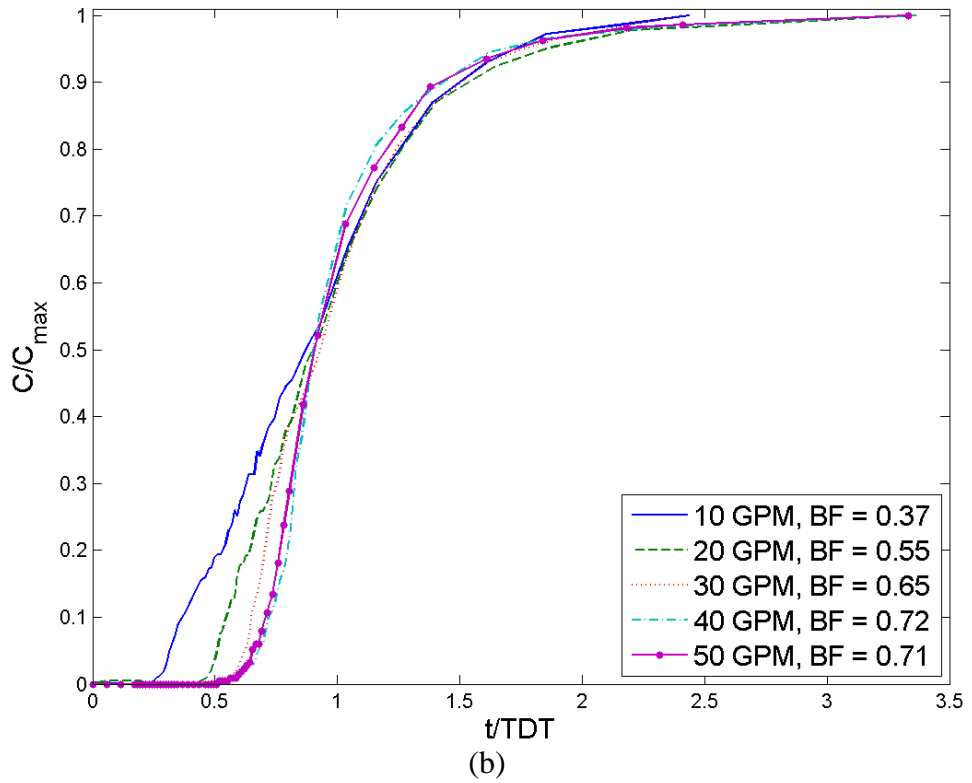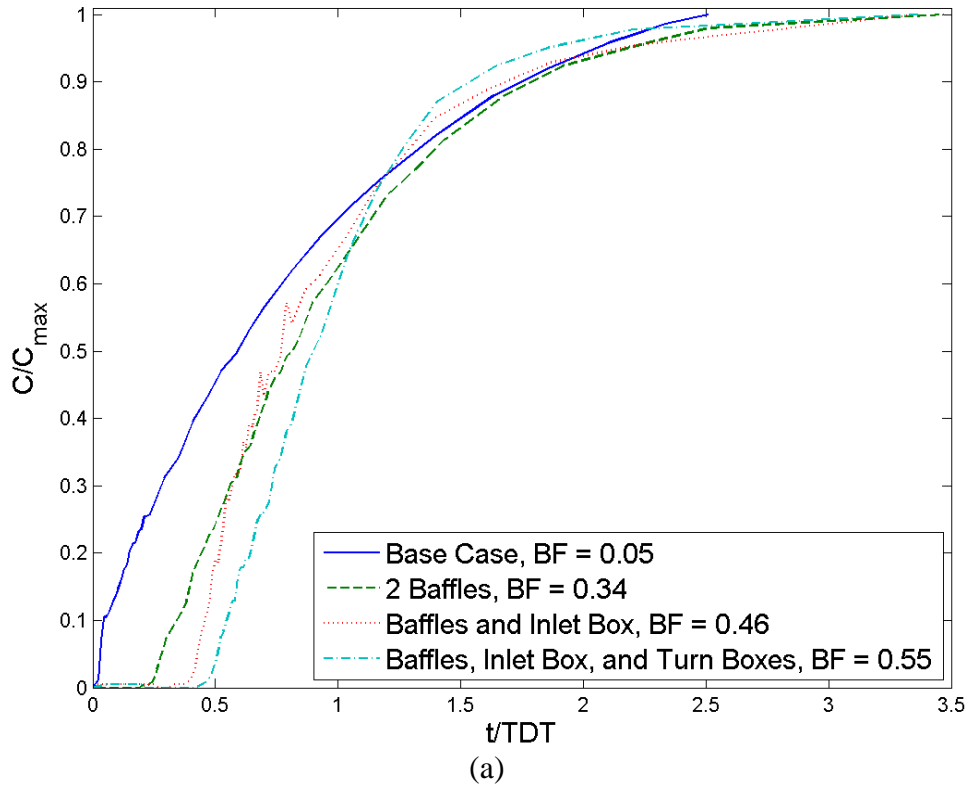
Figure 5.6: Resulting RTD Curves for (a) All Tested Systems at a Flow Rate of 20 GPM and (b) the Turn Box System at Various Flow Rates
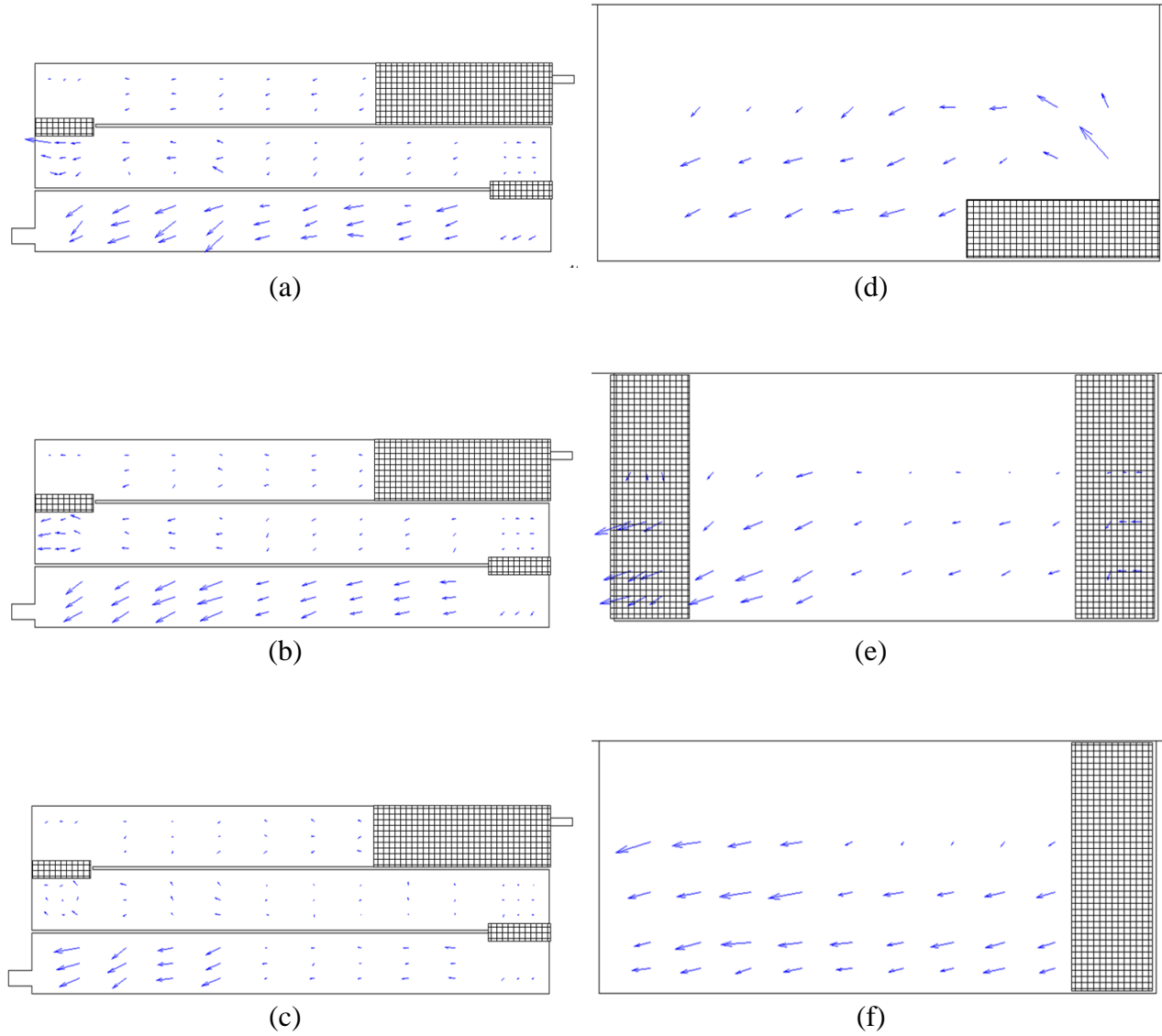
Figure 5.7: Resulting Velocity Vectors from ADV Measurements (a) 12 in. from the Bottom, (b) 24 in. from the Bottom, (c) 36 in. from the Bottom, (d) at the Center of the First Channel, (e) at the Center of the Second Channel, and (f) at the Center of the Third Channel
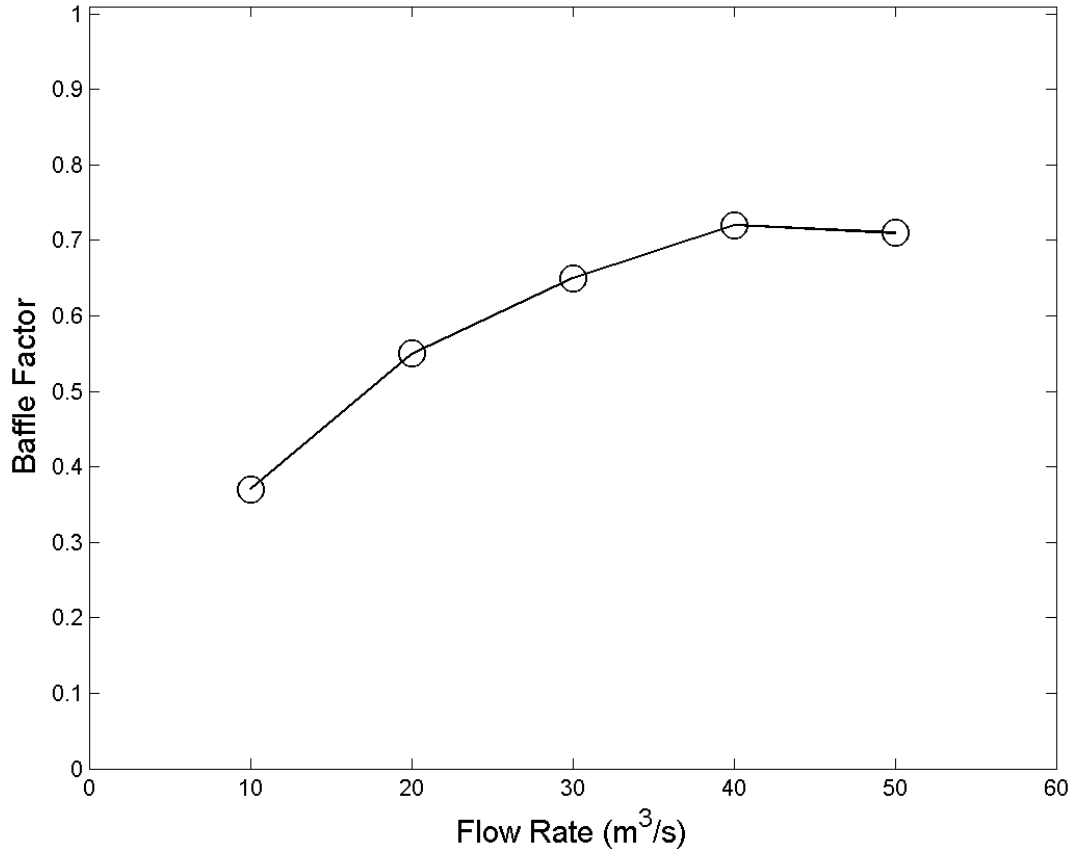
Figure 5.8: Flow Rate Vs. Baffling Factor for a Baffled System Employing and Inlet Box and Turn Boxes

5.6 Possible Alternatives

Gains in hydraulic disinfection efficiency using local application of random packing material only proved to be effective at larger flow rates or higher Reynolds numbers. Research conducted by Taylor and Barnett suggests that more simplistic means of inlet modification, such as the use of elbows or tees, are less dependent on changes in flow rate (Taylor, 2012; Barnett, 2014). Several additional CFD simulations were conducted to investigate some of these simpler modifications and to assess their potential for increasing hydraulic disinfection efficiency.

Additional modifications included complete reorientation of the inlet, use of a left facing elbow, and use of a right facing elbow. In addition to these cases an "idealized" case was simulated that utilized the entire channel wall as an inlet. This idealized case was simulated in

96

order to approximate a maximum obtainable baffling factor. All of these additional scenarios were run at a flow rate of 20 GPM. Resulting RTD curves from this analysis can be seen in Figure 5.9 and a comparison of velocity profiles can be seen in Figure 5.10(a-e). Use of simple tees as an inlet modification reduces the influential zone of the jet to the first channel. As a result, all modifications yield a baffling factor of around 0.60. If the investigated modifications perform independently of flow rate, then they would outperform the turn box system for inlet Reynolds numbers below 47,500. Installation of a simple elbow is much easier and more cost effective than constructing packing material structures, so these simple options appear more attractive. These conclusions should be experimentally validated and the performance of these simple modifications should be tested at different flow rates.
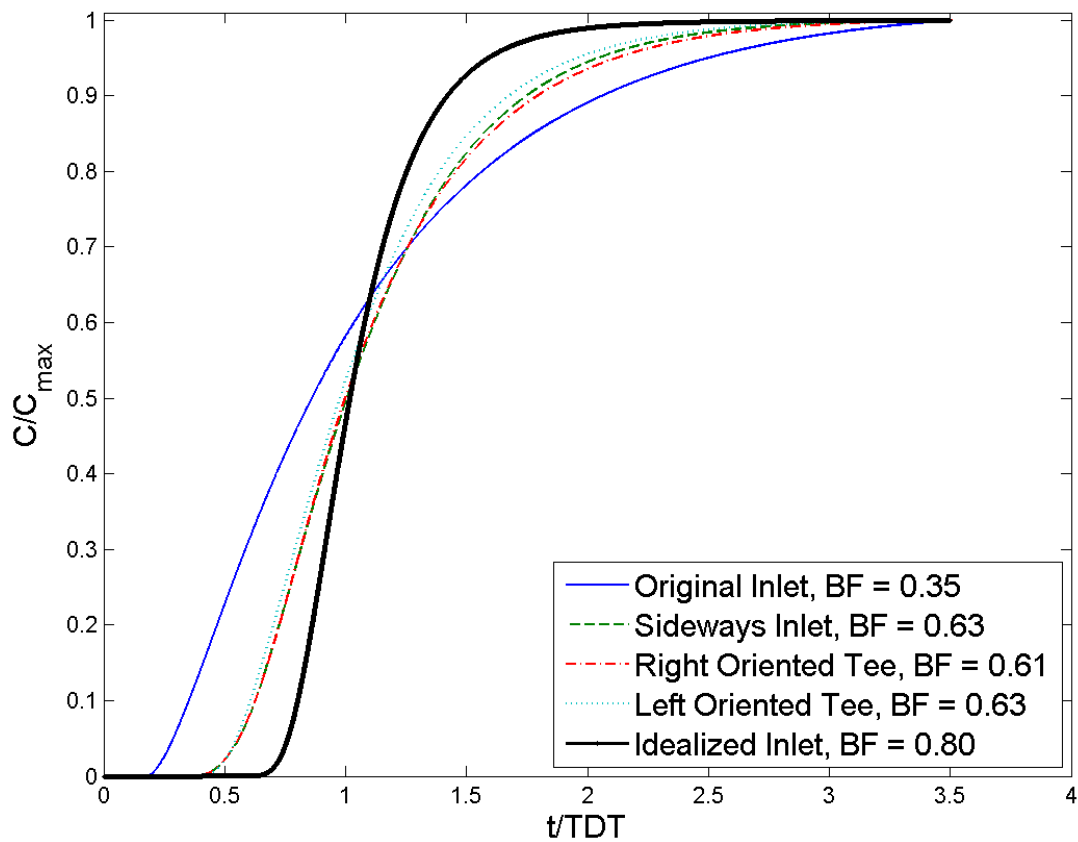

Figure 5.9: Resulting RTD Curves for Different Simple Inlet Modifications
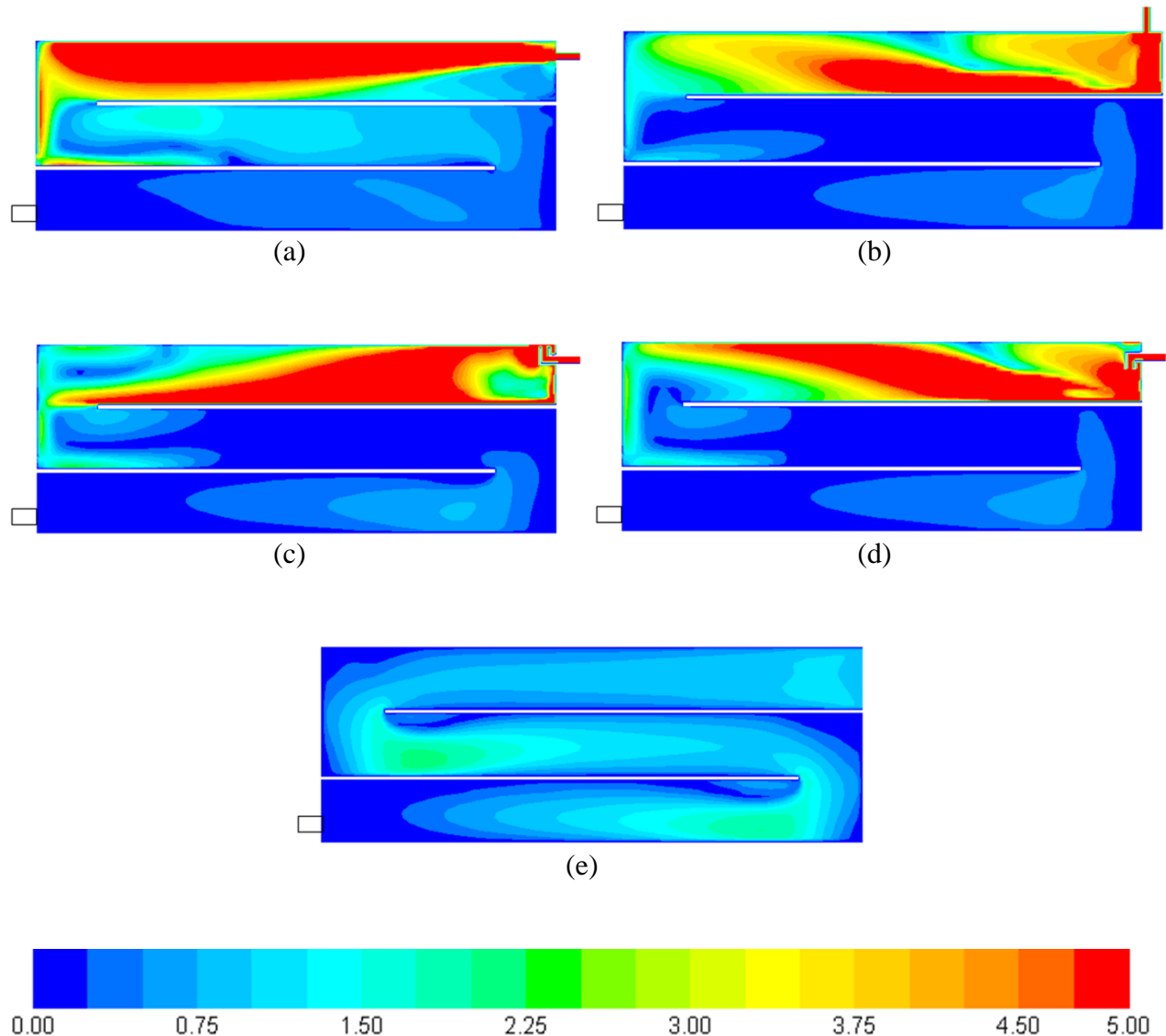
Figure 5.10: Normalized Velocity Contours (V/V_{average}) on a Plane at the Inlet within a Two Baffle System for (a) the Original Inlet Condition, (b) a Sideways Inlet, (c) a Right Facing Tee Inlet, (d) a Left Facing Tee Inlet, and (e) an Idealized Inlet

5.7 Conclusions

Local application of random packing material proved to be an effective means of increasing hydraulic disinfection efficiency within baffled systems. Physical tests showed that the application of random packing material to areas of high velocity and flow separation can lead to gains in efficiency. Successful application is dependent on flow rate and gains are most prominent when material is placed parallel to the main direction of flow. CFD was shown to be

an invaluable tool in designing these modifications, as knowledge of internal hydraulics is required to drive efficient design.

ADV measurements within a baffled packing material system demonstrated the ability of random packing material to disperse inlet momentum and redirect flow. However, existence of similar flow structures between CFD results and ADV measurements suggest that effects of the incoming jet were not completely eliminated by the placement of packing material. As a result, placement of turn boxes was deemed beneficial only as a means of further reducing the effects of a sharp inlet.

High dependence on Reynolds number for system performance led to the investigation of alternate inlet modifications. Using CFD it was found that the implication of a single tee or elbow could result in baffling factors around 0.6, outperforming packing material systems for a wide range of flow rates. These results need to be validated through physical testing of a corresponding prototype. Dependence on flow rate for these simpler inlet modifications should also be investigated.

As stated in Chapter 4, there is yet to be a study that considers the potential for bacterial growth on random packing material within chlorinated systems. This should be investigated and resulting effects on system performance should be quantified.

CHAPTER 6: SUMMARY AND CONCLUSIONS

6.1 Summary of Research

Research presented and conducted for this thesis summarizes work that is both unique and insightful. A combination of CFD, physical tracer studies, and acoustic doppler velocimetry were used to investigate the internal hydraulics of drinking water contact tanks. Results of these investigations were then used to develop and tests beneficial system modifications. Chapter 3 presented a detailed parametric study which extended the work of Taylor (2012) and Barnett (2013). This study considered baffled systems with a sharp inlet, providing new insight by looking at the placement of baffles parallel to the long axis of a tank. Over 39 CFD simulations were performed for this parametric study, and results from several CFD simulations were directly validated through physical testing of a full-scale prototype.

Chapter 4 considered the local application of packing material as an alternative to internal baffling. Packing material was organized in box-like structures and placed over the inlet in order to facilitate diffusion of the resulting jet. An extensive parametric study was then performed to investigate the importance of geometric characteristics on changes in system performance. This process involved the completion of 40 tracer studies.

Chapter 5 extended the work of Chapters 3 and 4 by considering placement of random packing material within a baffled system at areas of high velocity and flow separation (at the inlet and at baffle turns). Resulting systems were analyzed at a number of flow rates and then compared to simpler types of modification. Throughout this study three separate systems were physically tested using 22 different tracer studies. ADV measurements were then taken at 342 points within the most efficient system.

6.2 Major Conclusions

The parametric study presented in Chapter 3 showed that L_{bo}/W_{ch} should be minimized for baffled systems utilizing a poorly oriented sharp inlet and that the parameter L^* should be less than 40%. Systems with $L^* > 0.40$ exhibit channeling of flow around baffle tips, resulting in short circuiting and a loss in disinfection efficiency. Comparing results with the work of Taylor (2012) and Barnett (2013) showed that inlet type and orientation have a significant impact on potential gains in efficiency. Inlet type and orientation also significantly impact rates of increase for the baffling factor with respect to geometric parameters. If possible, the inlet should be directed towards a nearby wall or surface to allow for the distribution of momentum. Only then will large values of L_T/W_{ch} be beneficial. Study results also showed that the USEPA design tables are grossly non-conservative, overestimating the baffling factor by as much as 100%.

Research presented in Chapter 4 showed that the most effective inlet modification using random packing material covers the developmental region of a turbulent jet. Increasing H_{Bx} beyond the resulting diameter of a turbulent jet can be detrimental to system performance, resulting in lower baffling factors. In general the conditions $20 \leq L_{Bx}/D_{\text{inlet}} \leq 30$ and $H_{Bx} \approx 6D_{\text{inlet}}$ should be met for optimal performance. Increases in hydraulic disinfection efficiency were found to be highly dependent on flow rate and resulting RTD curves were significantly diffusive. Open systems using random packing material are limited to a maximum baffling factor of 0.36 due to recirculation that occurs outside of the packing zone region.

Results from the study in Chapter 5 showed that the most effective and inexpensive system could be obtained through a combination of internal baffling and inlet modification. The most beneficial packing material system was achieved through placement of random packing material at the inlet and at baffle turns. ADV results showed that packing material helps to

spread the incoming jet but does not completely remove its effects. Maximum obtainable baffling factors were around 0.7 and gains in baffling factor were heavily dependent on flow rate. Use of an elbow at the inlet to redirect the flow was investigated as an alternative to packing material modification. Different configurations of elbow inlets outperformed packing material flow rates for inlet Reynolds numbers below 47,500. These results still need to be validated with physical tracer studies.

6.3 Suggestions for Futures Research

In order to expand the observations made within this thesis, the following recommendations are made for future research:

- The parametric study from Chapter 3 should be extended through consideration of a variably sized inlet at different orientations. It is hypothesized that the ratio of the inlet area to the channel area will have a significant impact on study results. Head-loss near the inlet should also be quantified for a number of potential conditions and used as a scaling parameter.

- A study should be conducted in order to investigate the long term effects of using packing material in chlorinated contactors. Packing material is designed to have larger surface areas, which could potentially facilitate biofouling or attract unwanted mineral buildup. The likelihood of these occurrences should be quantified.

- Effects of stability stratified flow within disinfection contact tanks should be investigated to determine losses in effective volume. If a plant has a heated treatment area and is drawing from a naturally cold source it is possible for a stable gradient to develop and for effective volume to decrease. Hydraulic disinfection efficiency should be quantified for this particular case.

REFERENCES

Amini, R; Taghipour, R; & Mirgolbabaei, H. 2011. Numerical assessment of hydrodynamic characteristics in chlorine contact tank. *J. Numer. Meth. Fluids,* **67**, 885-898.

ANSYS. 2011. ANSYS FLUENT Theory Guide

Baawain, M.S; El-Din, M.G; & Smith, D.W. 2006. Computational fluid dynamics application in modeling and improving the performance of a storage reservoir used as a contact chamber for microorganism inactivation. *Journal of Environmental Engineering and Science*, **5**, 151-162.

Barnett, T.C. 2013. *Flow Dynamics and Scalar Transport in Drinking Water Contact Tanks*. Master's Thesis, Department of Civil and Environmental Engineering, Colorado State University, Fort Collins, CO.

Barnett, T.C.; Kattnig, J.J.; Venayagamoorthy, S.K; Whittaker, G. 2014. Improving Drinking Water Contact Tank Hydraulics Using Random Packing Material. *J. American Water Works Association* (AWWA). DOI: http://dx.doi.org/10.5942/jawwa.2014.106.0005

Chan, H.C; Huang, W.C; Leu, J.M; Lai, C.J. 2007. Macroscopic modeling of turbulent flow over a porous medium. *International Journal of Heat and Fluid Flow*, **28**, 1157-1166.

Chorin, A.J. 1968. Numerical Solution of the Navier-Stokes Equations. *Mathematics of Computation*, **104(22)**, 745-762.

Davis, M.L; Cornwell, D.A. 2008. *Introduction to Environmental Engineering*; McGraw Hill: New York.

Fei, W.Y; Wang, Y.D; Song, X.Y; Yin, Y.D; & Sun, LY. 2003. Intensification of random packing via CFD simulation, PIV measurement and traditional experiments. *Journal of Chemical Technology and Biochemistry*, **78**, 142-145.

Hannoun, I.A; Boulos, P.F; & List, J. 1998. Using hydraulic modeling to optimize contact time. *Journal American Water Works Association*, **90(8)**, 77-87.

Kavanaugh, M.C; & Trussell, R. Rhodes. 1980. Design of aeration towers to strip volatile contaminants from drinking water. *J. American Water Works Association* (AWWA), **72(12)**, 684-692.

Kazerooni1, R.B; & Hannail, S.K. 2009. Simulation of Turbulent Flow Through Porous Media Employing a v2f Model. *Scientia Iranica*, **16(2)**, 159-167.

Khan, L.A; Wicklein, E.A; & Teixeira, E.C. 2006. Validation of a Three-Dimensional Computational Fluid Dynamics Model of a Contact Tank. *J. Hydraulic Engineering*, **132**, 741-746.

Kothandaraman, V; Evans, R.L. 1974. *Design and Performance of Chlorine Contact Tanks*. State of Illinois, ISWS-74-CIR119.

Lansey, K.E; Boulos, P.F. 2005. *Comprehensive Handbook on Water Quality Analysis for Distribution Systems*. MWH Soft: 300 North Lake Avenue, Site 1200, Pasadena, California 91101 USA.

Letternam, R.D; ed. 1999. *Water Quality and Treatment, 5th ed.* American Water Works Association, McGraw-Hill: New-York.

Mahr, B; Mewes D. 2007. CFD Modelling and Calculation of Dynamic Two-Phase Flow in Columns Equipped with Structured Packing. *Chemical Engineering Research and Design,* **85(8A)**, 1112-1122.

Owens, S.A; Perkins, M.R; & Eldridge, R.B. 2013. Computational Fluid Dynamics Simulation of Structured Packing. *Industrial & Engineering Chemistry Research,* **52**, 2032-2045.

Pedras, M.H.J; de Lemos, M.J.S. 2001. Macroscopic turbulence modeling for incompressible flow through undeformable porous media. *International Journal of Heat and Mass Transfer*, **44**, 1081-1093.

Petre, C. F.; Larachi, F.; Iliuta, I.; Grandjean, B. P. A. 2003. Pressure drop through structured packings: Breakdown into the contributing mechanisms by CFD modeling. *Chem. Eng. Sci*, **58 (1)**, 163−177.

Pilling, M; Holden, B.S. 2009. Choosing Trays and Packing for Distillation. *CEP*, September, 44-50.

Pope, S.B. 2000. *Turbulent Flows*. Cambridge University Press: Cambridge, U.K.

Raschig Jaeger Technologies. 2006. Product Bulletin 400. Houston, TX.

Rauen, W.B; Lin, B; Falconer, R.A; Teixeira, Edmilson C. 2008. CFD and experimental model studies for water disinfection tanks with low Reynolds number flows. *Chemical Engineering Journal,* **137**, 550-560.

Rauen, W.B; Angeloudis, A; Falconer, R.A. 2012. Appraisal of chlorine tank modeling practices. *Water Research,* **46**, 5834-5847.

Richards, T; Rienhart, D. 1986. Evaluation of Plastic Media in Trickling Filters. *Journal Water Pollution Control Rederation*, **58 (7)**, 774.

Sherwood, T.K; Shipley, G.H. 1938. Flooding Velocities in Packed Columns. *Industrial and Engineering Chemistry*, **30(7)**, 765-769.

Shiono, K; Teixeira, E. C. 2000. Turbulent Characteristics in a Baffled Contact Tank. *Journal of Hydraulic Research*, **38(6)**, 403-416.

Stewart, R.W. 1968. *Turbulence*. Educational film under the National Committee for Fluid Mechanics Films, National Science Foundation.

Szulczewska, B; Zbicinski, Ir; & Gorak, A. 2003. *Chemical Engineering and Technology*, **26(5)**, 580-584.

Taylor, Z.H. 2012. *Towards Improved Understanding and Optimization of the Internal Hydraulics of Chlorine Contact Tanks.* Master's Thesis, Department of Civil and Environmental Engineering, Colorado State University, Fort Collins, CO.

U.S. Department of Energy, USDOE. 2001. *Distillation Column Modeling Tools*. Office of Industrial Technologies, Energy Efficiency and Renewable Energy, Washington, D.C.

United States Environmental Protection Agency, USEPA. 1991. *Guidance Manual for Compliance with the Filtration and Disinfection Requirements for Public Water Systems Using Surface Water Sources*. 68-01-6989. USEPA

United States Environmental Protection Agency, USEPA. 2003. *LT1ESWTR Disinfection Profiling and Benchmarking Technical Guidance Manual*. EPA 816-R-03-004, Office of Water, Washington, D.C.

United States Environmental Protection Agency, USEPA. 2004 (June). *Understanding the Safe Drinking Water Act*. Tech. rept. EPA 816-F-030. USEPA.

United States Environmental Protection Agency, USEPA. 2011 (July). *National Characteristics of Drinking Water Systems Serving Populations Under 10,000*. Tech. rept. EPA 816-R-10-022. USEPA

United States Environmental Protection Agency, USEPA. 2012. *Safe Drinking Water Act (SDWA)*. < http://water.epa.gov/lawsregs/rulesregs/sdwa/> (April 19, 2014).

United States Environmental Protection Agency, USEPA. 2012. *Small Systems and Capacity Development.* <http://water.epa.gov/type/drink/pws/smallsystems/> (Jan. 10, 2014).

United States Geological Survey (USGS). 2014. *How much water is there on, in, and above Earth?* < http://water.usgs.gov/edu/earthhowmuch.html> (April 19, 2014).

Venayagamoorthy, S.K; Stretch, D.D. 2010. On the turbulent Prandtl number in homogeneous stably stratified turbulence. *J. Fluid Mech*, **644**, 359-369.

Versteeg, H. K; Malalasekera, W. 2007. *An Introduction to Computational Fluid Dynamics: The Finite Volume Method, Second Edition*. Pearson Education: Harlow, England.

Wang, H; Falconer, R.A. 1998. Numerical Modeling of Flow in Chlorine Disinfection Tanks. *J. Hydraulic Engineering*, **124**, 918-931.

Wang, H; Falconer, R.A. 1998. Simulating Disinfection Processes in Chlorine Contact Tanks using Various Turbulence Models and High-order Accurate Difference Schemes. *Water Research*, **32(5)**, 1529-1543.

Wang, H; Shao, X; & Falconer, R.A. 2003. Flow and Transport Simulation Models for Prediction of Chlorine Contact Tank Flow-Through Curves. *Water Environment Research*, **75(5)**, 455-471.

Water.org. *Water Crisis Facts*. <water.org/water-crisis/water-facts/water/> (April, 19, 2014).

Wenjun, L.I.U; Zhipeng, D.U; Junwei, J.I.N. 2007. Optimizing the configuration of a clearwell by integrating pilot and full-scale tracer testing. *Front. Environ. Sci. Engin. China*, **1(3)**, 270-275.

Wen, X; Akhter, S; Afacan, A; Nandakumar, K; & Chuang, K. T. 2007. CFD modeling of columns equipped with structured packings: I. Approach based on detailed packing geometry. *Asia-Pacific Journal of Chemical Engineering,* **2**, 336-334.

Wilson, J. M; Venayagamoorthy, S.K. 2010. Evaluation of hydraulic efficiency of disinfection systems based on residence time distribution curves. *Environ. Sci. Technol*, **44**,9377-9382.

Wilcox, D.C. 2007. *Basic Fluid Mechanics*, *Third Edition*. DCW Industries, Inc: San Diego, California.

Wilson, J. M. 2011. *Evaluation of Flow and Scalar Transport Characteristics of Small Public Drinking Water Disinfection System using Computational Fluid Dynamics*. Master's Thesis, Department of Civil and Environmental Engineering, Colorado State University, Fort Collins, CO.

Wols, B.A; Hofman, J.A.M.H; Uijttewaal, W.S.J; Rietveld, L.C; van Dijk, J.C. 2010. Evaluation of different disinfection calculation methods using CFD. *Environmental Modeling and Software*, **25**, 573-582.

Xu, Qing. 2010. *Internal Hydraulics of Baffled Disinfection Contact Tanks Using Computational Fluid Dynamics*. Master's Thesis, Department of Civil and Environmental Engineering, Colorado State University, Fort Collins, CO.

Yakhot, V; Orszag, S.A. 1986. Renormalization Group Analysis of Turbulence. *J. Scientific Computing*, **1 (1)**, 3-51.

106

Yin, F. H; Sun, C.G;Afacan, A; Nandakumar, K; & Chuang, K. T. 2000. CFD Modeling of Mass-Transfer Processes in Randomly Packed Distillation Columns. *Ind. Eng. Chem. Res*, **39**, 1369-1380.

Zhang, J.M.; Lee, H.P.; Khoo, B.C; Teo,C.P; Haja, N; & Peng, K.Q. 2011. Modeling and Simulations of Flow Pattern, Chlorine Concentration, and Mean Age Distributions in Potable Water Service Reservoir of Singapore. *Journal of Environmental Engineering*, **137**, 575-584.

Zhang, J.M; Khoo, B.C; Lee, H.P; Teo, C.P; Haja, N; & Qi Peng, K. 2012. Effects of Baffle Configurations on the Performance of a Potable Water Service Reservoir. *Journal of Environmental Engineering*, **138**, 578-587.

APPENDIX A: UDF

```
#include "udf.h"

DEFINE_DIFFUSIVITY(diff_coeff,c,t,i)

{

return C_MU_T(c,t) / 0.7+0.001;

}
```

APPENDIX B: EC300A CONDUCTIVITY PROBE CALIBRATION PROCEDURE

A YSI EC300A conductivity meter was used to measure conductivity for all sodium-chloride tracer studies presented in this thesis. The EC300A handheld unit was cleaned after every test using de-ionized water and a manufacturer certified nylon brush. After every two to five tracer studies the unit was calibrated using the following set of steps:

1. Connect the conductivity probe and cable assembly to the unit.

2. Rinse the probe and calibration container with deionized water and scrub each electrode with the manufacturer provided nylon brush.

3. Rinse the conductivity probe and the calibration chamber using standardized calibration solution that has been stored at room temperature.

4. Turn the unit on. The screen will display CELL and the cell constant of the conductivity probe.

5. Allow temperature readings to stabilize, then press CAL to enter the calibration mode. Press MODE until Conductivity Calibration is reached.

6. Fill the calibration container with fresh standardized solution of a known conductivity and immerse the probe. Completely submerged the probe without touching the sides of the calibration container. Shake the probe lightly to remove and air bubbles trapped in the conductivity cell.

7. Allow the temperature to stabilize. After temperature stabilization, use the up and down arrow keys to adjust the conductivity value to that of the conductivity standard at 25°C. Press Enter to calibrate. The unit beeps twice to indicate a successful calibration, then automatically switches to normal operation mode.

8. Switch to temperature compensation mode and check that the conductivity matches the

    standard solution for the measured temperature. If it does not repeat steps 1-8.

APPENDIX C: EXPERIMENTAL ERROR

All physical tracer studies conducted in this thesis were subject to various sources of experimental uncertainty. Sources of error for conductivity based tracer studies included variability in flow rate measurement, temperature measurement, conductivity measurement, background conductivity, and inherent violations in the assumption of passivity. Reported manufacturer uncertainty for the Master Meter flow measurement device that was used in all tracer studies was $\pm 3\%$. Reported uncertainty for the EC300A conductivity meter that was implemented can be seen below in Table C1. For the range of tested conductivities the measurement error related to conductivity measurement was approximately $\pm 1\%$ of a given reading plus 2 μS/cm. Raw water used in all conductivity measurements was supplied from Horsetooth Reservoir and would vary in conductivity by as much as 5 mS/cm over a period of several days. Any tests that were significantly affected by changes in background conductivity were repeated a minimum of two times.

Initial testing of inlet box systems from Chapter 4 were done using both lithium-chloride and sodium-chloride solutions as conservative tracers. Results showed that higher concentrations of sodium-chloride introduced buoyancy effects within the studied system, violating the assumption of passivity (See Figure C1). A number of tests were conducted with decreasing tracer conductivities in order to prescribe acceptable concentrations for the obtainment of a passive system. However, it is still likely that small experimental error occurred from buoyancy effects in later tests

Buoyancy effects were assumed negligible for lithium-chloride studies due to low tracer concentrations. Experimental uncertainty for lithium chloride tests resulted from variations in flow rate, sample size, and error associated with inductively coupled plasma-atomic emission

spectroscopy. Samples were taken over a period of time and therefore represented average concentrations over the collected time interval. Measurement of lithium ion concentration was completed by the Colorado State University Soil, Water, and Plant testing laboratory using methods techniques with a small range of uncertainty ($< \pm 1\%$).

Table C1: YSI EC300A Product Specifications

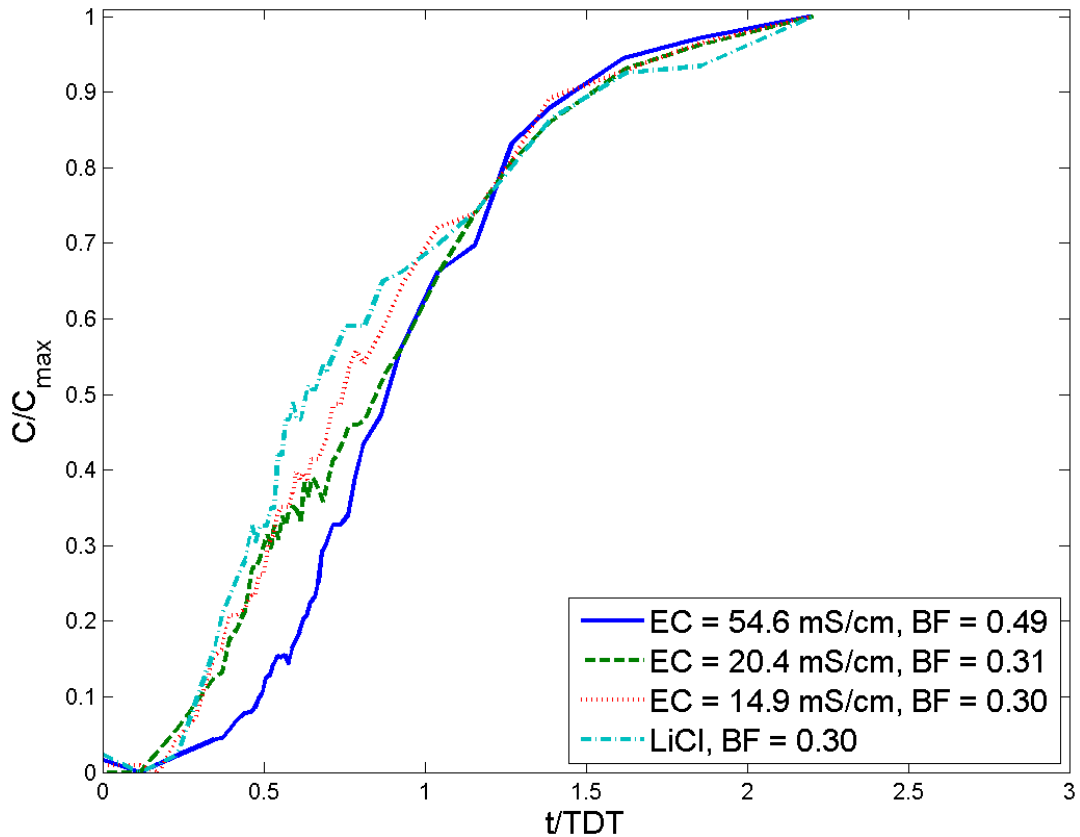| Display	Range	Accuracy
Conductivity, Auto-ranging	0.0 to 499.9 uS/cm	$\pm 1\%$ of reading plus 2 uS/cm
	500 to 4999 uS/cm	$\pm 1\%$ of reading plus 5uS/cm
	5.00 to 49.99 mS/cm	$\pm 1\%$ of reading plus 0.05 uS/cm
	50.0 to 200.0 mS/cm	$\pm 2.5\%$ of reading plus 0.5 mS/cm
Salinity	0.0 to 70.0 ppt	0.2% Full Scale
Temperature °C	-10.0 to 90 °C	$\pm 0.2°$ C or $\pm 0.4\%$ Full Scale, whichever is greater

Figure C1: Buoyancy Effects Induced by Higher Tracer Concentrations